ENERGY MATERIALS: MODELING, DESIGN AND APPLICATIONS OF ELECTROWETTING, THERMOELECTRIC AND SUPERCONDUCTING MATERIALS

BY

HANXIONG WANG

A dissertation submitted to the

School of Graduate Studies

Rutgers, The State University of New Jersey

In partial fulfillment of the requirements

For the degree of

Doctor of Philosophy

Graduate Program in Mechanical and Aerospace Engineering

Written under the direction of

Liping Liu

And approved by

_____

_____

_____

_____

New Brunswick, New Jersey

JANUARY, 2019

ABSTRACT OF THE DISSERTATION

Energy materials: modeling, design and applications of electrowetting, thermoelectric and superconducting materials

By Hanxiong Wang

Dissertation Director: Liping Liu

Energy materials play a significant role in modern material science. To understand the mechanism of functional materials, an energy functional formulation method can provide an efficient way to systematically describe the behavior of energy materials. Energy formulation method also has the advantage in dealing with the difficulties in the field formulation. In this thesis, we mainly have three parts of work based on energy formulation method.

First, an interesting problem on the equilibrium shape of a bubble/droplet in an electric field is investigated. This is important for electrowetting over dielectrics (EWOD), electrohydrodynamic enhancement for heat transfer, and electro-deformation of a single biological cell among others. In this part of work, we develop a general variational formulation on account of electro-mechanical couplings. In the context of electrohydrodynamics (EHD), we identify the free energy functional and the associated energy minimization problem that determines the equilibrium shape of a bubble in an electric field. Based on this variational formulation, we implement a fixed mesh level-set gradient method for computing the equilibrium shapes. This numerical scheme is efficient and validated by comparing with analytical solutions at the absence of electric field and experimental results at the presence of electric field. We also present simulation results for zero gravity which will be useful for space applications. The variational formulation and numerical scheme are anticipated to

have broad applications in areas of EWOD, EHD, and electro-deformation in biomechanics.

Secondly, based on the continuum theory of thermoelectric materials developed by Liu[71], we predict that the power factor of thermoelectric (TE) composites can be significantly enhanced by simple laminate structures. This prediction is numerically verified by the Finite Element Model (FEM) that is implemented to compute the local fields in heterogeneous TE structures of general geometries and boundary conditions. Among many other applications, the FEM enables to investigate the effects of small electrical contact on power generation. For a cylindrical sandwich TE structure, we show that the power output of the TE sandwich structure, though lowered by a small contact area, is still significantly larger than that of the constituent TE semiconductor.

Thirdly, we study the type II superconducting materials. Many applications of high-temperature superconductors(HTS) need a high critical current density J_c, especially under a strong external magnetic field. An effective way to enhance J_c is to pin the vortex array to avoid flux flow. Therefore, fluxing pinning plays an important role in the properties of HTS. Here, based on Ginzburg-Landau theory and classic Landau theory of micromagnetics, we formulate the total free energy of the system associated with superconducting materials coupling with paramagnetic inhomogeneities. Consider thin film scenario, pinning force which is related to the size of inhomogeneity, paramagnetic permeability and distance of vortex to inhomogeneity interface is investigated with/without external transport current at dilute limit. We develop a self-consistent model, leading to an estimation of paramagnetic interface effect on pinning force in different structures of the thin film composite. The theoretical results fit well with existing experiments in the literature qualitatively.

Acknowledgements

Foremost, I would like to express my sincere gratitude to my advisor and mentor, Prof. Liping Liu for his selfless help of both my PhD research and my life, for his patience, motivation, and immense knowledge. This dissertation is accomplished with his guidance in every aspect. His guidance helped me in all the time of research and writing of this thesis. I could not have imagined having a better advisor and mentor for my Ph.D study. He really made my PhD life and it was such a precious experience with him in the last 6 years.

Besides my advisor, I would like to thank the rest of my thesis committee: Prof. Andrew Norris, Prof. Aaron Mazzeo, and Prof. Zhengchao Han, for their insightful comments and encouragement, but also for the hard question which incented me to widen my research from various perspectives.

I would like to express my greatest gratitude to my parents, Jingkang Wang and Guoping Wu for their selfless support all the time throughout my life. I would like to thank my best friends, Renze Wang and Ruobing Bai, for helping me from work to life.

I am also grateful to my colleagues Wuhan Yuan, Yuqian Zhang, Hua Hong, Lixing Hu, Xiaobing Zhang, Wei Wang, Xiaoshi Su and many other important friends, without your help and considerations, it would not have been possible for me to realize this achievement.

Last but not the least, I would like to thank my most important one: my girl friend, Ning Li, for all her love and support. You raise me up and lighten my life during my dark day. I promise no matter how hard it gets, we will overcome it together with love. The future is bright and beautiful. May happiness be with us, always.

Table of Contents

List of Tables

List of Figures

Chapter 1

Introduction

Energy materials, e.g., thermoeletric materials and superconducting materials, are widely used in modern manufacturing and aerospace industry, where it is applied to statisfy the requirements such as energy conversion efficiency, critical electric current. In order to better apply these energy materials on the real devices, it is necessary to establish the self-consistent theories so that we can build reasonable models to describe and predict the behaviour of the specified materials.

Based on the subject of classic electrostatics, magnetostatics and electicity, the state variables of a continuum deformable body $\Omega \subset I\!R^3$ in static equilibrium shall necessarily satisfy the Maxwell equations and mechanical balance laws:

$$\begin{aligned} &\nabla \times \mathbf{E} = 0, \qquad \nabla \cdot \mathbf{D} = \rho^e, \qquad \mathbf{D} = \epsilon_0 \mathbf{E} + \mathbf{P} + \mathbf{P}^e, \\ &\nabla \times \mathbf{H} = 0, \qquad \nabla \cdot \mathbf{B} = 0, \qquad \mathbf{B} = \mu_0(\mathbf{H} + \mathbf{M} + \mathbf{M}^e), \\ &\mathbf{F} = \mathrm{Grad}\chi, \qquad \nabla \cdot \sigma_{\mathrm{tot}} = \mathbf{f}^e, \qquad \sigma_{\mathrm{tot}} = \sigma_{\mathrm{tot}}^T. \end{aligned} \tag{1.1}$$

where $\mathbf{E}$, $\mathbf{D}$, $\mathbf{H}$, $\mathbf{B}$:$V \to I\!R^3$ are respectively electric field, electric displacement, magnetic field and magnetic flux, $\mathbf{M}$ (resp. $\mathbf{M}^e$) : $V \to I\!R^3$ is intrinsic (resp. external) magnetization, $\mathbf{P}$ (resp. $\mathbf{P}^e$) : $V \to I\!R^3$ is intrinsic (resp. external) polarization, ϵ_0 (resp. μ_0) is electric permittivity (resp. magnetic permeability) of vacumn, $\chi : V \to I\!R^3$ is deformation, $\mathbf{F} : V \to I\!R^{3\times 3}$ is deformation gradient, $\mathbf{f}^e : V \to I\!R^3$ is external body force and $\sigma_{\mathrm{tot}} : V \to I\!R^{3\times 3}$ is the total stress. And theories for the continuum media are completed by the constitutive relations such that the system is well-posed upon specifying boundary conditions on ∂V:

$$C(\chi, \mathbf{F}; \mathbf{D}, \mathbf{E}, \mathbf{P}, \mathbf{P}^e, \mathbf{H}, \mathbf{B}, \mathbf{M}, \mathbf{M}^e) = 0. \tag{1.2}$$

The main problem of the above procedure is that the constitutive relations for the continuum medium has to be inferred from benchmark experiments or a more fundamental microscopic theory [25], instead of being derived within the framework of continuum theory. And the constitutive laws have to be consistent with the fundamental laws, frame independent and guarantee the symmetries of the medium. From the above arguments, an energy formulation has the advantage to avoid these two issues and address the difficulties in the field formulation [25]. After proposing an internal energy function, usually constitutive relations can be obtained by expanding and truncating the internal energy function. In this procedure, whether the constitutive laws conform to the fundamental laws can justify the success of the proposed energy function. Many poineers developed the above enegy functional formulation method. To the best knowledge of author's knowledge, Toupin (1956) firstly systematically began this theory associated with deriving the field equations and showed the equivalence between the field energy and principle of virtual work.

Generally speaking, the principle of virtual work can be regarded as a weak form of a variational principle. Therefore, it is naturally to think of a variational formulation for a continuum body based on the physical free energy and some intuitation. If the goal is to identify static equalibrium state of a body at a constant temperature, we shall assume the body has constant entropy and the equalibrium state is determined by the principle of minimum free energy(Gibbs, 1878, pg. 109). Moverover, the effects of general boundary conditions associated with free energy need to be considered and added to the proposed internal energy functional. The above two facts require us to determine the proper set of thermodynamic variables that can completely describe the thermodynamic state of the continuum body and the energy functional can interact with all the possible boundary conditions so that we can employ the minimum free energy.

There are several more advantages in the variational energy formulation method besides that the constitutive laws can be merged into the form of internal enegy function. First, the proposed energy provides a clear thermodynamic interpretation in the framework of Gibbs. Second, there is no need to artically seperate the local term and the nonlocal term, i.e., the Maxwell stress. This mechanism can be derived naturally from the first variation of the total free energy. Also, even a well-posed boundary value problem may admit multiple

solutions. It will be convenient to analyze the stability of these solutions to the system once we have the general total free energy form. Last but not least, energy formulation method can be applied to study many other physical phenomena, e.g., phase transitions. Once the state variables are determined, it is quite convenient and natural to calculate the conjugate driving forces and formulate the kinetic laws, which sometimes are the difficulties in the field equations.

As discussed in Liu (2013) [72], the field equations in general may enjoy many different variational energy formulation. However, the associated Euler-Lagrange equations (including the constitutive laws) must be consistent with the field equations. In another words, the state variables and energy functional could be different for some specified problem but the equivalence of various forms of total free energy need to be guaranteed.

In this dissertation, we first propose a general variational method in account of electro-mechanical couplings, dealing with the problem of determining the equilibrium shape of a bubble/droplet in an electric field in chapter 2. For this kind of evolution problems, the total free energy and the selection of possible variation of state variables are chosen based on the physical gound. We notice that this judgement completely depends on the physical meaning instead of mathematical form [72]. Later, in chapter 3, we study the thermoelectric effect including Seebeck effects, Peltier effects and Thomson effect by a continuum theory [71]. The effective properties of thermoelectric composite are also considered. In chapter 4, concerning the phase transitions of type II superconducting materials, we propose an energy formulation which is closely related with phenomenological Ginzburg-Landau theory and Landau theory of micromagnetics.

This dissertation is organized as follows: in Chapter 2 we develop a general variational formulation in account of electro-mechanical couplings, identify the free energy functional and the associated energy minimization problem that determines the equilibrium shape of a bubble in an electric field. A numerical simulation based on a level set method is employed, comparing with previous experimental results, to verify the correctness of our theory and algorithm. In Chapter 3 we review Liping Liu's continuum theory of thermoelectric bodies [71]. Starting from experimental observations and conservation laws, boundary value problems are formulated for various applied boundary conditions. Local fields in TE bodies

are solvable theoretically. Furthermore the effective properties of thermoelectric composites are defined; explicit formula of effective TE properties of thermoelectric composites with simple laminates structure are obtained. A TE composite system with a simple laminate microstructure which enhances power factor significantly is discussed. Chapter 4 is a study of magnetic vortex pinning by paramagnetic boundary in high temperature type II superconducting materials. The proposed free enenrgy is based on Ginzburg-Landau theory and classic Landau theory of micromagnetics. Assuming temperature is constant, we propose a general total free energy of the superconducting system. Then we derive the energy in planar form in thin film and deduce the pinning force for a individual vortex in dilute limit. Finally we study the impact of transport current on pinning effect in a thin film. In Chapter 5 we introduce two ideal devices: A high T_c superconducting magnet excited by thermoelectric composite; A thermoelectric cooler for superconducting transmission bulk. We conclude in Chapter 6.

Chapter 2

Energy description on a heterogeneous bubble in an electric field

2.1 Introduction

Electro-mechanical coupling is of fundamental importance for many applications. For solid and hard materials, electro-mechanical coupling manifests itself as piezoelectric or flexoelectric effects [43]. For soft materials and fluids, electro-mechanical coupling is often addressed by invoking the concept of Maxwell stress [28, 42]:

$$\mathbf{T}_{\mathrm{MW}} = \mathbf{E} \otimes \mathbf{D} - \frac{\epsilon(\mathbf{x})}{2}|\mathbf{E}|^2\mathbf{I}, \tag{2.1}$$

where $\mathbf{E}$ ($\mathbf{D}$) is the local electric field (displacement), $\mathbf{I}$ is the identity tensor and $\epsilon(\mathbf{x})$ is the local electric permittivity. Though widely used for many applications [44, 13], the fundamental concept of Maxwell stress is not free of contention [37, 4]. In the literature, the following quantity (see e.g. [30], ch. 3; [45])

$$\mathbf{T}_0 = \mathbf{E} \otimes \mathbf{D} - \frac{\epsilon_0}{2}|\mathbf{E}|^2\mathbf{I} \tag{2.2}$$

is also referred to as the Maxwell stress with ϵ_0 being the vacuum permittivity. Moreover, the physical interpretation of the Maxwell stress often relies on the formula that the electric body force is given by $\mathbf{f} = \mathrm{div}\mathbf{T}_{\mathrm{MW}}$ which, by direct calculations, yields body force terms called electrophoretic force, dielectrophoretic force, electrostrictive force, etc [16, 27]. It is somewhat mysterious what are the distinctions and physical origins of the above different formulas of Maxwell stress and various forces due to electro-mechanical interaction. This conceptual difficulty is not new and has been discussed in length in the literature ([28],

pg. 132; [30], ch. 3; [46]). In addition, for static equilibrium problems we anticipate the thermodynamic state of the system shall be such that the free energy of the system is minimized. This motivates us to establish a free-energy based variational formulation for continuum bodies that accounts for general electro-mechanical couplings [24, 25].

In this work we consider a particular class of electro-mechanical coupling problem: the equilibrium shape of an immersible bubble in an electric field. The field equation for the equilibrium interface is well-known, i.e., the generalized Young-Laplace equation with a force term contributed by the Maxwell stress [47, 32]. One may wonder whether the field equation admits a variational formulation, and if so, whether the formulation shall give a precise explanation on the origin of the Maxwell stress.

We remark that the problem of equilibrium shape and evolution of a bubble arises from a number of important applications including electrowetting over dielectrics (EWOD), electro-hydrodynamic (EHD) enhancement for heat transfer [31, 39], and electro-deformation of a single biological cell [17]. Similar problems also arise in the determination of the equilibrium shape of a pore channel embedded in a soft elastomer matrix coupled with electrostatics and diffusion [20, 23, 3]. To demonstrate our formulation, we focus on a single vapor bubble model for EHD since it represents a simple yet relevant model of EHD-enhanced boiling [19, 47, 32, 33, 34, 5, 22, 16, 48]. Experimental observations have confirmed that the electric field can alter the bubble dynamics dramatically, for instance, resulting in elongated bubble shape along the field direction, increased ebullition frequency and smaller departure volume [6, 8, 11, 33, 26]. Meanwhile, a few theoretical and computational studies have been conducted to understand the physical mechanisms for the effect of electric field on the behavior of EHD bubble [38, 32, 48, 9, 10, 15, 49, 50]. However, to the author's best knowledge, the existing theoretical treatments and numerical implementations are based on the field equations where the expression of Maxwell stress (2.1) is taken for granted. Moreover, the stability criterion for bubbles remains elusive in the field equation formulation, demanding a more systematic energetic analysis.

The energy-based approach in EHD has been employed by Cheng and Chaddock [7] to analyze the deformation and stability of spheroidal homogeneous bubbles in an electric field where the effect of the solid substrate is neglected. In the subsequent work [8], the authors

obtained the shape profile of a bubble elongating in the electric field and determined the departure size at different electric field strength. Cheng and Chaddock's [7, 8] approach was based on the assumption of ellipsoidal shapes and the closed-form solutions to the electrostatic problem where the concept of Maxwell stress was not needed at all, and hence cannot be directly used for numerical simulations. Our work extends the energy-based approach to heterogeneous bubbles of general geometries and under general boundary conditions. We remark that identifying the free energy of a continuum medium in an electric field has proven to be quite subtle. Alternative, sometimes contradictory, expressions of the total free energy (or internal energy) of the system (including or not including the effects of boundary devices) have been proposed in the literature. This has generated quite some confusions. The reader is referred to one of the Liu's recent works [24, 25] and references therein for the origins and relationship between different energy formulations pertaining to electro-mechanical coupling. Here, for the EHD model of a single bubble on solid substrate we identify the free energy of the system, carry out the derivation of electric contribution to the mechanical balance of the bubble interface, and obtain the variational principle (a minimization problem, as anticipated) that determines the equilibrium shape of a bubble in an electric field. This variational principle also implies a robust numerical algorithm for computing the equilibrium shape of a bubble. Following the framework of the level-set method [35, 41, 36] and sensitivity analysis [2], we implement a gradient scheme for minimizing the free energy of the system with a given volume and obtain the final equilibrium shape of the bubble. This numerical scheme is further verified by comparing with analytical results [7] at the absence of electric field and experimental results at the presence of electric field.

As is well-known, a key difficulty of simulating the equilibrium shape of a bubble in an electric field lies in computing the nonlocal Maxwell stress on the interface. A second difficulty in a Lagrangian scheme arises from tracking the interface. The level-set based gradient method is particularly convenient to address these issues. Roughly speaking, the level-set function is defined on a fixed mesh to characterize the shape of the bubble; the same mesh is used in the finite element model for solving the electrostatic problem. We

can then determine the driving forces on the interfaces by a sensitivity analysis. By enforcing a kinetic law that relates the normal velocity of the interface and driving force, the evolution of the level-set function follows a Hamilton-Jacobi equation and the total free energy decreases monotonically with respect to (fictitious) time until the final equilibrium shape is reached. We remark that our numerical scheme is particularly robust and suitable for stability analysis of the bubble since it is based on a minimization problem. It is also worthwhile to mention the work of Di Marco *et al.* [27] where the dynamic process of a growing bubble in an electric field has been studied via a scheme that combines the volume of fluid method, level-set method and ghost fluid approach.

This chapter is organized as follows. In Section 2.2 we begin with the field equation formulation of the problem including the Maxwell equation for the electric field, the equilibrium equations for the interfaces, and the associated boundary conditions. A variational formulation of the problem is presented in Section 2.3. We also show the associated Euler-Lagrange equations are equivalent to the field equations in Section 2.2 and derive the driving forces on the interfaces that will be useful for our numerical scheme. In Section 2.4, following [40, 1] we describe the level-set gradient method and the detailed algorithm for minimizing our energy functional. Some numerical examples are given in Section 2.5 including comparison with prior experimental data and analytical solutions. We conclude and summarize in Section 2.6.

Notation. We employ direct notation for brevity if possible. Vectors are denoted by bold symbols such as $\mathbf{e}, \mathbf{u}$, etc. When index notations are in use, the convention of summation over repeated index is followed. The inner (or dot) product of two vectors $\mathbf{a}, \mathbf{b} \in I\!R^3$ is defined as $\mathbf{a} \cdot \mathbf{b} := (\mathbf{a})_i (\mathbf{b})_i$ and $\mathbf{a} \cdot \mathbf{M}\mathbf{b} = a_i M_{ij} b_j$ for a matrix $\mathbf{M} \in I\!R^{3\times 3}$. From the viewpoint of matrices, the i^{th} row vector of the gradient of a vector field, e.g., $\nabla \mathbf{u}$, is the gradient of the i^{th} component of $\mathbf{u}$ whereas the "div" operates on the row vectors of a matrix field. Therefore, $\text{div}\nabla\mathbf{u} = \Delta\mathbf{u}$ and $\text{div}[(\nabla\mathbf{u})^T] = \nabla(\text{div}\mathbf{u})$. For a scaling parameter $\varepsilon \ll 1$, $O(\varepsilon)$ implies the asymptotic behavior $O(\varepsilon)/\varepsilon \to C \neq 0$ as $\varepsilon \to 0$ whereas $o(\varepsilon)/\varepsilon \to 0$ as $\varepsilon \to 0$.

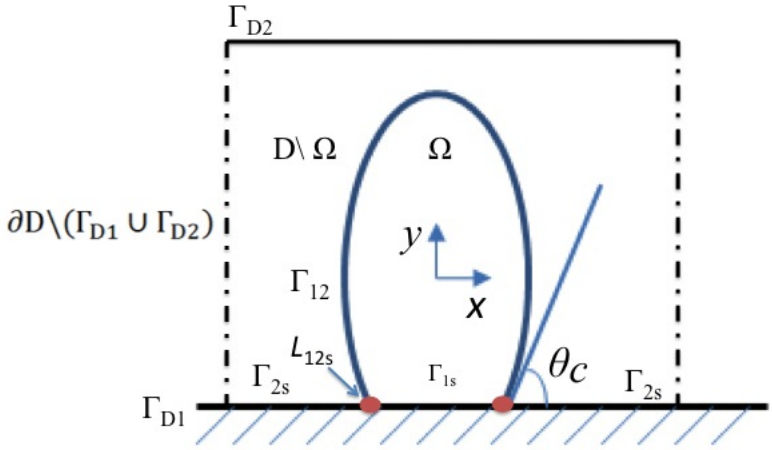

Figure 2.1: A bubble in an applied electric field.

2.2 Problem statement

Consider a two-phase immiscible fluid as shown in Fig. 2.1 and denote by $D \subset I\!R^3$ the domain occupied by the two-phase fluid. Let Ω and $\Omega^c = D\backslash\Omega$ denote the domain occupied by the first phase fluid and the second phase fluid with the density and permittivity given by

$$\rho(\mathbf{x}) = \begin{cases} \rho_1 & \mathbf{x} \in \Omega, \\ \rho_2 & \mathbf{x} \in D \setminus \Omega, \end{cases} \qquad \epsilon(\mathbf{x}) = \begin{cases} \epsilon_1 & \mathbf{x} \in \Omega, \\ \epsilon_2 & \mathbf{x} \in D \setminus \Omega, \end{cases}$$

respectively. We further assume that the domain Ω is regular, axisymmetric and open bounded. The fluid phases are in contact with the solid container and, in particular, the first fluid phase, the second fluid phase and the solid substrate meet at a line which we denote by L_{12s}. Denote by Γ_{12} the interface between the first and the second fluid phase, and by Γ_{1s} (Γ_{2s}) the interface between the first (second) fluid phase and the solid substrate. Let γ_{12}, γ_{1s}, and γ_{2s} be the surface tensions of the interfaces Γ_{12}, Γ_{1s}, and Γ_{2s}, respectively. The line tension in the junction line L_{12s} is denoted by l_{12s}.

We apply an external electric field on the two-phase fluid by maintaining a constant

potential difference between two planar electrodes on the boundary of the domain D (see Fig. 2.1). The bottom (resp. top) electrode occupying $\Gamma_{D1} \subset \partial D$ (resp. $\Gamma_{D2} \subset \partial D$) has the electrostatic potential $\varphi = V_1$ (resp. $\varphi = V_2$). By the Maxwell equation, the electrostatic potential $\varphi : D \to I\!R$ necessarily satisfies

$$\begin{cases} \mathrm{div}[\epsilon(\mathbf{x})\nabla\varphi] = 0 & \text{in } D, \\ \varphi = V_1 \quad \text{on } \Gamma_{D1}, \qquad \varphi = V_2 \quad \text{on } \Gamma_{D2}, \\ \hat{\mathbf{n}} \cdot \nabla\varphi = 0 & \text{on } \partial D \setminus (\Gamma_{D1} \cup \Gamma_{D2}). \end{cases} \tag{2.3}$$

Here, the last boundary condition follows from the assumption that the boundary $\partial D \setminus (\Gamma_{D1} \cup \Gamma_{D2})$ is far away from the bubble and hence the fringe field is negligible. We remark that the above boundary value problem uniquely determines the local electric field.

We seek to determine the equilibrium shape of the bubble Ω assuming that the inertial and hydrodynamic forces are negligible. To this end, we first notice that the boundary of Ω may in general consist of the interface between the two fluids Γ_{12}, the interface between the first phase fluid and the solid substrate Γ_{1s} and the junction line L_{12s}. The equilibrium of any sub-interface $\Sigma \subset \Gamma_{12}$ implies the classic Young-Laplace equation:

$$\int_{\partial\Sigma} \gamma_{12}\hat{\mathbf{t}} + \int_{\Sigma} (p_1 - p_2 + f_e)\hat{\mathbf{n}} = 0 \quad \Rightarrow \quad 2\gamma_{12}H = p_1 - p_2 + f_e \qquad \text{on } \Gamma_{12}, \tag{2.4}$$

where $\hat{\mathbf{n}}$ is the unit outward normal to the interface Γ_{12}, $\hat{\mathbf{t}}$ is the unit tangent on Γ_{12} that is perpendicular to and point away from $\partial\Sigma$, and H is the mean curvature of the interface Γ_{12}. To derive the second of (2.4) we have noticed that by the Stokes theorem (see, e.g., [29]), for any cotangent vector field $\mathbf{v}$ on Γ_{12},

$$\int_{\partial\Sigma} \mathbf{v} \cdot \hat{\mathbf{t}} = \int_{\Sigma} \nabla_s \cdot \mathbf{v},$$

where ∇_s denotes the surface gradient. Then for any constant unit vector $\hat{\mathbf{k}} \in I\!R^3$, the above identity with $\mathbf{v} = \hat{\mathbf{k}} - \hat{\mathbf{n}}(\hat{\mathbf{k}} \cdot \hat{\mathbf{n}})$ implies that

$$\hat{\mathbf{k}} \cdot \int_{\partial\Sigma} \hat{\mathbf{t}} = \int_{\Sigma} \nabla_s \cdot [\hat{\mathbf{k}} - \hat{\mathbf{n}}(\hat{\mathbf{k}} \cdot \hat{\mathbf{n}})] = -\hat{\mathbf{k}} \cdot \int_{\Sigma} \hat{\mathbf{n}} \nabla_s \cdot \hat{\mathbf{n}}.$$

Inserting the above equation into the first of (2.4), from the arbitrariness of the sub-interface Σ, by the definition $2H = \nabla_s \cdot \hat{\mathbf{n}}$, we obtain the differential form of the equilibrium equation, i.e., the second of (2.4).

Further, we assume the two-phase fluid is in a uniform downward gravitational field of strength g. Therefore, within a non-consequential additive constant, e.g., the actual pressure at a point on the plane $\{y = 0\}$ in the second phase, the pressure in the second phase is given by

$$p_2 = -\rho_2 g y \qquad \text{in } D \setminus \Omega, \tag{2.5}$$

whereas the pressure in the first phase is given by

$$p_1 = -\rho_1 g y + p_* \qquad \text{in } \Omega. \tag{2.6}$$

Here the unknown constant $p_* \in I\!R$ is the pressure difference inside and outside the bubble Ω at $y = 0$ and depends on the volume of the bubble. Finally, the term f_e is the normal stress on Γ_{12} due to the electric interactions between the fluids and the applied electric field and is given by

$$f_e = \hat{\mathbf{n}} \cdot [\![\mathbf{T}_{\mathrm{MW}}]\!] \hat{\mathbf{n}}, \qquad \mathbf{T}_{\mathrm{MW}} = \mathbf{E} \otimes \mathbf{D} - \frac{\epsilon(\mathbf{x})}{2} |\mathbf{E}|^2 \mathbf{I}, \tag{2.7}$$

where $\mathbf{E} = -\nabla \varphi$ is the local electric field. Here and subsequently we denote by $[\![*]\!] = (*)|_+ - (*)|_-$ the jump across the interface with $+$ $(-)$ side being the exterior (interior) side of $\partial\Omega$.

Moreover, the equilibrium of any subinterval on the junction line L_{12s} implies that

$$\kappa l_{12s} = \gamma_{2s} + \gamma_{12} \cos\theta_C - \gamma_{1s} \qquad \text{on } L_{12s}, \tag{2.8}$$

where θ_C is the contact angle between the first fluid phase and the solid phase and κ is the curvature of the junction line L_{12s}. The above equation may be regarded as the boundary condition of the Young-Laplace equation (2.4). There are also situations, e.g., the first fluid

is ejected into the second fluid from a pipette of radius r_0. In this case it is the junction line that is prescribed and we shall require L_{12s} coincides with the wall of the pipette:

$$r(y)|_{y=0} = r_0. \tag{2.9}$$

For a given volume of the bubble Ω, we anticipate that equations (2.3), (2.4) and (2.8) or (2.9) admit a solution that determines the equilibrium shape of Ω for some constant p_*. At the absence of electric field and neglecting the line tension, the solutions to (2.3), (2.4) and (2.8) can be obtained by solving an ordinary differential equation, see Cheng and Chaddoock (1986) [7]. At the presence of electric field, the nonlocal Maxwell stress (2.7) makes the analytical and numerical solutions to (2.3), (2.4) and (2.8) or (2.9) challenging problems. Below we present an alternative formulation of the problem that justifies the formula (2.7) of Maxwell stress and furnishes a convenient numerical scheme for computing the equilibrium shapes.

2.3 An equivalent variational formulation

In this section we reformulate the problem of determining the equilibrium shape of the bubble as an energy minimization problem. This approach clarifies the origin of the formula (2.7) of Maxwell stress on the interface and gives rise to a convenient gradient method for solving (2.3), (2.4) and (2.8) or (2.9).

For the system of two immiscible fluids as shown in Fig. 2.2, we describe the thermodynamic state of the system by the shape and size of the bubble Ω and the polarization $\mathbf{P} : D \to I\!R^3$ in both fluids. In terms of state variables (Ω, $\mathbf{P}$), we identify the total free energy of the system as

$$\mathcal{E}_{\text{tot}}[\Omega, \mathbf{P}] = \int_{\Omega} (\rho_1 - \rho_2) gy + \int_{\Gamma_{12}} \gamma_{12} + \int_{\Gamma_{1s}} (\gamma_{1s} - \gamma_{2s}) + \int_{L_{12s}} l_{12s} + \mathcal{E}^{\text{elect}}[\Omega, \mathbf{P}], \tag{2.10}$$

where the first three terms arise from the gravity, surface tension of the interface between two fluids, and surface tensions between two fluids and solid substrate, respectively. Also, following Liu (2013, 2014) we write the electric part of free energy of the system $\mathcal{E}^{\text{elect}}[\Omega, \mathbf{P}]$

as

$$\mathcal{E}^{\text{elect}}[\Omega, \mathbf{P}] = \frac{\epsilon_0}{2}\int_D |\nabla\varphi|^2 + \int_{\partial D} \varphi[(-\epsilon_0\nabla\varphi + \mathbf{P})\cdot\hat{\mathbf{n}}] + \int_D \frac{|\mathbf{P}|^2}{2(\epsilon(\mathbf{x}) - \epsilon_0)}, \tag{2.11}$$

where the potential φ is determined by the boundary value problem (2.3). In the above equation, the first term denotes the energy of the electric field, the second term is contributed by the electric loading device, say, a battery used to maintain the potential difference, and the last term arises from polarizing the molecules in the fluids. For a fixed volume Λ_0 of Ω, by the principle of minimum free energy the equilibrium shape of the bubble shall be dictated by the minimization problem

$$\min\Big\{\mathcal{E}_{\text{tot}}[\Omega, \mathbf{P}] :\ vol(\Omega) = \Lambda_0,\ \mathbf{P}\in\mathbb{P}\Big\}, \tag{2.12}$$

where $vol(\Omega)$ denotes the volume of the domain Ω, $\mathbb{P} := \{\mathbf{P} : \int_D |\mathbf{P}|^2 < +\infty\}$ consists of all square integrable polarizations and $\mathbf{P}$ satisfies

$$\begin{cases} \operatorname{div}[-\epsilon_0\nabla\varphi + \mathbf{P}] = 0 & \text{in } D, \\ \varphi = V_1 \quad \text{on } \Gamma_{D1}, \qquad \varphi = V_2 \quad \text{on } \Gamma_{D2}, \\ \hat{\mathbf{n}}\cdot\nabla\varphi = 0 & \text{on } \partial D\setminus(\Gamma_{D1}\cup\Gamma_{D2}). \end{cases} \tag{2.13}$$

Since the mechanical part of free energy (i.e., the first three terms of (2.10)) is independent of polarization $\mathbf{P}$, it will be convenient to a priori solve the minimization problem with respect to polarization $\mathbf{P}$ and introduce an effective electric energy that depends only on Ω:

$$\mathcal{E}_*^{\text{elect}}[\Omega] := \min_{\mathbf{P}\in\mathbb{P}, vol(\Omega)=\Lambda_0} \mathcal{E}^{\text{elect}}[\Omega, \mathbf{P}]. \tag{2.14}$$

The Euler-Lagrange equations associated with the above minimization problem can be

calculated by considering variations of polarization $\mathbf{P} \to \mathbf{P}_\delta = \mathbf{P} + \delta\mathbf{P}_1$. Standard first-variation calculation yields that the minimizing polarization necessarily satisfy

$$\mathbf{P} = -(\epsilon(\mathbf{x}) - \epsilon_0)\nabla\varphi \qquad \text{in } D, \tag{2.15}$$

as one would expect from the definition of permittivity and polarization: $\mathbf{D} = \epsilon(\mathbf{x})\mathbf{E} = \epsilon_0\mathbf{E} + \mathbf{P}$. Inserting the above equation into (2.11), by the divergence theorem we find the minimum can be written as

$$\mathcal{E}_*^{\text{elect}}[\Omega] = \int_D \frac{\epsilon_0}{2}|\nabla\varphi|^2 + \int_D \frac{\epsilon(\mathbf{x}) - \epsilon_0}{2}|\nabla\varphi|^2 + \int_{\partial D} \varphi[-\epsilon(\mathbf{x})\nabla\varphi]\cdot\hat{\mathbf{n}} = -\frac{1}{2}\int_D \epsilon(\mathbf{x})|\nabla\varphi|^2. \tag{2.16}$$

By (2.10), (2.14) and (2.16), we rewrite the total free energy of the system as a functional of the bubble shape Ω:

$$\hat{\mathcal{E}}_{\text{tot}}[\Omega] = \int_\Omega (\rho_1 - \rho_2)gy + \int_{\Gamma_{12}} \gamma_{12} + \int_{\Gamma_{1s}} (\gamma_{1s} - \gamma_{2s}) + \int_{L_{12s}} l_{12s} - \frac{1}{2}\int_D \epsilon(\mathbf{x})|\nabla\varphi|^2. \tag{2.17}$$

We claim that equilibrium equation (2.4) for the interface Γ_{12} and (2.8) for the junction line L_{12s} can be regarded as the Euler-Lagrange equation of the variational principle (2.12). To see this, without change of notation we denote by Ω a local minimizer of the energy functional $\hat{\mathcal{E}}_{\text{tot}}[\Omega]$ in (2.17). We now consider small variations of the domain Ω such that the boundary points of the new domain Ω_δ consisting of $\mathbf{y} = \mathbf{x} + \delta\mathbf{y}_1(\mathbf{x})$, where $\mathbf{x} \in \partial\Omega$, $\mathbf{y}_1 : \partial\Omega \to I\!R^3$ can be interpreted as the velocity and δ as a small (fictitious) time interval. Since Ω is a local minimizer, we infer that for any volume-conserving velocity $\mathbf{y}_1$ and any number $\delta \in I\!R$ small enough,

$$\hat{\mathcal{E}}_{\text{tot}}[\Omega_\delta] - \hat{\mathcal{E}}_{\text{tot}}[\Omega] =: T1 + T2 + T3 + T4 + T5 \geq 0. \tag{2.18}$$

In the above equation, for brevity we have defined the quantities Ti $(i = 1, \cdots, 5)$ as:

$$T1 = \int_{\Omega_\delta} (\rho_1 - \rho_2) gy - \int_{\Omega} (\rho_1 - \rho_2) gy, \qquad T2 = \int_{\Gamma_{12}^\delta} \gamma_{12} - \int_{\Gamma_{12}} \gamma_{12},$$
$$T3 = \int_{\Gamma_{1s}^\delta} (\gamma_{1s} - \gamma_{2s}) - \int_{\Gamma_{1s}} (\gamma_{1s} - \gamma_{2s}), \qquad T4 = \int_{L_{12s}^\delta} l_{12s} - \int_{L_{12s}} l_{12s},$$
$$T5 = -\frac{1}{2} \int_D \epsilon_\delta(\mathbf{x}) |\nabla \varphi_\delta|^2 + \frac{1}{2} \int_D \epsilon(\mathbf{x}) |\nabla \varphi|^2,$$

where $\epsilon_\delta(\mathbf{x})$ takes the value of ϵ_1 if $\mathbf{x} \in \Omega_\delta$ and ϵ_2 if $\mathbf{x} \in D \setminus \Omega_\delta$, φ_δ is the solution to (2.3) for this new dielectric function $\epsilon_\delta(\mathbf{x})$, Γ_{12}^δ is the new interface between the first and second fluids, Γ_{1s}^δ is the new interface between the first fluid and the solid phase, and L_{12s}^δ is the new junction line between the first, second fluids and the solid substrate.

The implications of (2.18) depend on the choices of the velocity $\mathbf{y}_1$. First of all, to conserve the volume of Ω_δ the velocity $\mathbf{y}_1$ necessarily satisfies

$$\int_{\partial\Omega} \mathbf{y}_1 \cdot \hat{\mathbf{n}} = 0. \tag{2.19}$$

If the velocity $\mathbf{y}_1$ is supported on Γ_{12} (which implies the interfaces between the fluids and the solid substrate remain unchanged if δ is small enough), without loss of generality we can assume the velocity $\mathbf{y}_1$ is normal to the interface Γ_{12} and given by $\mathbf{y}_1 = v\hat{\mathbf{n}}$. Then it is clear that $T3 = T4 = 0$,

$$T1 = \delta \int_{\Gamma_{12}} (\rho_1 - \rho_2) gyv + o(\delta), \tag{2.20}$$

and (see e.g. [21])

$$T2 = \delta\gamma_{12} \int_{\Gamma_{12}} 2Hv + o(\delta). \tag{2.21}$$

Moreover, we find that the change of the electrostatic energy $\mathcal{E}_*^{\text{elect}}$ with respect to a small variations of the domain Ω is given by (see *Appendix* 2.7 for details)

$$T5 = -\delta \int_{\Gamma_{12}} f_e v + O(\delta^2) = -\delta \int_{\Gamma_{12}} v f_e + o(\delta). \tag{2.22}$$

where the stress f_e, defined in equation (2.7), is contributed by electrostatic interaction, i.e., the Maxwell stress. From (2.22), the Maxwell stress on the interface between two fluids can be regarded as a configurational force that determines the change of electric energy of the system when the interface is perturbed.

We remark that the derivation of (2.22) is quite technical, involving variations of phase boundary Γ_{12} or "inner variation" of the electrostatic potential φ, and henceforth postponed to Appendix. For a history and applications of this technique, the interested reader is referred to Eshelby (1970 [12]) in the context of elasticity for his celebrated energy-moment tensor, Simon (1980 [18]) for a general concept of shape derivatives, and to recent works of Grabovsky *et al.* (2011 [14]), Liu (2014 [25]) and references therein.

From (2.20), (2.21), (2.22) and taking into account the constraint (2.19) by a Lagrangian multiplier $-p_* \int_{\Gamma_{12}} v$, we obtain the Euler-Lagrange equation associated with the variational principle (2.12):

$$2\gamma_{12}H + (\rho_1 - \rho_2)gy - f_e - p_* = 0 \qquad \text{on } \Gamma_{12},$$

which can be identified with the Young-Laplace equation (2.4).

We now calculate the boundary conditions on the junction line L_{12s}. To this end, we shall consider variations with nonzero velocity on L_{12s}. Without loss of generality, assume that

$$\mathbf{y}_1 = v_x(u_1, u_2)\mathbf{e}_x \qquad \text{on } \Gamma_{12},$$

where v_x decays to zero away from the junction line, $\mathbf{e}_x$ is unit vector in x direction. Let $\hat{\mathbf{t}}$ be the outward tangential unit vector on the boundary line of Γ_{12}. Then

$$\begin{aligned} T1 &= \delta \int_{\Gamma_{12}} (\rho_1 - \rho_2)gyv_x\mathbf{e}_x \cdot \hat{\mathbf{n}} + o(\delta), \\ T2 &= \delta \int_{\Gamma_{12}} 2H\gamma_{12}v_x\mathbf{e}_x \cdot \hat{\mathbf{n}} + \delta \int_{L_{12s}} \gamma_{12}v_x\mathbf{e}_x \cdot \hat{\mathbf{t}} + o(\delta), \end{aligned} \tag{2.23}$$

and

$$T3 = \delta \int_{L_{12s}} (\gamma_{1s} - \gamma_{2s}) v_x + o(\delta), \qquad T4 = \delta \int_{L_{12s}} l_{12s}\kappa v_x + o(\delta). \tag{2.24}$$

In addition, by (2.22) we have

$$T5 = -\delta \int_{\Gamma_{12}} f_e v_x \mathbf{e}_x \cdot \hat{\mathbf{n}} + o(\delta). \tag{2.25}$$

For boundary conditions we shall assume the trial function v_x decays so quickly away from the boundary that all area integrals in (2.23)-(2.25) are negligible as compared with the line integrals. Therefore, by (2.18) we obtain

$$l_{12s}\kappa + \gamma_{1s} - \gamma_{2s} - \gamma_{12}\cos\theta_C = 0 \qquad \text{on } \ L_{12s},$$

which can be identified with the equilibrium equation (2.8) for the junction line.

Based on the variational formulation (2.12), we now describe the gradient method for computing the equilibrium shape Ω with a prescribed volume $vol(\Omega) = \Lambda_0$ satisfying equations (2.4) and (2.8) or (2.9). For an initial guess of the shape Ω_0, we let the domain evolve in the descent direction of the total energy and obtain the shape Ω_t as a function of the fictitious time t. As shown above, if Ω_t is not in equilibrium, then for a small variation

$$\partial\Omega_t \ni \mathbf{x} \to \mathbf{y} = \mathbf{x} + \delta v \hat{\mathbf{n}} \in \partial\Omega_{t+\delta}, \tag{2.26}$$

the change of total energy is given by

$$\hat{\mathcal{E}}_{\text{tot}}[\Omega_{t+\delta}] - \hat{\mathcal{E}}_{\text{tot}}[\Omega_t] = -\delta \int_{\Gamma_{12}} v f_{12}^d - \delta \int_{L_{12s}} v\hat{\mathbf{n}} \cdot \mathbf{e}_x f_{12s}^d + o(\delta), \tag{2.27}$$

where

$$f_{12}^d = -2\gamma_{12}H - (\rho_1 - \rho_2)gy + f_e, \qquad f_{12s}^d = -l_{12s}\kappa - \gamma_{1s} + \gamma_{2s} + \gamma_{12}\cos\theta_C.$$

may be called the *driving force* on the boundary $\partial\Omega_t$ and the junction line L_{12s}, respectively.

If we enforce a kinetic law

$$v = cf_{12}^d \quad \text{on } \Gamma_{12}, \qquad v = cf_{12s}^d \hat{\mathbf{n}} \cdot \mathbf{e}_x \quad \text{on } L_{12s}, \tag{2.28}$$

for some positive constant $c > 0$ and let the boundary evolves according to (2.26), by (2.27) the change of total energy is given by

$$\hat{\mathcal{E}}_{\text{tot}}[\Omega_{t+\delta}] - \hat{\mathcal{E}}_{\text{tot}}[\Omega_t] = -\delta \int_{\Gamma_{12}} c|f_{12}^d|^2 - \delta \int_{L_{12s}} c|f_{12s}^d|^2 |\hat{\mathbf{n}} \cdot \mathbf{e}_x|^2 + o(\delta),$$

and is negative for small enough time step δ; the domain Ω_t is anticipated to converge to an equilibrium shape as t increases.

2.4 Numerical algorithm based on the level-set method

The above variational formulation implies a natural fixed mesh scheme to compute the equilibrium shape of the bubble. Following Osher and Sethian (1988 [35]), we employ the level-set method and use a scalar function $\psi : D \times [0, +\infty) \to I\!R$ to characterize the shape of the bubble Ω_t:

$$\begin{cases} \psi(\mathbf{x}, t) < 0 & \Longleftrightarrow \quad \mathbf{x} \in \Omega_t, \\ \psi(\mathbf{x}, t) = 0 & \Longleftrightarrow \quad \mathbf{x} \in \partial\Omega_t, \\ \psi(\mathbf{x}, t) > 0 & \Longleftrightarrow \quad \mathbf{x} \in D \setminus \bar{\Omega}_t. \end{cases}$$

In account of the axis-symmetry of Ω_t, we denote by (r, y) a point in the xy-plane $\{(x, y, z) : z = 0\}$, where $r = \sqrt{x^2 + z^2}$. Let $\hat{\mathbf{n}} = \nabla\psi/|\nabla\psi|$ be the outward normal on the boundary of the domain $\{(r, y) : \psi(r, y) \leq const.\}$. Upon initiating the level-set function $\psi(r, y, t)$, we need to determine the velocity field $v(r, y, t)$ by the kinetic law (2.28) and let the level-set function accordingly evolve. Since a point $(r(t), y(t))$ on $\partial\Omega_t$ satisfies $\psi(r(t), y(t), t) = 0$, differentiating with respect to t we obtain

$$\frac{\partial}{\partial t}\psi + v(r, y, t)|\nabla\psi| = 0, \tag{2.29}$$

where the velocity field $v(r, y, t)$ is given by (2.28) when restricted to $\partial\Omega_t$.

Below we compute the velocity field contributed by various driving forces. In terms of the level-set function $\psi(r, y, t)$, the mean curvature is given by (cf., Eq. (5.33), page 58, Sethian 1996 [40])

$$2H = \nabla \cdot \hat{\mathbf{n}} = \frac{(\psi_{yy} + \frac{\psi_r}{r})\psi_r^2 + \psi_y^2(\psi_{rr} + \frac{\psi_r}{r}) - 2\psi_r\psi_y\psi_{ry}}{(\psi_r^2 + \psi_y^2)^{3/2}}, \qquad \hat{\mathbf{n}} = \frac{(\frac{x\psi_r}{r}, \psi_y, \frac{z\psi_r}{r})}{(\psi_r^2 + \psi_y^2)^{1/2}}, \tag{2.30}$$

where ψ_r, ψ_y denote the derivatives of ψ with respect to r, y, respectively. By the kinetic law (2.28) it contributes a velocity field

$$v_H(r, y) = -2c\gamma_{12}H(r, y) \qquad \forall\ (r, y) \in D. \tag{2.31}$$

A second velocity field is contributed by the density difference between the two fluids. By (2.20) we have

$$v_g(r, y) = -c(\rho_1 - \rho_2)gy \qquad \forall\ (r, y) \in D. \tag{2.32}$$

Thirdly, to compute the velocity field contributed by the Maxwell stress

$$v_e(r, y) = cf_e \qquad \forall\ (r, y) \in D, \tag{2.33}$$

we need to a priori solve the Maxwell equation (2.3) and obtain the electric field $\mathbf{E}(r, y) = -(\varphi_r, \varphi_y)$. Then the Maxwell stress defined by (2.7) on the interface Γ_{12} is given by

$$f_e = [\![(\hat{\mathbf{n}} \cdot \mathbf{E})(\hat{\mathbf{n}} \cdot \mathbf{D}) - \frac{\epsilon(\mathbf{x})}{2}|\mathbf{E}|^2]\!].$$

Since the interface Γ_{12} is implicit in our scheme, the above formula is replaced by

$$f_e = s\hat{\mathbf{n}} \cdot \nabla f_{\mathrm{MW}}, \qquad f_{\mathrm{MW}} := (\hat{\mathbf{n}} \cdot \mathbf{E})(\hat{\mathbf{n}} \cdot \mathbf{D}) - \frac{\epsilon(\mathbf{x})}{2}|\mathbf{E}|^2$$

and applied to the entire domain D, where s is the grid size for computing the gradient in the numerical scheme (c.f., step 1 in the subsequent description of the algorithm). Finally,

to constrain the volume, the velocity field v_{p_*} contributed by the Lagrangian multiplier p_* shall be such that

$$\int_{\partial\Omega}(v_{p_*}+v_H+v_g+v_e)=0.$$

However, in our scheme it is inconvenient to compute integrals over the boundary $\partial\Omega_t$. We shall simply define

$$v_{p^*}(r,y)=\begin{cases}\delta_1 & \text{if } \Lambda_t<\Lambda_0\\ -\delta_1 & \text{if } \Lambda_t>\Lambda_0\end{cases}\qquad \forall\ (r,y)\in D, \tag{2.34}$$

where Λ_0 be the prescribed volume of the first fluid, Λ_t is the volume of the domain $\Omega_t:=\{(x,y,z):\psi(r,y)\le 0\}$, and $\delta_1>0$ is a small positive number. Note that the above velocity field v_{p_*} will induce small fluctuations of the volume of Ω_t. Depending on the stage of simulations, we can adaptively choose the number δ_1 such that the fluctuation is within, e.g., 0.1% of Λ_0. The overall velocity field is given by

$$v(r,y)=v_H(r,y)+v_g(r,y)+v_e(r,y)+v_{p_*}(r,y)\qquad \forall\ (r,y)\in D. \tag{2.35}$$

Further, by the second of (2.28) the boundary condition (2.8) can be implemented by introducing

$$v(r,y)\Big|_{y=0}=cf_{12s}^d\hat{\mathbf{n}}\cdot\mathbf{e}_x, \tag{2.36}$$

whereas the boundary condition (2.8) is enforced by

$$v(r,y)\Big|_{y=0}=0. \tag{2.37}$$

We remark that a key advantage of fixed-mesh level-set method lies in that the interface $\partial\Omega_t$ is implicit in the scheme. In other words, we simulate the evolution the level-set function ψ instead of the interface itself. Therefore, the velocity field (2.31)-(2.37) are extended to all grid points in the entire computation domain D instead of being restricted to the boundary

$\partial\Omega$. The evolution of the level-set function ψ apparently depends on the extension, but the evolution of the domain Ω_t and the converged equilibrium shape is independent of the particular extension.

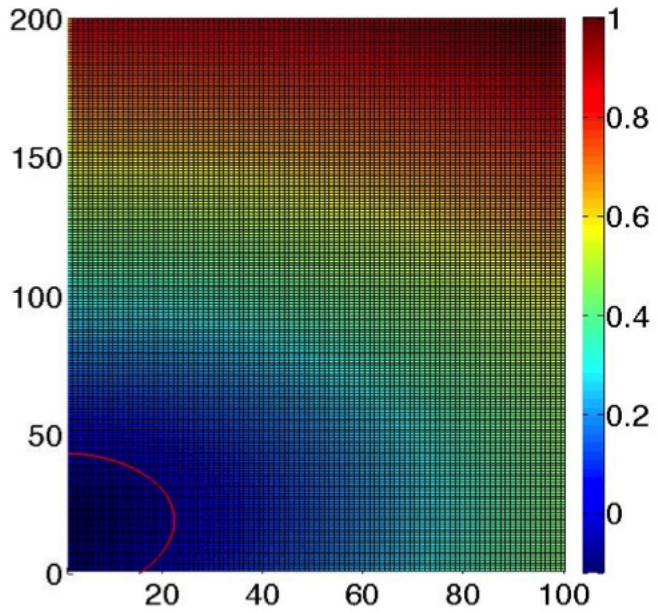

Figure 2.2: The contour plot of the level set function in a typical simulation. The domain D is a rectangle of ratio $1:2$ with meshsize 100×200. The solid red line shows the zero contour representing the interface of the bubble.

With the overall velocity field defined, we summarize our algorithm as follows:

1. Generating a uniform fixed mesh on the spatial domain D of interval size s_r in r-direction and s_y in y-direction. In all subsequent simulations and shown in Fig. 2.2, the domain D is a rectangle of ratio $1:2$ with a regular mesh of size 100×200, and hence $s_r = s_y =: s$.

2. Initializing the level-set function $\psi^0 = \psi(r, y, t = 0)$. In practice, we always start from a very small hemisphere and let it evolve according to the kinetic law (2.35) to eliminate the potential dependence of the final equilibrium shape on the initialization.

3. For $n \geq 0$, let $\psi_{ij}^n = \psi(r_i, y_j, t_n)$, and $r_i = is_r$, $y_j = js_y$, $t_n = nt_1$. Here $t_1 \ll 1$ is the fictitious time step.

(a) Finding the solution φ^n to the Maxwell equation (2.3) based on the finite element method. Computing the overall velocity field v_{ij}^n defined by (2.35)-(2.37). Here we do not remesh to track the interface; the material properties of each element are either of the first fluid or the second as determined by the level-set function.

(b) Computing the new level-set function $\psi_{ij}^{n+1} = \psi(r_i, y_j, t_{n+1})$ by the Hamilton-Jacobi equation (2.29). In particular we will use an explicit first-order upwind scheme described in Sethian (1996, page 55, [40]):

$$\frac{\psi_{ij}^{n+1} - \psi_{ij}^n}{t_1} + \max(v_{ij}, 0) g_{ij}^+ + \min(v_{ij}, 0) g_{ij}^- = 0,$$

where

$$\begin{aligned}
g_{ij}^+ &= [\max(D_{ij}^{-r}, 0)^2 + \min(D_{ij}^{+r}, 0)^2 + \max(D_{ij}^{-y}, 0)^2 + \min(D_{ij}^{+y}, 0)^2]^{1/2}, \\
g_{ij}^- &= [\max(D_{ij}^{+r}, 0)^2 + \min(D_{ij}^{-r}, 0)^2 + \max(D_{ij}^{+y}, 0)^2 + \min(D_{ij}^{-y}, 0)^2]^{1/2}, \\
D_{ij}^{+r} &= \frac{\psi_{ij}^n(r_{i+1}, y_j) - \psi_{ij}^n(r_i, y_j)}{r_{i+1} - r_i}, \quad D_{ij}^{-r} = \frac{\psi_{ij}^n(r_i, y_j) - \psi_{ij}^n(r_{i-1}, y_j)}{r_i - r_{i-1}}, \\
D_{ij}^{+y} &= \frac{\psi_{ij}^n(r_i, y_{j+1}) - \psi_{ij}^n(r_i, y_j)}{y_{j+1} - y_j}, \quad D_{ij}^{-y} = \frac{\psi_{ij}^n(r_i, y_j) - \psi_{ij}^n(r_i, y_{j-1})}{y_j - y_{j-1}}.
\end{aligned}$$

4. For stability we reinitialize the level-set function such that it is the signed distance function:

$$\psi^{n+1}(r, y) = \{\mathrm{sgn}(\psi^{n+1}) \mathrm{dist}((r, y), \partial\Omega_{t_{n+1}}) : (r, y) \in D\}.$$

This is an important step in practice since the level-set function may become too steep, resulting in bad approximations to the unit normal $\hat{\mathbf{n}}$ and the mean curvature H.

5. Iterating the above step 2 - step 4 until the total energy converges.

A few remarks are in order here regarding the present numerical scheme based on the variational formulation. First, for the initialization described above our simulations always yield the same final shapes for a prescribed final volume and electric field, though we cannot rigorously prove the uniqueness of the final solution. Second, the Young-Laplace

equation (2.4) coupled with the nonlocal Maxwell stress could be solved by a self-consistent scheme. Roughly speaking, one could describe the interface $\partial\Omega$ by Lagrangian coordinates and iterate the boundary $\partial\Omega$ until the Young-Laplace equation (2.4) is satisfied. This self-consistent scheme is, to the best of our knowledge, not as efficient as compared with present gradient method since (i) every iteration requires remeshing of the entire domain for solutions of the Maxwell equation (2.3), (ii) the gradient or the "optimal" direction of iteration is not known, and (iii) there is no physics-based criterion for convergence and for topological changes of the domain in some more general problems, e.g., splitting or merging of the bubble. Last, though not addressed in the present work, the variational formulation can yield stability criterion for the equilibrium shape by computing the second variations of the total free energy [14] and the numerical scheme can capture the onset of departure of the bubble from the substrate.

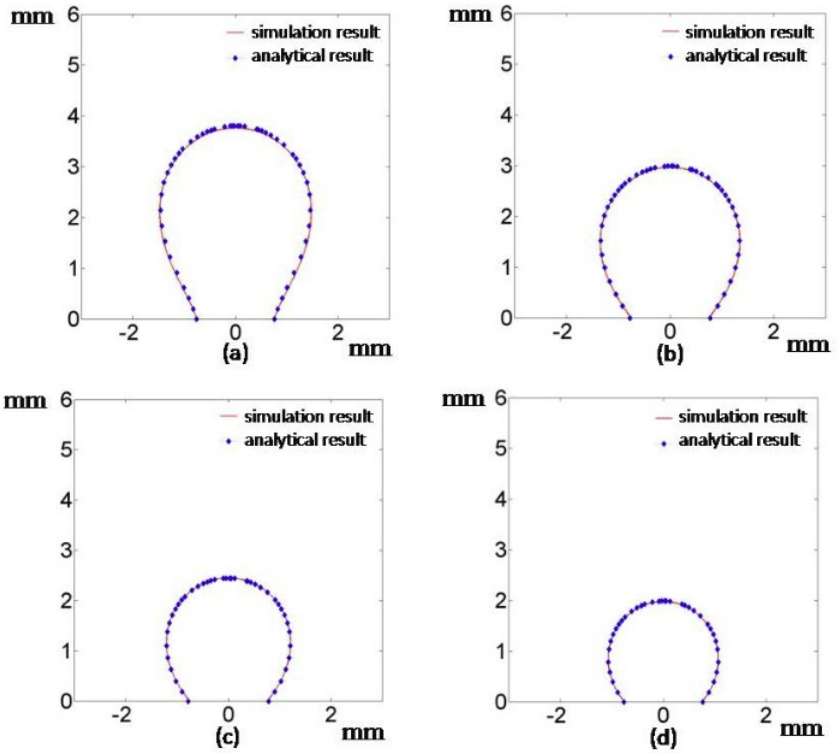

Figure 2.3: Comparison of analytical and simulated equilibrium shapes of the bubble at the absence of electric field: the solid line represents the equilibrium shapes implied by (2.38); the dotted line represents the simulated equilibrium shapes. The volume of the bubble is 17.1mm^3, 11.8mm^3, 8.1mm^3 and 5.3mm^3 in (a), (b), (c) and (d), respectively.

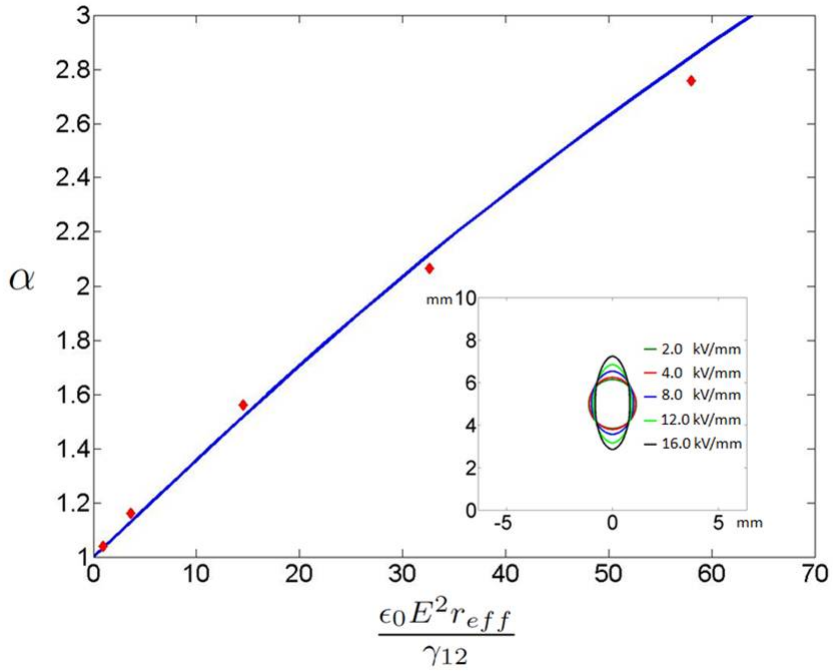

Figure 2.4: Aspect ratio α as a function of dimensionless electric field strength $\epsilon_0(E_y^e)^2 r_{\text{eff}}/\gamma_{12}$. The solid line represents the analytical solutions implied by (2.40); the diamond points represent the simulated results. The inset picture is the corresponding simulated equilibrium shape of the bubble under different electric field 2.0 kV/mm, 4.0 kV/mm. 8.0 kV/mm, 12.0 kV/mm and 16.0 kV/mm, respectively.

2.5 Numerical examples and validation

2.5.1 Comparison with analytical results

We verify our scheme by comparing with analytical results of Cheng and Chaddock (1986) [8] in two scenarios. First, at the absence of electric fields, Cheng and Chaddock (1986) [8] have shown that the equilibrium shape $y = y(r)$ satisfies the following dimensionless nonlinear ordinary differential equation:

$$-\frac{\frac{d^2y}{dr^2}}{\{1+(\frac{dy}{dr})^2\}^{3/2}} + \frac{\frac{dy}{dr}}{r\{1+(\frac{dy}{dr})^2\}^{1/2}} = 2 - B_o y, \tag{2.38}$$

where $1/R_0$ is the curvature at the apex of the bubble, r and y are the nondimensional coordinate with respect to R_0, $_\Delta\rho = \rho_1 - \rho_2$ is the density difference of two phases, γ_{12} is the surface tension and $B_o = \frac{\Delta \rho g R^2}{\gamma_{12}}$ is Bound number .

We choose material properties as

$$\rho_1 = 1.165\,\mathrm{kg/m^3}, \qquad \rho_2 = 849\,\mathrm{kg/m^3}, \qquad \gamma_{12} = 0.044\,\mathrm{N/m}, \tag{2.39}$$

and use the boundary condition (2.9) with $r_0 = 0.75$mm. These particular material properties and boundary conditions are chosen to be consistent with the experiments described in the next section. To compare our computational results with the analytical solutions in the absence of electric field, we first solve (2.38) for appropriate y_0, R_0 such that the contact area of the bubble with the substrate has a radius $r_0 = 0.75$mm. We then compute the volume Λ_0 of the bubble and use the numerical algorithm described in the last section to find the simulated equilibrium shapes. Figure 2.3 (a), (b), (c), and (d) show the analytical solutions and simulation results for $\Lambda_0 = 17.1\mathrm{mm}^3$, $11.8\mathrm{mm}^3$, $8.1\mathrm{mm}^3$ and $5.1\mathrm{mm}^3$, respectively. The solid line represents the equilibrium shapes implied by (2.38); the dotted line represents the simulated equilibrium shapes. From Fig. 2.3, we see that the simulated and analytical equilibrium shapes are in excellent agreement which verifies our numerical approach at the absence of electric field.

Second, in the presence of electric field and neglecting gravity, by assuming the shape would remain as prolate spheroids Cheng and Chaddock (1986) [8] have shown that the aspect ratio $\alpha :=$ long-axislength/short-axislength of the spheroid in a uniform external electric field $\bar{\mathbf{E}} = E_y^e \mathbf{e}_y$ are determined by

$$\frac{\partial}{\partial \alpha}(\alpha^{-2/3} + \alpha^{1/3}\frac{\sin^{-1} e}{e}) - \frac{\epsilon_0 (E_y^e)^2 r_{\mathrm{eff}}}{3\gamma_{12}}\frac{\partial H}{\partial \alpha} = 0, \tag{2.40}$$

where r_{eff} is the initial radius of the spherical bubble at the absence of electric field, $\epsilon_0 = 8.85 \times 10^{-12}\mathrm{F/m}$ is the vacuum permittivity, ϵ_1 and ϵ_2 are the electric permittivity of two phases, $e(\alpha) = (1 - 1/\alpha^2)^{1/2}$ is the eccentricity of the spheroid, $n = \frac{1-e^2}{2e^3}(\ln\frac{1+e}{1-e} - 2e)$, and

$$H(\alpha) = \frac{(\epsilon_2 - \epsilon_1)\epsilon_1}{(1 - n(\alpha))\epsilon_1 + n(\alpha)\epsilon_2}.$$

Figure 2.4 shows the dependence of the aspect ratio α on the external electric field: the solid line is obtained by (2.40); the diamond points are our simulation results. Also, the

inset shows the simulated equilibrium shapes of the bubble in different external fields, which shows that the equilibrium shapes indeed look much like spheroids and verifies the assumption of Cheng and Chaddock (1986). Also, the aspect ratios' dependence on the external electric field from simulations agrees well with the prediction of (2.40).

In summary, from Fig. 2.3 and Fig. 2.4 we see that the simulated and analytical equilibrium shapes are in excellent agreement which verifies our numerical approach, both at the absence of electric fields and in the presence of electric fields. In the next section, we will compare our simulations with experimental results in the presence of an external electric field and gravity.

2.5.2 Comparison with experiments

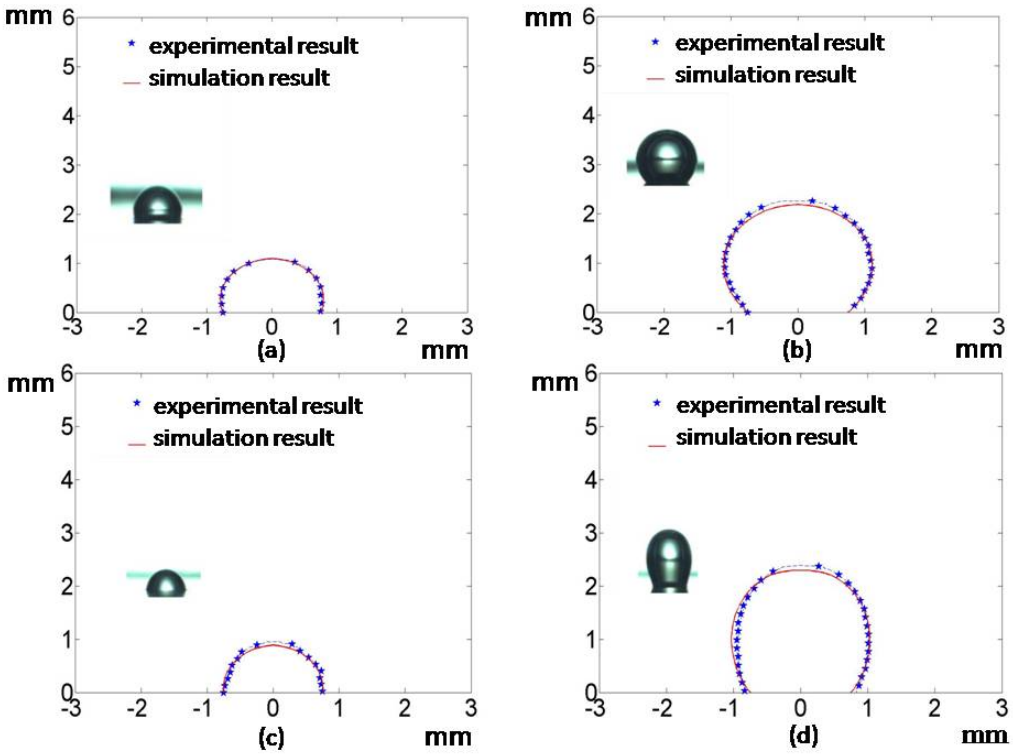

Figure 2.5: Comparison simulation result with experiment. The solid line represents the shape of the simulation result and the dotted line represents the shape of the experiment result. The volume is 1.56mm^3, 6.20mm^3, 1.10mm^3 and 6.10mm^3 from (a) to (d). Electric field 2 kV/mm is applied on (a) and (b) and Electric field 3 kV/mm is applied on (c) and (d). The inset pictures in (a), (b), (c) & (d) are reproduced from Chen *et al.* (2007 [6]) with Elsevier permission.

In the presence of electric field, analytical solutions to the equilibrium shapes are not available. We shall validate our numerical approach by the experimental results obtained by Chen *et al* (2007 [6]). In the experiments, a single nitrogen bubble is injected into transformer oil through an orifice of radius 0.75mm. A voltage is applied between the top and bottom electrodes. The densities of two phases and surface tension are given by (2.39). In addition, the electric permittivity of two phases are given by

$$\epsilon_1 = \epsilon_0, \qquad \epsilon_2 = 2.1\epsilon_0,$$

More details about the experimental setup can be found in Chen *et al* (2007 [6]).

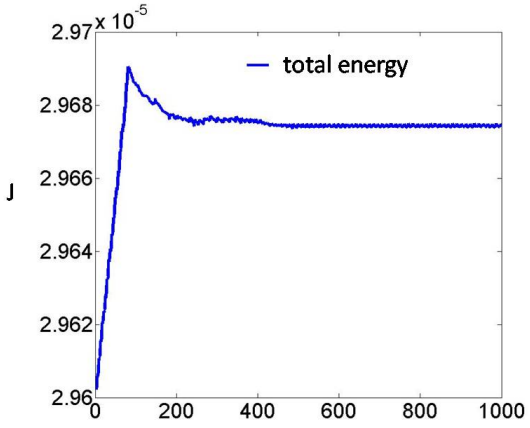

Figure 2.6: Convergence of the total energy.

The volume of the nitrogen bubble in the transformer oil increases as nitrogen is being injected. A high speed camera records the bubble formation and evolution in a DC electric field. From the recorded images of the bubble (cf., the inset photos in Fig. 2.5), we can find the contour of the bubble and the volume Λ_0 of the bubble by MATLAB. We then compute the equilibrium shape of the bubble for the prescribed electric voltage and volume Λ_0 by the algorithm described in § 2.4. Figure 2.5 shows the experimental results and simulated equilibrium shapes in an external electric field of 2 kV/mm (Fig. 2.5 (a) & (b)) and 3kV/mm (Fig. 2.5 (c) & (d)). The volumes of the bubbles are fixed by the experimental images and given by 1.56mm^3 (a), 6.20mm^3 (b), 1.80mm^3 (c), and 6.10mm^3 (d). The solid

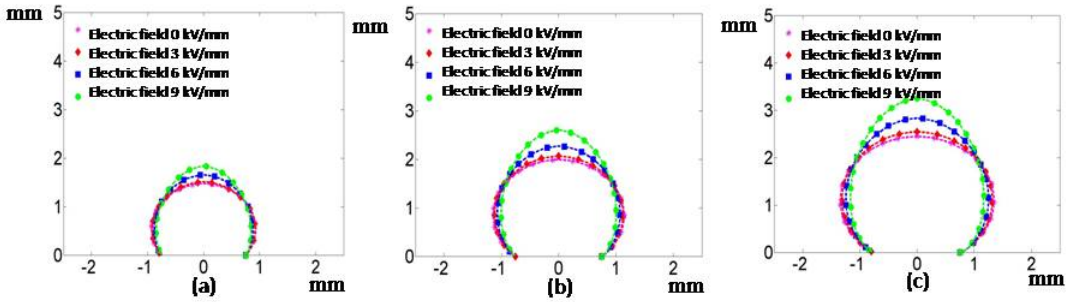

Figure 2.7: Simulated equilibrium shapes at the absence of gravity. The fixed volume is 3.0mm^3, 6.0mm^3 and 10.0mm^3 in (a), (b) and (c). Electric field from 0 kV/mm to 9 kV/mm is applied on each case.

line represents the shape of the simulation results and the dotted line represents the shape of the experimental results. From Fig. 2.5 (a), (b), (c), and (d), we see that the simulation results agree well with the experiment which validates our numerical approach.

During the simulations, we also monitor the convergence of the total energy as shown in Fig. 2.6 for Fig. 2.5 (b). For all simulations, the initial shape of the bubble is chosen as a hemisphere of radius $r_0 = 0.75\text{mm}$. For a final volume $\Lambda_0 > \frac{2\pi}{3} r_0^3$, by (2.34) the volume and total energy of the bubble increases at the beginning until reach Λ_0. Then by (2.34) the volume of the bubble fluctuate negligibly around Λ_0 while the shape of the bubble is driven to minimize the total free energy as shown in Fig. 2.6. For a typical case, the total energy converges after a few hundreds of iterations. We remark that the convergence of the total energy is also observed for all cases in Fig. 2.3, 2.5 and 2.7.

The numerical scheme developed here can be conveniently used for simulating equilibrium shapes of bubbles of different materials and at different environments. As an example, we consider the injection of nitrogen bubble into transformer oil at zero gravity. This can be achieved by simply setting $g = 0$ in our simulation. Figure 2.7 (a), (b) and (c) show the simulated equilibrium shapes for a fixed contact radius of $r_0 = 0.75\text{mm}$ and different volumes at 3.0mm^3, 6.0mm^3 and 10.0mm^3. The electric fields vary from 0.0kV/mm,

3.0kV/mm, 6.0kV/mm to 9.0kV/mm. From Fig. 2.7 we observe that the equilibrium shape is elongated as the intensity of electric field increases. Based on these simulation results, we can find the relationship between bubble volume, surface area and the applied electric field. Among many other applications, these results can be further used to develop model of EHD enhancement of boiling at zero gravity and predict rate of heat transfer.

2.6 Summary and discussion

We have developed a variational formulation for the equilibrium shape of heterogeneous bubbles in an electric field and shown that it is equivalent to the classic field equation approach based on the Young-Laplace equation and the concept of Maxwell stress. Based on this energy formulation, we implement a fixed mesh level-set gradient method for simulating the equilibrium shapes of the bubble in an electric field. The numerical scheme is validated by comparing with analytical solutions and experimental results in some different scenarios. We anticipate that the variational formulation and numerical scheme will find broad applications in areas of EWOD, EHD and electro-deformation of soft materials among others.

2.7 Appendix: derivation of Maxwell stress

We now proceed to details of deriving (2.22). First, we extend the deformation $\mathbf{y}(\mathbf{x})$ such that the deformation $\mathbf{y}(\mathbf{x}) = \mathbf{x} + \delta\mathbf{y}_1(\mathbf{x})$ is continuously differential on the entire domain D, equal to $\mathbf{x}$ slightly away from $\partial\Omega$ (i.e., $|\mathbf{y}_1|$ decays quickly to zero away from $\partial\Omega$). Moreover, we notice that the new potential φ_δ is defined by the Maxwell equation (2.3) with Ω replaced by Ω_δ. Let

$$\begin{aligned} &\mathbf{F}_\delta = \nabla\mathbf{y} = \mathbf{F} + \delta\mathbf{F}_1 + o(\delta), \quad \mathbf{F} = \nabla\mathbf{x} = \mathbf{I}, \quad \mathbf{F}_1 = \nabla\mathbf{y}_1, \\ &J_\delta = J[1 + \delta\mathrm{Tr}(\mathbf{F}_1))] + o(\delta), \quad \mathbf{C}_\delta = \mathbf{F}_\delta^T\mathbf{F}_\delta = \mathbf{I} + \delta\mathbf{F}_1^T + \delta\mathbf{F}_1 + o(\delta). \end{aligned} \tag{2.41}$$

Upon a change variables $\mathbf{y} \to \mathbf{x}$, we find the new electrostatic potential φ_δ is also determined by

$$\begin{cases} \operatorname{div}(-\epsilon(\mathbf{x}) J_\delta \mathbf{C}_\delta \nabla \varphi_\delta) = 0 \qquad \text{in } D, \\ \varphi_\delta = V_1 \qquad \text{on } \Gamma_{D1}, \qquad \varphi_\delta = V_2 \qquad \text{on } \Gamma_{D2}, \\ \hat{\mathbf{n}} \cdot \nabla \varphi_\delta = 0 \qquad \text{on } \partial D \setminus (\Gamma_{D1} \cup \Gamma_{D2}). \end{cases} \tag{2.42}$$

In addition, the electric energy (2.16) can be written as

$$\mathcal{E}_*^{\text{elect}}[\Omega_\delta] = -\frac{1}{2} \int_D \epsilon(\mathbf{x}) J_\delta |\mathbf{F}_\delta^{-T} \nabla \varphi_\delta|^2. \tag{2.43}$$

To calculate the first variation of the electric energy $\mathcal{E}_*^{\text{elect}}[\Omega_\delta]$, we assume the new electric potential can be written as

$$\varphi_\delta = \varphi + \delta \varphi_1 + o(\delta). \tag{2.44}$$

Comparing (2.42) with (2.3), we find that the potential φ_1 shall satisfy

$$\begin{cases} \operatorname{div}[-\epsilon(\mathbf{x}) \nabla \varphi_1 - \epsilon(\mathbf{x}) \operatorname{Tr}(\mathbf{F}_1) \nabla \varphi + \epsilon(\mathbf{x})(\mathbf{F}_1 + \mathbf{F}_1^T) \nabla \varphi] = 0 \qquad \text{in } D, \\ \varphi_1 = 0 \qquad \text{on } \Gamma_{D1}, \qquad \varphi_1 = 0 \qquad \text{on } \Gamma_{D2}, \\ \hat{\mathbf{n}} \cdot \nabla \varphi_1 = 0 \qquad \text{on } \partial D \setminus (\Gamma_{D1} \cup \Gamma_{D2}). \end{cases} \tag{2.45}$$

Further, by (2.43) and (2.41) we find

$$\mathcal{E}_*^{\text{elect}}[\Omega_\delta] = \mathcal{E}_*^{\text{elect}}[\Omega] + \delta \text{Var1} + o(\delta), \tag{2.46}$$

where

$$\text{Var1} = -\frac{1}{2} \int_D \epsilon(\mathbf{x}) [\operatorname{Tr}(\mathbf{F}_1) |\nabla \varphi|^2 - \nabla \varphi \cdot (\mathbf{F}_1 + \mathbf{F}_1^T) \nabla \varphi + 2 \nabla \varphi \cdot \nabla \varphi_1]. \tag{2.47}$$

By (2.45) and the divergence theorem we obtain

$$\int_D \epsilon(\mathbf{x})\nabla\varphi\cdot\nabla\varphi_1 = \int_D [\mathrm{div}(\varphi_1\epsilon(\mathbf{x})\nabla\varphi) - \varphi_1\mathrm{div}(\epsilon(\mathbf{x})\nabla\varphi)] = 0.$$

Therefore, (2.47) can be rewritten as

$$\mathrm{Var1} = \int_D \mathbf{F}_1\cdot\mathbf{T}_{\mathrm{MW}}, \qquad \mathbf{T}_{\mathrm{MW}} = \nabla\varphi\otimes(\epsilon(\mathbf{x})\nabla\varphi) - \frac{\epsilon(\mathbf{x})}{2}|\nabla\varphi|^2\mathbf{I}, \tag{2.48}$$

where $\mathbf{T}_{\mathrm{MW}}$ is precisely the "Maxwell stress" for a linear medium. From the Maxwell equation (2.3), it is clear that

$$\mathrm{div}\mathbf{T}_{\mathrm{MW}} = 0 \qquad \text{in } D\setminus\partial\Omega,$$

which means the Maxwell stress has body force contribution at an interior point in the two fluids. However, for the interface Γ_{12}, by the divergence theorem we have

$$\mathrm{Var1} = -\int_{\partial\Omega}\mathbf{y}_1\cdot[\![\mathbf{T}_{\mathrm{MW}}]\!]\hat{\mathbf{n}} = -\int_{\partial\Omega} v\hat{\mathbf{n}}\cdot[\![\mathbf{T}_{\mathrm{MW}}]\!]\hat{\mathbf{n}} = -\int_{\partial\Omega} v f_e, \tag{2.49}$$

which complete the proof of (2.7).

Chapter 3

Continuum theory for thermoelectric materials

3.1 Introduction

In recent years, there has been renewed interest in engineering thermoelectric (TE) materials for energy and refrigeration applications [51, 52, 53, 54, 55, 56]. The energy conversion efficiency of a TE material is characterized by the dimensionless figure of merit ZT. For a thermoelectric device separating two heat reservoirs for power generation, the electrical power output can be written as

$$\dot{W}_{\text{elect}} = \eta\eta_{\text{carnot}}\dot{Q}, \tag{3.1}$$

where $\eta_{\text{carnot}} = \frac{T_h - T_c}{T_h}$ is the ideal Carnot efficiency, T_h (T_c) is the temperature of the hot (cold) reservoir, $\dot{Q}$ is the rate of heat transfer, and $\eta = (\sqrt{ZT+1}-1)/(\sqrt{ZT+1}+1)$ is the relative efficiency. The figure of merit ZT of typical "good" TE semiconductors, e.g., Bi_2Te_3, is about $1-2$, corresponding to a relative efficiency $\eta = 10\% - 20\%$. Also, the thermal conductivity of Bi_2Te_3 is about three orders of magnitude smaller than that of typical metals, e.g., copper, meaning that the rate of heat transfer across TE semiconductors is significantly less than conventional heat exchanger with copper separating two heat reservoirs. In other words, for a target electrical power output $\dot{W}_{\text{elect}}$, the TE generator costs significant amount of TE materials that are much more expensive than copper. The low conversion efficiency and high cost of TE materials have limited their large-scale applications in power generation and refrigeration.

From (3.1), an important approach to improving electrical power output is to improve the figure of merit ZT, i.e., the relative efficiency η. There have been a great deal of efforts in enhancing ZT through *ab initio* material designs and nanostructured composites

[57, 58, 59, 60, 61, 62, 62, 63] in the past decade. However, improving ZT has proven to be extremely difficult; the latest progress [62, 64] has a ZT at around 2.4 ($\eta = 30\%$). Also, from a continuum viewpoint Bergman and Levy have shown that the figure of merit of a two-phase composite cannot exceed the highest ZT of their constituent phases [65].

On the other hand, if the goal is to improve the electrical power output $\dot{W}_{\text{elect}}$, by (3.1) an alternative route is to improve the rate of heat transfer $\dot{Q}$ between two heat reservoirs. This corresponds to improve the power factor P of the TE material. From a cost viewpoint, improving figure of merit ZT lowers the cost of heat resources, i.e., the cost of maintaining the temperature difference between two heat reservoirs; improving power factor lowers the amount of TE materials needed for a target power output (cf., (3.31)). Though the conversion efficiency may be suboptimal for a high power factor TE material, the overall cost of power generation can be significantly lowered if the heat resources themselves are of low cost or even costless, e.g., the waste heat from a conventional nuclear/chemical fuel power plant [66], geothermal resources, oceanic thermocline [67] among others. Therefore, improving the power factor of TE materials can be as important, if not more, as improving the the figure of merit for economically competitive applications.

Unlike the figure of merit ZT, it has been predicted that the power factor P can be significantly enhanced by engineering nanostructures or even macroscopic composites [68, 69, 70, 71, 82]. Also, experimentally it has been shown that heterogeneous TE composites can have a power factor larger than the power factor of constituent TE materials [73, 74, 75, 76, 77, 78].

In this chapter, we first review the continuum theory of thermoelectric bodies developed by Liu [71]. Under the conditions of small variations of electrochemical potential, temperature and their gradients, the governing equations of thermoelectric bodies can be reduced from a nonlinear system to a linear elliptic system. Therefore the local fields in thermoelectric bodies can be determined by the specified boundary conditions.

Furthermore, from a macroscopic viewpoint, effective properties of thermoelectric composites can be predicted, espeically by an explicit formula of effective properties for an simple laminate structure. In particular, we show that the power factor of a good TE semiconductor, e.g., Bi_2Te_3, and a good conductor, e.g., copper, can be improved by two orders

of magnitude at an optimal microstructure [71]. Later, we present a numerical verification of this prediction by computing local fields in the TE structure. The numerical model can be used to address TE structures of general geometries in real-world working conditions. We study the effect of electrical contacts between the TE structure and external circuit, and show that the power output of the TE structure, though lowered by a small electrical contact area, is still significantly larger than that of the TE semiconductor of the same size and boundary conditions.

3.2 A continuum theory of thermoelectric bodies

Consider a homogeneous thermoelectric body $\Omega \subset I\!R^3$, we postulate the thermodynamic state of the system is described by electrochemical potential μ and absolute temperature T. And we have the identities

$$\mathbf{q} = T\mathbf{j}_s, \qquad r = T\eta, \tag{3.2}$$

where $\mathbf{q}$ is heat flux, $\mathbf{j}_s$ is entropy flux, r is external heat supply inside the body and η is the entropy supply. Suppose there is no external heat supply, i.e., $r = 0$; the only way to exchange heat is through the boundary of Ω by conduction. And for a time-independent boundary condition, the thermodynamic system will eventually evolve into a steady state. Through the experimental observations, i.e., *Ohm's Law*, *Fourier's Law*, Seebeck effects and Peltier effect, we could have the following phenomenological relation between fluxes and driving-forces, i.e., gradients of electrochemical potential $\mathbf{e} = -(\nabla\mu)^T$ and gradients of temperature $\mathbf{g} = -(\nabla T)^T$:

$$\mathbf{j}_1 = \mathbf{L}_1\mathbf{f}_1, \qquad \mathbf{j}_1 := \begin{bmatrix} \mathbf{j}_e \\ \mathbf{j}_s \end{bmatrix}, \qquad \mathbf{f}_1 := \frac{1}{T}\begin{bmatrix} \mathbf{e} \\ \mathbf{g} \end{bmatrix}, \qquad \mathbf{L}_1 := \begin{bmatrix} T\sigma & T\sigma\mathbf{s} \\ \beta\sigma & \kappa + \beta\sigma\mathbf{s} \end{bmatrix}, \tag{3.3}$$

where σ is electric conductivity tensor, β is Peltier coefficient matrix, κ is thermal conductivity tensor, $\mathbf{s}$ is Seebeck coefficient matrix and $\mathbf{j}_e$ is electric flux. Remark that the coefficient matrix $\mathbf{L}_1$ shall depend on temperature T but be independent of electrochemical potential μ. Further, by Thomson or Kelvin relations, $\mathbf{L}_1$ is symmetic, i.e., $\mathbf{L}_1 = \mathbf{L}_1^T$.

Denote by u the internal energy density, it can be written as

$$u = u_0 + C_v T + \rho\mu, \tag{3.4}$$

where C_v is the volumetric specific heat and u_0 a constant which is independent of T, μ.

Then denote by ρ the free charge density, the conservation of electric charges implies

$$\nabla \cdot \mathbf{j}_e = -\partial_t \rho \qquad \text{on } \Omega \tag{3.5}$$

And the conservation of internal energy u is

$$\nabla \cdot \mathbf{j}_u = \mathbf{j}_s \cdot \nabla T + T\nabla \cdot \mathbf{j}_s + \mathbf{j}_s \cdot \nabla\mu + \mu\nabla \cdot \mathbf{j}_e = -\partial_t u \qquad \text{on } \Omega. \tag{3.6}$$

To derive a constitutive model for thermoelectric materials, we need first determine the fluxes and driving-forces. From a simple dimension analysis in [71], there is no unique choice for these two terms and the inner products of pairs of driving-forces and fluxes remain invariant for the tranformation

$$(\mathbf{j}_1, \mathbf{f}_1) \to (\mathbf{j}_2, \mathbf{f}_2) = (\Lambda\mathbf{j}_1, \Lambda\mathbf{f}_1). \tag{3.7}$$

Denote by γ the rate of entropy production per unit volume, it cannot depend on the choice of fluxes and driving-forces according to the fundamental thermodynamics for irreversible process and by definition, it has the following relation with the conjugate pair of fluxes and driving-force $(\mathbf{j}, \mathbf{f})$

$$\gamma = \mathbf{j} \cdot \mathbf{f}. \tag{3.8}$$

From [29], we have

$$\gamma = \partial_t \sigma + \nabla \cdot \mathbf{j}_s, \tag{3.9}$$

where σ is the entropy density. By the first law of thermodynamics we have

$$\partial_t u(\mathbf{x}, t) = T\partial_t \sigma(\mathbf{x}, t) + \mu\partial_t \rho(\mathbf{x}, t). \tag{3.10}$$

By conservation of electric charges (3.5) and conservation of energy (3.6), we have

$$T\nabla \cdot \mathbf{j}_s = -\partial_t u - \mathbf{j}_s \cdot \nabla T - \mathbf{j}_e \cdot \nabla \mu + \mu\partial_t \rho. \tag{3.11}$$

Therefore by the above equations (3.9), (3.10) and (3.11) we obtain

$$\gamma = (-\mathbf{j}_e \cdot \nabla \mu - \mathbf{j}_s \cdot \nabla T)/T. \tag{3.12}$$

The above equation illustrates that $(\mathbf{j}_e, \mathbf{j}_s)$ and $(-\nabla\mu/T, -\nabla T/T)$ are a conjugate pair of fluxes and driving-forces. For steady state, electric flux and energy flux $(\mathbf{j}_e, \mathbf{j}_u)$ are better choices to describe the thermoelectric body since they are divergence free by the conservation laws. Notice that we identify energy flux $\mathbf{j}_u$ as

$$\mathbf{j}_u = T\mathbf{j}_s + \mu\mathbf{j}_e, \tag{3.13}$$

The conjugate driving-force and the coefficient matrix between the fluxes $\mathbf{j}$ and driving-forces $\mathbf{f}$ can be written as

$$\mathbf{f} := \begin{bmatrix} [\nabla(-\mu/T)]^T \\ [\nabla(1/T)]^T \end{bmatrix}, \tag{3.14}$$

$$\mathbf{L}(\mu, T) := \begin{bmatrix} T\sigma & \mu T\sigma + T^2\sigma\mathbf{s} \\ \mu T\sigma + T^2\sigma\mathbf{s} & \mu^2 T\sigma + \mu T^2(\mathbf{s}^T\sigma + \sigma\mathbf{s}) + T^2(\kappa + T^2\mathbf{s}^T\sigma\mathbf{s}) \end{bmatrix} \tag{3.15}$$

Thus by the conservation laws, we have

$$\nabla \cdot [\mathbf{L}(\mu, T)\mathbf{f}] = \begin{bmatrix} -\partial_t \rho \\ -\partial_t u \end{bmatrix}. \tag{3.16}$$

Especially for steady state, we have

$$\nabla \cdot [\mathbf{L}(\mu, T)\mathbf{f}] = 0. \tag{3.17}$$

Just to be clear, if we choose $\mathbf{u} = (u_1, u_2) = (-\mu/T, 1/T)$ as the state variables, we identitify that

$$\mathbf{F} = \begin{bmatrix} \nabla u_1 \\ \nabla u_2 \end{bmatrix}, \qquad \mathbf{J} = \begin{bmatrix} \mathbf{j}_e^T \\ \mathbf{j}_u^T \end{bmatrix}, \qquad \mathbf{J} = \mathbf{C}(\mathbf{u})\mathbf{F}, \tag{3.18}$$

where the associated fourth-order tensor $\mathbf{C}(\mathbf{u}) \subset I\!R^{2\times n\times 2\times n}$ is given by

$$(\mathbf{C})_{1i1j} = T(\sigma_{ij}), \qquad (\mathbf{C})_{1i2j} = (\mathbf{C})_{2j1i} = \mu T(\sigma)_{ij} + T^2(\sigma\mathbf{s})_{ij}, \tag{3.19}$$

$$(\mathbf{C})_{2i2j} = [\mu^2 T\sigma + \mu T^2(\mathbf{s}^T\sigma + \sigma\mathbf{s}) + T^2(\kappa + T\mathbf{s}^T\sigma\mathbf{s})]. \tag{3.20}$$

And the conservation law (3.16) can be rewritten as

$$\nabla \cdot [\mathbf{C}(\mathbf{u})\nabla\mathbf{u}] = 0 \qquad \text{on } \Omega. \tag{3.21}$$

For a heterogeneous thermoelectric body Ω, its material properties in general depends on position $\mathbf{x}$. Applying a time independent boundary conditions to the body, the system will eventually envolve into a steady state. We suppose that the driving-forces to the carriers and the variations of (μ,T) are small in the body. Therefore, we assume that the fourth-order thermoelectric tensor $\mathbf{C}(\mathbf{u}(\mathbf{x}), \mathbf{x})$ is given as

$$\mathbf{C}(\mathbf{u}(\mathbf{x}), \mathbf{x}) = \mathbf{C}(\mathbf{u}_0, \mathbf{x}) \qquad \text{in } \Omega, \tag{3.22}$$

where $\mathbf{u}_0 = (-\mu_0/T_0, 1/T_0)$ and (μ_0, T_0) are electrochemical potential and temperature of the body in the equilibrium state. Remark that (μ_0, T_0) are uniform and in practice we can choose T_0 as the average temperature of the body and $\mu_0 = 0$ since the electrochemical potential μ has no physical consequence. A more detailed discussion can be found in [71].

We then infer that in steady state, the boundary value problem shall satisfy

$$\begin{cases} \nabla \cdot [\mathbf{C}_0(\mathbf{x})\nabla \mathbf{u}] = 0 & \text{on } \Omega, \\ \text{time independent boundary conditions} & \text{on } \partial\Omega, \end{cases} \tag{3.23}$$

where

$$[\mathbf{C}_0(\mathbf{x})]_{1i1j} = T_0[\sigma(\mathbf{x})]_{ij}, \qquad [\mathbf{C}_0(\mathbf{x})]_{1i2j} = [\mathbf{C}_0(\mathbf{x})]_{2i1j} = T_0^2[\sigma(\mathbf{x})\mathbf{s}(\mathbf{x})]_{ij},$$
$$[\mathbf{C}_0(\mathbf{x})]_{2i2j} = T_0^2[\kappa(\mathbf{x}) + T_0\mathbf{s}^{\mathbf{T}}\sigma(\mathbf{x})\mathbf{s}(\mathbf{x})]_{ij}. \tag{3.24}$$

3.3 A Sandwich Structure Model

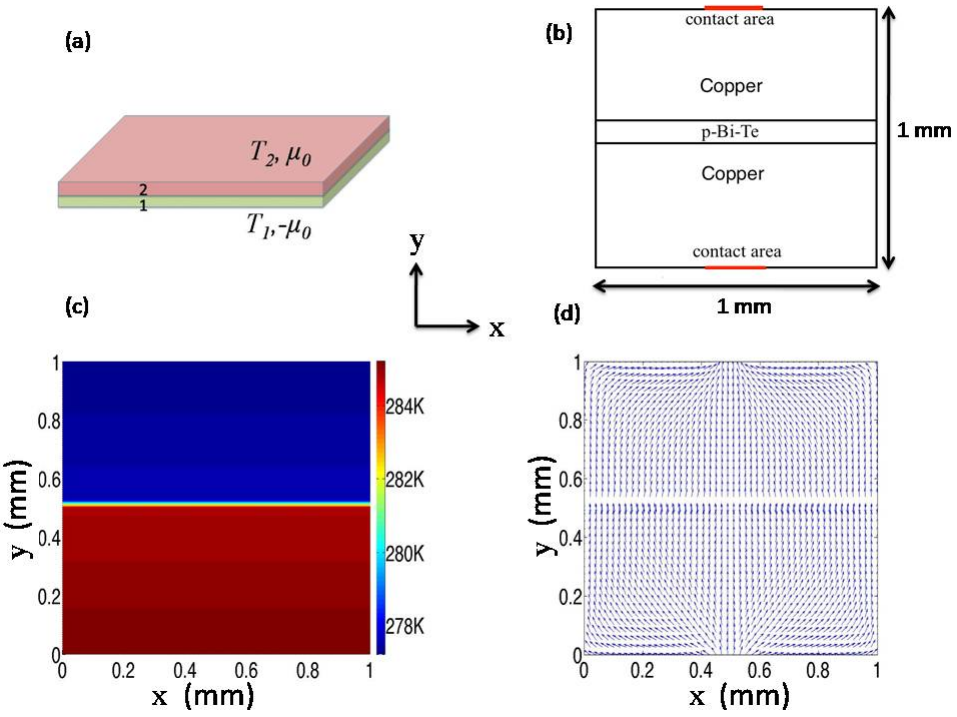

Figure 3.1: (a) A simple laminate of two TE materials. (b) The cross section of the cylinder of the sandwich of Cu/p-Bi-Te/Cu. (c) & (d) Temperature distribution and electric current in the cross section shown in (b) for 99.75% Cu-layers, 1% electrical contact area, $\delta T = 20K$, $T_0 = 288K$ and $\mu_0 = 1mV$.

Our theoretical prediction and numerical model are based on the continuum theory for TE materials as briefly introduced above [71]. Consider a heterogeneous TE body $\Omega \subset I\!R^3$ with electrical conductivity $\sigma = \sigma(\mathbf{x})$, thermal conductivity $\kappa = \kappa(\mathbf{x})$ and Seebeck coefficient

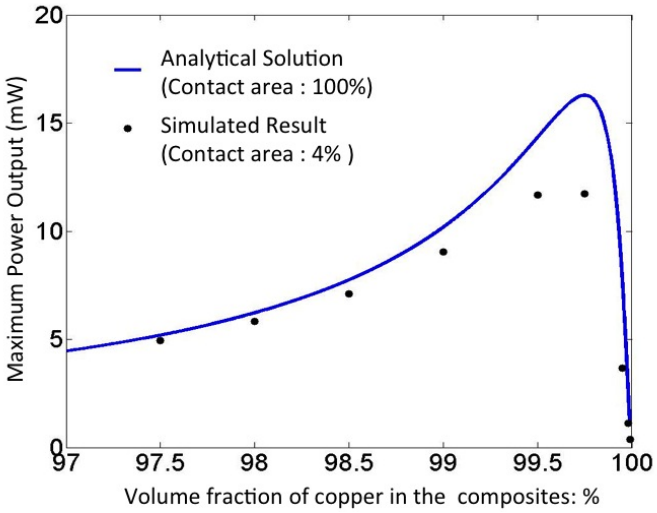

Figure 3.2: Maximum power output versus volume fraction of Cu-layers in the sandwich structure: solid line — analytical prediction by (5.1); '·' — numerical results for 4% electrical contact area.

$s = s(\mathbf{x})$. Let $T, \mu : \Omega \to I\!R$ be the local temperature and electrochemical potential, and $(u_1, u_2) = (-\mu/T, 1/T)$. For TE materials with *small* variations of temperature and electrochemical potential, the constitutive relation for TE materials can be written as [79, 80, 81]:

$$\begin{cases} \mathbf{j}_e = T_0\sigma\nabla u_1 + T_0^2\sigma s\nabla u_2, \\ \mathbf{j}_u = T_0^2\sigma s\nabla u_1 + T_0^2[\kappa + T_0\sigma s^2]\nabla u_2, \end{cases} \tag{3.25}$$

where $\mathbf{j}_e, \mathbf{j}_u$ are the electric current density and energy flux, respectively, and T_0 is the average temperature of the body. Then for a steady-state, conservations of energy and electric charges imply that

$$\mathrm{div}\mathbf{j}_e = 0, \qquad \mathrm{div}\mathbf{j}_u = 0 \quad \text{in } \Omega. \tag{3.26}$$

Upon specifying appropriate boundary conditions, the above equations can be solved for the local fields and determine the effective properties of TE composites.

As an example, we consider a simple laminate of two TE materials with TE properties given by σ_r, κ_r and s_r $(r = 1, 2)$. As shown in Fig. 3.1(a), we denote by L the total thickness

and specify the boundary temperature and electrochemical potential as

$$\begin{cases} T = T_2, \quad \mu = \mu_0, & \text{on top surface,} \\ T = T_1, \quad \mu = -\mu_0, & \text{on bottom surface,} \end{cases} \tag{3.27}$$

Assuming small temperature difference (i.e., $\delta T = T_2 - T_1 \ll T_0$) and upon linearization, we can explicitly solve the boundary value problem formed by (5.3), (3.26) and (5.2). In particular, by (3.26) we find that the electric current and energy fluxes along direction $\mathbf{e}_Y$ shall be constant and given by

$$\begin{aligned} j_e &= -\frac{\sigma^e \mu_0}{L} - \frac{\delta T \sigma^e s^e}{L}, \\ j_u &= -\frac{2T_0 \mu_0 \sigma^e s^e}{L} - \frac{\delta T[\kappa^e + T_0 \sigma^e (s^e)^2]}{L}, \end{aligned} \tag{3.28}$$

where the constants σ^e, κ^e, s^e can be regarded as the the effective electrical conductivity, effective thermal conductivity and effective Seebeck coefficient of the overall laminate and satisfy [71]:

$$\begin{aligned} &\begin{bmatrix} \sigma^e & T_0 \sigma^e s^e \\ T_0 \sigma^e s^e & T_0[\kappa^e + T_0 \sigma^e (s^e)^2] \end{bmatrix} = \\ &\left\{ \theta_1 \begin{bmatrix} \sigma_1 & T_0 \sigma_1 s_1 \\ T_0 \sigma_1 s_{\mathrm{mt}} & T_0[\kappa_1 + T_0 \sigma_1 (s_1)^2] \end{bmatrix}^{-1} \right. \\ &\left. + \theta_2 \begin{bmatrix} \sigma_2 & T_0 \sigma_2 s_2 \\ T_0 \sigma_2 s_2 & T_0[\kappa_2 + T_0 \sigma_2 (s_2)^2] \end{bmatrix}^{-1} \right\}^{-1}, \end{aligned} \tag{3.29}$$

where θ_1 (θ_2) is the volume fraction of material 1(2).

Further, by (3.28) we find the electrical power generated per unit volume is given by

$$\dot{W} := \frac{2\mu_0 j_e}{L} = -\frac{2}{L^2}(2\mu_0^2 \sigma^e + \mu_0 \delta T \sigma^e s^e). \tag{3.30}$$

For fixed temperature difference δT, upon maximizing the power output over μ_0 we find

Table 3.1: TE properties of Copper and p-type doped $(Bi_{0.25}Sb_{0.75})_2$ Te_3 [63].

Material	σ (Ωm)	s $(\mu V/K)$	κ (W/mK)
Cu	5.85 $\times 10^7$	1.90	401
p-Bi-Te	0.33 $\times 10^5$	245	0.559

the maximum power generated per unit volume is given by

$$\dot{W}_{\max} = \frac{P^e}{4}(\frac{\delta T}{L})^2, \qquad P^e = \sigma^e (s^e)^2, \tag{3.31}$$

where the maximum is achieved at $\mu_0 = -\frac{\delta T s^e}{4}$ and P^e can be interpreted as the effective power factor of the laminate.

For a simple laminate of a metallic material with good electric and thermal conductivity and a TE semiconductor with large Seebeck coefficient, we anticipate that electrochemical potential and temperature drop mainly occurs across the semiconducting TE layer, and hence the effective Seebeck coefficient s^e of the overall laminate remains roughly to be that of the semiconductor. Therefore, the effective power factor can be roughly improved as much as the effective electrical conductivity σ^e can be improved. By (5.1) and (3.31), we plot the power output of cylindrical Cu/p-Bi-Te/Cu sandwich versus the volume fraction of Cu-layers in Fig. 3.2 for $\delta T = 20K$, $T_0 = 288K$, $L = 1mm$ and base area $\frac{\pi}{4}mm^2$. The TE properties of Cu and p-Bi-Te are listed in Table 1. From Fig. 3.2 we see that the power output achieves its maximum at about 99.75% volume fraction of Cu-layers, which is about two order of magnitude larger than that of the p-Bi-Te of the same geometry and boundary condition (5.2).

3.4 Simulation

The above calculation has assumed that the electric current is uniform on the xz-plane. In applications, for heat conduction and electrical connections the electrical contact is typically a fraction of the surface area of the TE structure. It may be dubious that equations (3.31) and (5.1) correctly characterize the power output of the TE structure in such a working condition. To verify this result, we implement a Finite Element Model (FEM) that

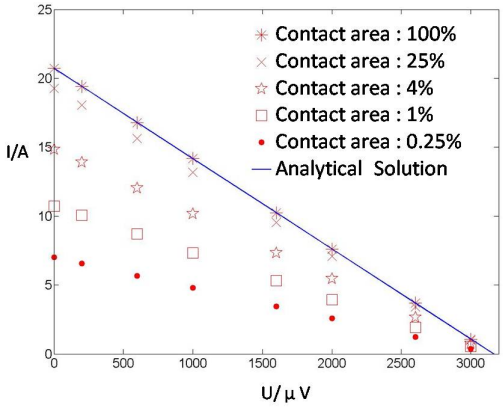

Figure 3.3: I-V curves for different electrical contact areas, 99.75 % Cu-layers, $\delta T = 20K$ and $T_0 = 288K$.

numerically solves the partial differential equation formed by (5.3)-(3.26). As sketched in Fig. 3.1(b) we consider a cylindrical Cu/p-Bi-Te/Cu sandwich structure of 1 mm diameter and 1 mm height. While the temperature on the top and bottom surfaces remains the same as (5.2) with $\delta T = T_2 - T_1 = 20K$ and $T_0 = (T_1 + T_2)/2 = 288K$, we only prescribe the electrochemical potential on the electrical contact areas that locate at the center of the top and bottom surfaces. We set the normal electric current equal to zero on the rest of top and bottom surfaces, and the normal electric current and thermal flux equal to zero on the side surface of the cylinder. Adjusting the electrical contact areas, prescribed electrochemical potential and volume fraction of Cu-layers, we study their influence on the thermal to electrical energy conversion by monitoring the normal electric current output (from the electrical contacts).

Figure 3.1(c) shows the temperature on a cross-section whereas Fig. 3.1(d) shows the electric currents for 99.75% Cu-layers, 1% electrical contact area, $\delta T = 20K$, $T_0 = 288K$ and $\mu_0 = 1mV$. We observe that the temperature on the two Cu-layers are nearly constant. The temperature across the p-Bi-Te layer changes abruptly. By (3.31), this large temperature gradient implies a large electrical power output. On the other hand, the electric current is far from uniform due to small electrical contact area. To see its effect on the overall power output, in Fig. 3.3 we plot the I-V (Current vs. Voltage) curves for different electrical contact area, 99.75 % Cu-layers, $\delta T = 20K$ and $T_0 = 288K$. It is clear that electrical contact area does have a significant effect on the I-V curves and hence overall electrical

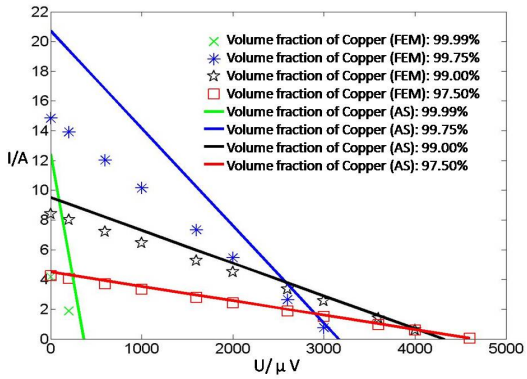

Figure 3.4: I-V curves for 4% electrical contact areas, $\delta T = 20K$, $T_0 = 288K$ and different volume fractions of Cu-layers. The solid line shows the analytical solution for fixing contact area 100 %.

power output.

To verify our prediction of two order of magnitude improvement of power factor in a working condition and the optimal volume fraction of Cu-layers, we numerically compute the I-V curves for 4% electrical contact area, $\delta T = 20K$, $T_0 = 288K$ and a variety of volume fraction of Cu-layers. From Fig. 3.4, we observe that the computed I-V curves are roughly straight lines, implying that the maximum power output is roughly half of the area of the triangle. The maximum power outputs for 4% electrical contact area versus volume fraction of Cu-layers is also plotted in Fig. 3.2 by '·'. From Fig. 3.4 we see that the deviation of the I-V curves from the theory (3.28) can be significant for optimal volume fraction (99.75%) of Cu-layers. Nevertheless, from Fig. 3.2 we see that the power output of the TE sandwich at the optimal volume fraction (99.75%) of Cu-layers is still about 75 times larger if the Cu-layers are replaced by the p-Bi-Te.

3.5 Conclusion

In conclusion, we have shown that the power factor can be significantly improved by heterogeneous TE structures. For a simple laminate of Cu/p-Bi-Te, assuming uniform electric current density and heat flux we show the effective power factor can be about 100 higher than that of the p-Bi-Te. We implement a FEM to solve generic TE boundary value problems for general geometries, heterogeneities, and boundary conditions. In particular, to

account for the effect of small electrical contacts, we numerically compute the local fields and electrical power output of a cylindrical Cu/p-Bi-Te/Cu sandwich in a real-world working condition. The numerical results show that though small electrical contacts do have a significant effect on electrical power output, the optimal power output of the TE sandwich is still 75 times larger than that of the p-Bi-Te structure at the same size and boundary conditions.

Chapter 4

Ginzburg-Landau for superconductors

4.1 Introduction

Recent advances in microfabrication techniques arise from the study in the application of high temperature superconductor-based wire, films and tapes. In order to seek superconductor materials which are capable of carrying high current without loss of energy, a number of theoretical and experimental papers on flux pinning, which is a central topic of research in type II superconductors, have suggested that by introducing ferromagnetic/nonferromagnetic particles, layers or other special structures in superconductor materials like M_gB_2, $YBCO$, etc, magnetic flux will be pinned and critical current can be enhanced. This kind of improvement in flux pinning and consequently critical current density J_c is a determining factor in the use of second genaration high-temperature superconductor (HTS).

Measurements of critical current density in pure superconductor materials grown on different substrates are reported in many literatures [129, 130], etc. The magnetic field dependence of superconducting critical current density J_c is measured from the magnetization hysteresis loops at various temperatures. Also the angular dependences of J_c with respect to the external field is reported. Eun-Mi *et al* [129] found deviations in angular dependence for fields nearly parallel to the *ab* plane. Haage *et al* found another interesting phenomena that anisotropic flux pinning and resistivity appears in the substrate of $YBCO$ thin films grown on vicinal $SrTiO_3(001)$ with *c* axis oriented along the $SrTiO_3$ [001] direction, which indicates that critical current density of HTS can be enhanced by growing thin films on tailored substrate surface. People also investigated the dependence of the critical current density J_c on temperature, magntic field, thin film thickness in some related papers [128, 127]

The magnetic and electric properties of HTS can be controlled by many other engineering methods during the fabrication procedure. As early as 2002, Dou [126] pointed out the enhancement of the critical current density and flux pining of M_gB_2 superconductor by nanoparticle SiC doping. The critical current J_c could be at most an order of magnitude higher than the undoped one. Sudesh [125] reported similar results by adding $F_eC_{10}H_{10}$ in the M_gB_2 sample. It shows that current density J_c is enhanced in the entire magnetic field region with affecting little transition temperature. The ferromagnetic inclusions provide efficient pinning centers to improve J_c behavior. Rare-earth compouds are also considered as new additives in superconductor films or tapes due to their excellent chemical inertness to and large lattice mismatches with $YBCO$, which is one kind of traditional superconducting materials. Sung [124, 123] reported that $YBCO + BYNO$ films exhibited no T_c reduction as well as superior J_c performance and exhibited a strong J_c peak for $H||c$ indicative of strong $c-$axis correlated flux-pinning. Selvamanickam [122] made a series of work on engineered defects by addition of dopants, and particularly examined the influence of rare-earth content and type in $(Gd, Y)Ba_2Cu_3O_7$ films with Zr addition. As mentioned above, studies introducing self-assembled pinning centers have been very active for improving the flux pinning properties in magnetic fields parallel to the c-axis [121, 116, 120, 119, 143]

4.1.1 Nucleation of superconductivity in S/F hybrids

Due to a number of advanced nanotechnology, for instance, the development of material deposition techniques and the lithographic methods, it is possible to fabricate the superconductor(S) and ferromagnetic(F)/paramagnetic subsystem in artificial heterostructure at nanometer scales[132, 133, 134, 135]. This is a different method to control and enhance the transport properties of HTS materials compared to the nanoparticle doping. Unlike the coexistance of superconductivity of ferromagnetism superconductors, this subsystem can be physically seperated. Several theoretical, experimental and numerical studies concerning the thermodynamical and transport properties of such hybrid system which consists of spatially separated superconductor and ferromagnets have been reported in the literatures[136, 137, 138, 139], etc.

We restrict our disscussion that all superconducting and ferrormagnetic are electrically

insulated and there is no proximity effect. This means the transport properties in the S/F hydrid system is dominated by their electromagnetic interaction. Based on these assumptions, different behavior of such S/F system is anticipated for variation of temperature and external field. We seperate our discussion into two senarios: 'hard' magnets and 'soft' magnets. For 'hard' magnets, when the phase is rather close to the superconducting transition line, the magnetization of ferromagnet is solely determined by its own magnetic history and won't be affected by the supercurrent generated in the superconductor. On the other hand, the nonuniform magnetic field induced by the ferromagnet can strongly affect the nucleation of superconductivity in S/F system, consequently the critical current density and temperature. For 'soft' magnets, the magnetization of the ferromagnet is no longer fixed. Instead, it can be influenced by the superconducting current. Thus, the superconductor and ferromagnet have more complicated coupling relationship than 'hard' S/F structure. What is more, both the 'hard' and 'soft' S/F system with pure electromagnetic coupling can be described by Ginzburg-Landau theory, which is a famous phenomenological second phase theory on superconducting area. We give some brief literature reviews on 'hard' S/F system and 'soft' S/F system in following.

Starting from a toy model, Milosevic and Peeters [140, 115] considered formulation of giant vortices of vortex and anti-vortex structure by a ferromagnetic disc with out-of-plane magnetization embedded in a thin superconducting film using the full nonlinear self-consistent Ginzburg-Landau theory. They concluded that antivortices are stabilized in shells around a central core of vortices with magnetization-controlled "magic numbers." The transition between the different vortex phases occurs through the creation of a vortex-antivortex pair under the magnetic disk edge. Moreover, they [112] discussed the influence of the magnet geometry.

Besides the effect of a single magnetic dot, the effect of magnetic pinning arrarys are also widely studied[114, 118, 117]. Milosevic and Peeters made a series of work on the effect of superconductivity of superconducting thin film nanostructured by a lattice of magnetic particles[114, 113, 110, 111, 109]. Dependence of vortice configuration on the size of the magnetic dots, polarity and the properties of the superconductor are shown in the work[113].

They investigated the superconducting thin film under a square array of rectangular ferromagnets with in-plane magnetization [109], and the results showed that vortex-antivortex pairs coexistence exists with/without the presence of external magnetic field. Doria[141] studied a rectangular array of magnetic moments embedding in a superconductor, and the behavior of the vortex phase formulation was predicted in the work. Carneiro[142] analyzed the interaction between vortices in planar superconducting films and magnetic dipole array placed outside the film.

In the meantime, many experimental results enrich people's knowledge[108, 107, 106, 105], etc. As early as 1997, Martin fabricated triangular arrays of submicrometer magnetic dots, with typical spacing of 400-600 nm and diameters close to 200 nm by electron beam lithography and studied the pinning effects on Nb thin films. The angular, current and temperature dependencies of the resistivity imply synchronized pinning by the magnetic array which is relevent at high vortex velocities, when the order in the vortex lattice increases. Silhanek *et al* [108] investigated the nucleation of superconductivity in an Al film deposited on top of an array of micromagnets with perpendicular anisotropy by dc transport measurements. Through controlling the magnetic state of the ferromagnets, they explored the superconductor-normal-metal phase boundary as a function of the magnetization of the dots. And critical current for a given temperature could be further enhanced by properly adjusting the size of the magnetic dots.

Multilayers is another special structure for S/F hybrid system, like bilayers or sandwich structure. Earlier in 1991, Ledvij *et al* [104] investigated the superconducting nucleation fields for ferromagnetic-superconducting-ferromagnetic triple layers when the magnetic field was applied parallel to the S/M interfaces. Koorevaar [103] analyzed the interplay between superconductivity and magnetism in various S/F multilayers. Zdravkov *et al* [132] studied the reentrant superconductivity in superconductor/ferromagnetic-alloy bilayers.

In the above work, magnetic defects and superconductor in the composite have a strong interaction with each other, resulting in strong flux-line pinning force because of the magnetic pinning mechanism. The enhancement of pinning force of vortices can stabilize the vortex phase in type II superconductor. Furthermore, critical current as an important property of superconducting material can be reached when driving force is balanced by pinning

force due to inhomogeneities.

4.1.2 Superconductor/soft magnet hybrids

In the above discussion, we assume the magnetization of ferromagnet remains unaltered in the S/F hybrids. Another topic is related to the soft ferromagentic materials or paramagnetic materials with low coercive field. In this kind of hybrid, the magnetization can be changed either by the external magnetic field or by the induced superconducting current.

The formation of vortices in the superconducting materials and magnetic domains in the ferromagnetic materials with S/F bilayers with perpendicular magnetization can be induced by the magnetostatic interaction between a vortex-free superconducting film and a uniformly magnetic domains in the ferromagnet film at zero external field. Erdin *et al* [102] pointed out that the ground state of the S/F system could be unstable with respect to the formation of vortices in the superconducting materials. The reason is that formation of vortices is energetically favorable once the total energy of a single vortex line influenced by magnetostatic interaction between superconductor and ferromagnet is negative. However, the energy will increase once the lateral size of the S/F system increases, due to the constant magnetic field along z direction generated by the averaged vortex density. Thereforce, the ferromagnetic film would split into domains with alternating magnetization in a finite temperature range in order to let the vortex phase to survive. It is also interesting to notice that for a thin film system consisting of a superconducting and a magnetic film, the interaction between a single vortex in the superconducting domain and the nanomagnet crosses over from attractive to repulsive at a short distance [101].

The interaction between vortices and a superparamagnetic particle with constant dipolar moment was investigated by Carneiro [142, 99, 98, 100, 97]. In his work, he pointed out the energy potential for the superconducting vortices differs significantly from that for a permanent dipole due to the rotational degree of freedom. The vortex pinning by a magnetic dipole is tunable by applying an in-plane external field. And the critical current could be controllable in the same way.

In order to modify the superconducting properties of such soft hybrid system, an alternative way is to utilize paramagnetic inhomogeneities, which are generally characterized

by zero or very low remanent magnetization. The magnetization of paramagnetic material completely depends on the external magnetic field and the magnetic permeability μ. Such kind of superconductor-paramagnet hybrids were studied theoretically and numerically by Geneko. In Genenko's paper[96], the concept of magnetic shielding for the enhancement of superconductor critical currents was discussed. Even in the *Meissner State*, the magnetically shielded superconductors are able to carry without dissipation rather high transport current comparable with the typical current values for a regime of strong flux pinning. Moreover, it [95] was numerically shown that transport current distributions in a flux-free superconductor strip located near a soft magnet wall of arbitrary thickness, the reduction of the edge current peaks caused by magnetic shielding saturates rapidly with increasing thickness of the magnet. The effect of magnetic shielding on the current and field distributions in a thin, flat superconductor ring located between two coaxial cylindrical soft magnets of high permeability was also studied Genenko *et al*[94]. Such a heterostructure keeps the flux-free state of the ring with high magnetic fields and low electromagnetic losses in ac applications, even in the presence of strong total supercurrents. The problem concerning the transport current distribution in a superconducting filament aligned parallel to the flat surface of a semi-infinite bulk magnet with the assumption that the superconductor is in the *Meissner State* was considered by Yampolskii *et al* [93]. Genenko *et al* [92] studied a similar problem that the distribution of magnetic field inside and outside a superconducting filament sheathed by a magnetic layer, as well as the magnetization of such a structure in the region of reversible magnetic behavior in the *Meissner State*. Moveover, a number of literatures about the formation of the mixed state in various superconductor/paramagnet structures in the presence of transport current, or an external magnetic field or the field of hard-magnetic dipoles, in the framework of the London model, was analyzed by Genenko *et al* [91], Genenko and Rauh [90], Yampolskii and Genenko [89], etc.

The implementation of paramagnetic and ferromagentic coatings in high-T_c superconducting materials raises lots of attention due to the improvement of the critical current and reduction of the ac losses [143, 144]. While good critical currents can be achieved in the absence of a magnetic field, there is still a challenge in reaching high critical currents in the presence of a magnetic field.

4.1.3 Enhancement of pinning effect and critical current

Flux pinning is one of the crucial problems in the development of high temperature superconductors (HTS). The defects of the nano-scale could be introduced into HTS by nanotechnology in order to strongly pin the quantized vortices. Tremendous efforts have been focusd on the enhancement on pinning effect and consequently critical current theoretically and experimentally. Since the normal core of quantized vortex or the shielding current surrounding the core locally interacts with the defects and impurities in the superconducting materials, a spatial perturbation of free energy of the quantized vortices is caused. For this reason, the flux pinning is generated. Generally speaking, the lorentz force $\mathbf{F}_L$ acts on the quantized vortices when the current exists under the magnetic field. The critical current is determined by the balance between pinning force $\mathbf{F}_p$ and lorentz force $\mathbf{F}_L$. The global pinning force $\mathbf{F}_p$ depends on the pinnng mechanics. Even the pinning phenomenon that rules the critical current is complex, including the effect of pinning energy, elastic energy between quantized vortices and the thermal energy, the most general method to generate and increase the pinning force is to introduce the different kinds of artificial defects.

As early as 2000, Adamopoulos and Patapis [145] studied the role of interfaces with large nonsuperconducting particles in vortex pinning. Based on the modified second London equation, they showed that the spatial variation of the magnetic penetration depth can lead to pinning of the vortices and increased critical current density under sharp interface. Even the model is one-dimension, they give a qualitative information of the bulk pinning force under a specified mircostructure. The interaction of a vortex in the vicinity of the normal phase particle with the normal phase causes a reduction of the magnetic energy of the vortex and creates a pinning site acting an attractive force to the vortex. And it is shown that as the interface sharpness decreases, the pinning force is reduced. Kayali [146] presented analytical study of a system consisting of a superconducting thin film pierced by ferromagnetic columnar defects. It is shown that the interaction between magnetic field of vortices and the magnetization outside the plane of the film leads to very strong pinning and a spontaneous vortex phase will appear if the magnetization of the columnar defect exceeds a critical value. Vortices in this system are pinned by pinning forces that increase linearly

with the magnetization of the magnetic defects. They also show that vortex pinning is strongly enhanced due to the contribution from the interaction between the magnetic field of vortices and the magnetization of the ferromagnetic columnar defect outside the plane of the superconductor and its close proximity. Blamire [147] reported that a magnetic inclusion can also reduce the lorentz force on a vortex, resulting in a substantially enhanced critical current density for given pinning force. They have shown that paramagnetic or ferromagnetic pinning centers have the potential to create a significant enhancement of the critical current density of a type II superconductor. They concluded that the enhancement is likely to be limited to fields below $1T$ by the saturation magnetization of the magnetic inclusions.

In the case of conventional superconductors, regular arrays of submicron holes substantially increase the critical current I_c and critical temperature T_c. Silhanek *et al* [88] used electric transport measurement to study the effect of placing an additional small antidot in the unit cell of the array. This composite antidot lattice consists of two interpenetrating antidot square arrays with a different antidot size and the same lattice period. The smaller antidots are located at the centers of the cells of the large antidots array. They showed that the composite antidot lattice can trap a higher number of flux quanta per unit cell inside the antidots compared to a reference antidot film without the additional small antidots. Moreover, the field range in which an enhanced critical current observed is considerably expanded. Wu *et al* [87] fabricated a superconducting Nb thin film with triangular arrays of pinning sites to investigate the commensurate vortex lattices. The interactions of vortices in this pattern film make the observed anisotropy in the pinning properties. The transport properties at near critical temperature show anisotropic pinning properties related to the configuration of pinning centers. The critical current is depressed when the driving force is applied along the short diagonal in the rhombic unit cell of pinning array, which implies that the pinning potential along the short diagonal creates a moving channel of vortices in triangular arrays of defects. The effect of different dimension of artificial pinning centers on pinning the quantized vortices were studied by Matsumoto *et al*[86]. In their work, critical current dentsities $\mathbf{J}_c$ of the HTS fillms are dramartically improved by the controlled artifical pinning centers. The in-field current density $\mathbf{J}_c$ of the high-quality, epitaxial films

was improved by one order of magnitude or more compared with the values of the past experimantally. Gurevich [84] calculated the thickness dependence of the critical current density $J_c(d)$ in films due to the two-dimensional/three-dimensional pinning crossover at low magnetic fields, taking into account the spatial correlation of pinning cernters, effect of bulk and surface pinning and the effect of thermal fluctuations. Bezotosny *et al* [85] observed the asymmetry in the magnetic field dependence of pinning force F_p for two opposite directions of the transport current. They found that the effect is less significant for thin and thick films where single vortex pinning and pinning of internal vortices is relevent. However, at the intermediate thickness, an asymmetry in the F_p depencence is obviously due to the pinning mechanism caused by surface effects.

Generally speaking, the theoretical model of the system consisting of magnetic inhomogeneities and superconductor matrix is complicated, what is more, in the presence of an applied magnetic field. So far, early work on this field give an invaluable qualitative information[145, 146, 147]. Nethertheless, to author's best knowledge, there is no explicit explaination to the problem from the energy viewpoint. The superconductor nanocomposite can be described phenomenologically using Ginzburg-Landau formalism. Both the microscopic level and the macroscopic level shall be considered, that is on the scale of the flux line spacing and on the scale of bulk superconductor and its physical surroundings. In the former case one is concerned with the details of the arrangement of flux vortices and their interaction with an array of pinning centers. In the latter case one is interested in the relation of the electrodynamics arrangement to a static or dynamic mixed state.

In this chapter, we begin with the interaction energy between a single vortex and a magnetic non-superconducting boundary in the equilibrium mixed state. This shall be considered firstly in order to obtain the interaction force caused by the inhomogeneities. Moreover, we shall notice that pinning is caused by the local fluctuations in the properties of the materials. The free energy of the system depends on the position of the vortices. We try to find the free energy of the system as a function of the position of the vortices with respect to the pinning center. The nature of the pinning force consists of the energy associated with the condensation energy and the core energy. However in the London limit (i.e. $\kappa \to \infty$), the core is reduced to a line discontinuity at the center of the current vortex

and the problem reduces to one of classical hydrodynamics. This assumption is the one to yield results in the range $H_{c1} \leq H \leq H_{c2}$ even the physical model is a bit unrealistic. Thus, we ignore the core energy here and focus on the magnetic energy and the supercurrents outside the core. Furthermore, the results of the model are likely to remain valid for the temperature other than near to critical temperature T_c. On account of these facts we give a full treatment of the problem based on Ginzburg-landau theory and classic Landau theory of micromagnetics to describe the total free energy for the two phases composite. The flux line which varies along x direction as well as y direction is modeled. Moreover, we restrict our study to the thin film so that the vortex line is expected to be straight and we ignore the proximity effect by assuming an insulting buffer material between the interface.

This chapter is organized as follows. A general total free energy of the superconductor composite system is proposed in section 4.2. Then we derive the planar energy form in the thin film case with zero transport current and deduce the pinning force for a single vortex in dilute limit in section 4.3. In section 4.4, driving force on a single force in pure superconducting film, which is usually so-called lorentz force is derived. Then the interaction with paramagnetic inhomogeneity under the external transport current is discussed in section 4.5. Section 4.6 is summary.

4.2 Free energy of superconductors with magnetic inhomogeneities

4.2.1 Free energy of the system

Consider a superconductor body with magnetic inhomogeneities in the vacuum. Denote by Ω (resp. Ω_s, Ω_m, Ω_v) the regime occupied by the overall body (resp. superconductor, magnetic inhomogeneities, vacuum). We postulate that the thermodynamic state of the system is described by the order parameter $\psi : \Omega_s \to \mathbb{C}$ for the superconductor, the magnetization $\mathbf{M} : \Omega_m \to I\!R^3$ for the magnetic inhomogeneities, and the magnetic vector potential $\mathbf{A} : I\!R^3 \to I\!R^3$ ($\mathbf{B} = \nabla \times \mathbf{A}$, where $\mathbf{B}$ is the magnetic field). At a constant temperature T close to the critical temperature T_c and under the application of an external

constant magnetic field $\mathbf{H}^e$, we identify the total free energy of the system as

$$\begin{aligned} G[\psi, \mathbf{A}, \mathbf{M}; \mathbf{H}^e] = & \int_{\Omega_s} \left[f_{n0} + \frac{\beta}{2}(|\psi|^2 + \frac{\alpha}{\beta})^2 + \frac{1}{2m^*}|(\frac{\hbar}{i}\nabla - \frac{e^*}{c}\mathbf{A})\psi|^2 \right] \\ & + \int_{\Omega_m} [\frac{a_{\text{ex}}}{2}|\nabla \mathbf{M}|^2 + \phi(\mathbf{M}) - \mathbf{H}^e \cdot \mathbf{M}] \\ & + \frac{1}{8\pi}\int_{I\!R^3} |\nabla \times \mathbf{A} - \mathbf{H}^e - 4\pi \mathbf{M}\chi_{\Omega_m}|^2, \end{aligned} \tag{4.1}$$

where $\hbar$ (resp. e^*, m^*, c) are the Planck constant, effective charge, effective mass of Cooper pairs and speed of light, f_{n0} is the free energy density in the normal state in the absence of external magnetic field, $\alpha = -\frac{e^{*2}}{m^* c^2} H_c^2(T)\lambda_{\text{eff}}^2(T), \beta = \frac{4\pi e^{*4}}{m^{*2} c^4} H_c^2(T)\lambda_{\text{eff}}^4(T)$ are phenomenological constants as in the classic Ginzburg-Landau theory (Tinkham, 1975), $a_{\text{ex}} > 0$ is the exchange constant in the theory of micromagnetics (Landau, 1933; Landau and Lifshitz, 1995), and $\phi : I\!R^3 \to I\!R$ describes the internal energy density associated with magnetization in the magnetic inhomogeneities. To be consistent, the state variables $(\psi, \mathbf{A}, \mathbf{M})$ should satisfy the following conditions:

$$\int_{\Omega_s} |\nabla \psi|^2 < +\infty, \ |\nabla \times \mathbf{A} - \mathbf{H}^e| \to 0 \ \text{ as } \ |\mathbf{x}| \to +\infty, \ \int_{\Omega_m} |\mathbf{M}|^2 < +\infty. \tag{4.2}$$

We expect the free energy (4.1) reasonably describes the interactions between superconductors and magnetic inhomogeneities based on the following observations: (i) At the absence of magnetic inhomogeneities (i.e., $\Omega_m = \emptyset$), equation (4.1) precisely degenerates into the Ginzburg-Landau theory for a pristine superconductor (Tinkham, 1975). (ii) At the absence of superconductor (i.e., $\Omega_s = \emptyset$), equation (4.1) is precisely the Landau theory of micromagnetics (Landau and Lifshitz, 1995).

In this work, we employ Gauss unit system such that

$$\mathbf{B} = \mathbf{H} \qquad \text{in } \ \Omega_s \cup \Omega_v, \qquad \mathbf{B} = \mathbf{H} + 4\pi\mathbf{M} \qquad \text{in } \ \Omega_m, \tag{4.3}$$

and the Maxwell equation is written as

$$\nabla \cdot \mathbf{B} = 0 \quad \text{ and } \quad \nabla \times \mathbf{H} = \frac{4\pi}{c}\mathbf{J} \qquad \text{in } \ I\!R^3, \tag{4.4}$$

where **J** is the current density.

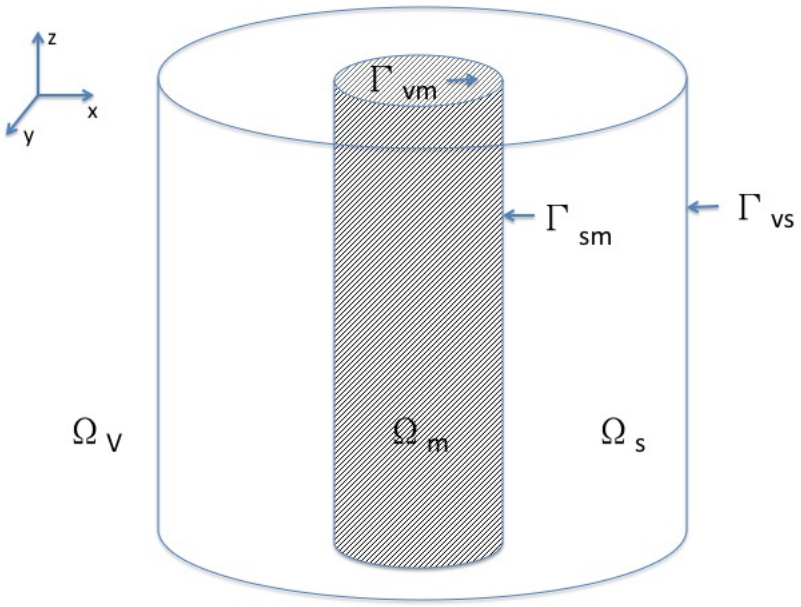

Figure 4.1: Schematic diagram

By the principle of free energy we claim the equilibrium state of the system is determined by the variational principle:

$$\min\{G[\psi, \mathbf{A}, \mathbf{M}; \mathbf{H}^e] : (\psi, \mathbf{A}, \mathbf{M}) \in \mathbb{S}\}, \tag{4.5}$$

where the admissible space for $(\psi, \mathbf{A}, \mathbf{M})$ is defined as

$$\mathbb{S} = \{(\psi, \mathbf{A}, \mathbf{M}) : \Omega_s \times I\!R^3 \times \Omega_m \to \mathbb{C} \times I\!R^3 \times I\!R^3 \ \text{ satisfy } (4.2)\}.$$

The Euler-Lagrange equations associated with the principle of free energy (4.5) necessarily satisfies (see *Appendix* 4.7.1 for details)

$$\begin{cases} \alpha\psi + \beta|\psi|^2\psi + \frac{1}{2m^*}(\frac{\hbar}{i}\nabla - \frac{e^*}{c}\mathbf{A})^2\psi = 0 & \text{in } \Omega_s, \\ \nabla \times (\nabla \times \mathbf{A} - 4\pi\mathbf{M}\chi_{\Omega_m}) = \frac{4\pi}{c}\mathbf{J}_s\chi_{\Omega_s} & \text{in } I\!R^3, \\ -\nabla \times \mathbf{A} + 4\pi\mathbf{M} + D_{\mathbf{M}}\phi(\mathbf{M}) - a_{\text{ex}}\Delta\mathbf{M} = 0 & \text{in } \Omega_m, \end{cases} \tag{4.6}$$

where

$$\mathbf{J}_s = [\frac{\hbar e^*}{2m^*i}(\psi^*\nabla\psi - \psi\nabla\psi^*) - \frac{e^{*2}}{m^*c}\psi\psi^*\mathbf{A}] \qquad \text{in } \Omega_s. \tag{4.7}$$

is the supercurrent. When linear paramagnetic material is applied, the associated boundary conditions derived from the variational calculus are

$$\begin{cases} \left[(\frac{\hbar}{i}\nabla - \frac{e^*}{c}\mathbf{A})\psi\right] \cdot \mathbf{N} = 0 & \text{on } \partial\Omega_s, \\ [\![\nabla \times \mathbf{A} - \mathbf{M}]\!]\big|_{\Gamma_{s\text{inh}}} \times \mathbf{N} = 0 & \text{on } \Gamma_{s\text{inh}}, \\ [\![\nabla \times \mathbf{A} - \mathbf{M}]\!]\big|_{\Gamma_{v\text{inh}}} \times \mathbf{N} = 0 & \text{on } \Gamma_{v\text{inh}}, \\ (\nabla\mathbf{M})\mathbf{N} = 0 & \text{on } \partial\Omega_m, \end{cases} \tag{4.8}$$

where we denote by $\Gamma_{s\text{inh}}(\Gamma_{v\text{inh}})$ the interface between the supreconductor(vacuum) and magnetic inhomogeneity. $\mathbf{N}$ is the unit outward normal on the boundary.

The Ginzburg-Landau energy (4.1) is Gauge-invariant in the sense that for any scalar potential $\theta' : I\!R^3 \to I\!R$,

$$G[\psi', \mathbf{A}', \mathbf{M}; \mathbf{H}^e] = G[\psi, \mathbf{A}, \mathbf{M}; \mathbf{H}^e] \quad \text{if } \mathbf{A} \to \mathbf{A}' = \mathbf{A} + \nabla\theta', \quad \psi \to \psi' = \psi e^{ie^*\theta'/c\hbar}.$$

It is sometimes convenient to rewrite the Ginzburg-Landau energy (4.1) directly in terms of Gauge-invariant quantities, i.e., Cooper pair density $|\psi|^2$, supercurrent density $\mathbf{J}_s$ (cf. (4.7)) and magnetic field $\mathbf{B} = \nabla \times \mathbf{A}$. To this end, we rewrite the wave function ψ as $\psi = u\exp(i\theta)$ with u^2 being the density of Cooper pairs and θ the phase. For brevity, we

introduce notation:

$$\tilde{\theta} = \frac{c\hbar}{e^*}\theta, \qquad \tilde{\mathbf{A}} = \mathbf{A} - \frac{c\hbar}{e^*}\nabla\theta. \tag{4.9}$$

From quantum mechanics, we identify $m^*\mathbf{v} = \hbar\nabla\theta - e^*\mathbf{A}/c$ as the momentum of Cooper pairs, and hence

$$\mathbf{J}_s = e^* u^2 \mathbf{v}, \qquad \mathbf{v} = \frac{\hbar}{m^*}(\nabla\theta - \frac{e^*}{c\hbar}\mathbf{A}) = -\frac{e^*}{m^* c}\tilde{\mathbf{A}}, \tag{4.10}$$

which is consistent with (4.7). We can identify $\tilde{\mathbf{A}}$ as the vector potential in London's gauge (Bardeen, 1950). Let $\mathbf{A}^e$ be the magnetic vector potential associated with external magnetic field such that $\nabla \times \mathbf{A}^e = \mathbf{H}^e$ on $I\!R^3$, and $\mathbf{A}^{\rm sf} = \mathbf{A} - \mathbf{A}^e$ be the self magnetic vector potential induced by the supercurrent and magnetization. By the Maxwell equation $(4.6)_2$ and boundary condition $(4.2)_2$, we can separate the contributions of supercurrent and magnetization:

$$\mathbf{A}^{\rm sf} = \mathbf{A}^{\rm sf}_s + \mathbf{A}^{\rm sf}_m, \tag{4.11}$$

where $\nabla \times \mathbf{A}^{\rm sf}_{s,m}$ is the self magnetic field associated with the supper current $\mathbf{J}_s$ and magnetization $\mathbf{M}$, and are respectively determined by

$$\begin{cases} \nabla \times \nabla \times \mathbf{A}^{\rm sf}_s = \frac{4\pi}{c}\mathbf{J}_s\chi_{\Omega_s} = \frac{1}{\lambda^2}[-\mathbf{A}^{\rm sf}_s - \mathbf{A}^{\rm sf}_m - \mathbf{A}^e + \nabla\tilde{\theta}]\chi_{\Omega_s} & \text{in } I\!R^3, \\ \nabla \times \mathbf{A}^{\rm sf}_s \to 0 & \text{as } |\mathbf{x}| \to +\infty, \end{cases} \tag{4.12}$$

and

$$\begin{cases} \nabla \times (\nabla \times \mathbf{A}^{\rm sf}_m - 4\pi\mathbf{M}\chi_{\Omega_m}) = 0 & \text{in } I\!R^3, \\ \nabla \times \mathbf{A}^{\rm sf}_m \to 0 & \text{as } |\mathbf{x}| \to +\infty. \end{cases} \tag{4.13}$$

From the classic theory of electromagnetism (Jackson, 1995), the magnetic field determined

by (4.13) can be written as $\mathbf{B}_m^{\rm sf} := \nabla \times \mathbf{A}_m^{\rm sf} = -\nabla\zeta_m + 4\pi\mathbf{M}\chi_{\Omega_m}$, and

$$\begin{cases} \nabla \cdot (\nabla\zeta_m + 4\pi\mathbf{M}\chi_{\Omega_m}) = 0 & \text{in } I\!R^3, \\ \nabla\zeta_m \to 0 & \text{as } |\mathbf{x}| \to +\infty. \end{cases} \tag{4.14}$$

In addition, the external magnetic field can also be written as

$$\mathbf{H}^e = -\nabla\zeta^e \qquad \text{in } I\!R^3.$$

We remark that the self magnetic fields $\mathbf{B}_{s,m}^{\rm sf} := \nabla \times \mathbf{A}_{s,m}^{\rm sf}$ are completely determined by independent real-valued variables $(u, \tilde{\mathbf{A}}, \mathbf{M})$. By the divergence theorem, the nonlocal energy in associated with magnetic field (i.e. the last term in (4.1)) can be written as

$$\frac{1}{8\pi}\int_{I\!R^3} |\nabla \times \mathbf{A}^{\rm sf} - 4\pi\mathbf{M}\chi_{\Omega_m}|^2 = \frac{1}{8\pi}\int_{I\!R^3} |\nabla \times \mathbf{A}_s^{\rm sf} - \nabla\zeta_m|^2 = F^s + F^m, \tag{4.15}$$

where

$$F^s[u, \tilde{\mathbf{A}}, \mathbf{M}; \mathbf{A}^e] = \frac{1}{8\pi}\int_{I\!R^3} |\nabla \times \mathbf{A}_s^{\rm sf}|^2, \qquad F^m[\mathbf{M}; \mathbf{A}^e] = \frac{1}{8\pi}\int_{I\!R^3} |\nabla\zeta_m|^2.$$

In addition, by direct calculation we find that the kinetic energy satisfies

$$\begin{aligned} \frac{1}{2m^*}|(\frac{\hbar}{i}\nabla - \frac{e^*}{c}\mathbf{A})\psi|^2 - \frac{\hbar^2}{2m^*}|\nabla u|^2 &= \frac{(e^*u)^2}{2m^*c^2}|\nabla\tilde{\theta} - \mathbf{A}|^2 = \frac{1}{8\pi\lambda^2}|\tilde{\mathbf{A}}|^2 \\ &= \frac{m^*}{2(e^*u)^2}|\mathbf{J}_s|^2 = -\frac{1}{2c}\mathbf{J}_s \cdot \tilde{\mathbf{A}}. \end{aligned}$$

Therefore, in terms of $(u, \tilde{\mathbf{A}}, \mathbf{M})$ the free energy (4.1) can be equivalently expressed as

$$G[u, \tilde{\mathbf{A}}, \mathbf{M}; \mathbf{A}^e] = G^s[u, \tilde{\mathbf{A}}, \mathbf{M}; \mathbf{A}^e] + G^m[\mathbf{M}; \mathbf{A}^e], \tag{4.16}$$

where G^s (G^m) represents the free energy associated with the superconductor Ω_s (resp.

magnetizable medium Ω_m), and is given by

$$\begin{aligned} G^s[u,\tilde{\mathbf{A}},\mathbf{M};\mathbf{A}^e] &= \int_{\Omega_s}\Big[\frac{\hbar^2}{2m^*}|\nabla u|^2+\frac{\beta}{2}(u^2+\frac{\alpha}{\beta})^2+\frac{1}{8\pi\lambda^2}|\tilde{\mathbf{A}}|^2\Big]+F^s[u,\tilde{\mathbf{A}},\mathbf{M};\mathbf{A}^e],\\ G^m[\mathbf{M};\mathbf{A}^e] &= \int_{\Omega_m}[\frac{a_{\rm ex}}{2}|\nabla\mathbf{M}|^2+\phi(\mathbf{M})+8\pi|\mathbf{M}|^2-\mathbf{H}^e\cdot\mathbf{M}]+F^m[\mathbf{M};\mathbf{A}^e]. \end{aligned} \tag{4.17}$$

In addition, the variational problem (4.5) is equivalent to

$$\min\{G[u,\tilde{\mathbf{A}},\mathbf{M};\mathbf{A}^e]:\ (u,\tilde{\mathbf{A}},\mathbf{M})\}. \tag{4.18}$$

By the standard calculus of variations or directly taking the real part and imaginary part of $(4.6)_1$, we rewrite the Euler-Lagrange equations (4.6) for $(u,\mathbf{M},\tilde{\mathbf{A}})$ as

$$\begin{cases} -\dfrac{\hbar^2}{2m^*}\Delta u+\alpha u+\beta u^3+\dfrac{u}{8\pi\hat{\lambda}^2}|\tilde{\mathbf{A}}|^2]=0 & \text{in } \Omega_s,\\ \nabla\times(\nabla\times\tilde{\mathbf{A}}-4\pi\mathbf{M}\chi_{\Omega_m})=-\dfrac{u^2}{\lambda^2}\tilde{\mathbf{A}}\chi_{\Omega_s} & \text{in } I\!R^3,\\ -\nabla\times\tilde{\mathbf{A}}+4\pi\mathbf{M}+D_{\mathbf{M}}\phi(\mathbf{M})-a_{\rm ex}\Delta\mathbf{M}=0 & \text{in } \Omega_m, \end{cases} \tag{4.19}$$

which, combined with the boundary and interfacial conditions (4.2) and (5.2), are presumably sufficient for determining the equilibrium state of the system.

$$\begin{aligned} &\hat{G}=G/\frac{2\alpha^2}{\beta}, \qquad \hat{u}=u/u_\infty, \qquad \hat{\mathbf{A}}=\tilde{\mathbf{A}}/\sqrt{\alpha^2/\beta},\\ &u_\infty=\sqrt{-\frac{\alpha}{\beta}}, \qquad \lambda=\sqrt{\frac{m^*c^2}{4\pi(e^*u_\infty)^2}}, \qquad \xi=\sqrt{-\frac{\hbar^2}{2m^*\alpha}}. \end{aligned} \tag{4.20}$$

We remark that λ and ξ is the London's penetration depth and superconducting coherence length. We can rewrite the free energy in a dimensionless form:

$$\hat{G}^s[u,\hat{\mathbf{A}},\hat{\mathbf{M}};\mathbf{A}^e]=\int_{\Omega_s}\Big[\xi^2|\nabla\hat{u}|^2+\frac{1}{2}(\hat{u}^2-1)^2+\frac{\hat{u}^2}{8\pi\lambda^2}|\hat{\mathbf{A}}|^2\Big]+\frac{1}{8\pi}\int_{I\!R^3}|\nabla\times\hat{\mathbf{A}}_s^{\rm sf}|^2,$$

4.2.2 Some classic solutions at the absence of magnetic inhomogeneities

At the absence of magnetic inhomogeneities (i.e. $\Omega_m = \emptyset$), equations (4.6)-(5.2) can be rewritten as

$$\begin{cases} \xi^2 \Delta \hat{u} + \hat{u} - \hat{u}^3 - \dfrac{\hat{u}}{8\pi\lambda^2}|\hat{\mathbf{A}}|^2 = 0 & \text{in } \Omega_s, \\ \nabla \times \nabla \times \hat{\mathbf{A}} = -\dfrac{\hat{u}^2}{\lambda^2}\hat{\mathbf{A}}\chi_{\Omega_s} & \text{in } I\!R^3. \end{cases} \tag{4.21}$$

with boundary conditions:

$$\begin{cases} \nabla \hat{u} \cdot \mathbf{N} = 0 & \text{on } \partial\Omega_s, \\ \nabla \times \hat{\mathbf{A}} \to \hat{\mathbf{H}}^e & \text{as } |\mathbf{x}| \to +\infty. \end{cases} \tag{4.22}$$

Enforcing the GL equations (4.21), the free energy can be significantly simplified. In particular, by $(4.21)_1$ and the divergence theorem we have

$$\int_{\Omega_s} \Big[-\xi^2 |\nabla \hat{u}|^2 + \hat{u}^2 - \hat{u}^4 - \frac{\hat{u}^2}{8\pi\lambda^2}|\hat{\mathbf{A}}|^2 \Big] = 0$$

Thus,

$$\hat{G}^s[u, \hat{\mathbf{A}}; \mathbf{A}^e] = \int_{\Omega_s} \frac{1}{2}(1 - \hat{u}^4) + \frac{1}{8\pi} \int_{I\!R^3} |\nabla \times \hat{\mathbf{A}}_s^{\text{sf}}|^2. \tag{4.23}$$

The Ginzburg-Landau boundary value problems (4.21)-(4.22) associated with variational principle (4.5) admits a few classic solutions. Below we briefly outline these solutions which will be the basis for our study of the heterogeneous system.

1. Normal solution/state: $(u, \nabla \times \tilde{\mathbf{A}}) = (0, \mathbf{H}^e)$.

$$\hat{G}^s = \frac{1}{2}|\Omega_s|.$$

2. Messiner solution/state. If $\alpha < 0$, one can verify that

$$(\hat{u}, \nabla \times \hat{\mathbf{A}}) = (1, \mathbf{B}_0), \tag{4.24}$$

where $\mathbf{B}_0 = 0$ in Ω_s and $\mathbf{B}_0\Big|_{I\!R^3\setminus\Omega_s}$ is the unique solution to the following boundary value problem:

$$\begin{cases} \Delta \mathbf{B}_0 = 0 & \text{in } I\!R^3 \setminus \Omega_s, \\ \mathbf{B}_0 \cdot \mathbf{N} = 0 & \text{on } \partial\Omega_s, \\ \mathbf{B}_0 \to \hat{\mathbf{H}}^e & \text{as } |\mathbf{x}| \to +\infty. \end{cases} \tag{4.25}$$

Strictly speaking, the Messiner solution described by (4.24)-(4.25) does not fully satisfy the Ginzburg-Landau boundary value problems (4.21)-(4.22).

$$\hat{G}^s = |\Omega_s|\frac{1}{8\pi}|\hat{H}^e|^2(1+d)$$

3. Mixed state with a planar interface.

We seek a solution of the form

$$\hat{u} = \hat{u}(x), \qquad \hat{\mathbf{A}} = \hat{A}_y(x)\mathbf{e}_y,$$

and

$$(u, A_y') \to \begin{cases} (u_\infty, 0) & \text{as } x \to +\infty, \\ (0, H^e) & \text{as } x \to -\infty. \end{cases}$$

Then (4.21) can be written as

$$\begin{cases} \xi^2 \dfrac{d^2}{dx^2}\hat{u} + \hat{u} - \hat{u}^3 + \dfrac{\hat{u}\hat{A}_y^2}{8\pi\hat{\lambda}^2} = 0 & \forall\, x \in I\!R, \\ \lambda^2 \dfrac{d^2}{dx^2}\hat{A}_y = \hat{u}^2\hat{A}_y & \forall\, x \in I\!R, \end{cases}$$

We focus on the type II superconductor with $\lambda \gg \xi$.

4. No-vortex solution with transport supercurrent and at the absence of external magnetic field. There are two configurations of interest. The first is that the superconductor is a film of thickness t with transport current in $\mathbf{e}_y$ direction. In this case, we assume $\Omega_s = (0,t) \times I\!R^2$ and seek a solution satisfying

$$\hat{u} = \hat{u}(x), \qquad \hat{\mathbf{A}} = \hat{A}_y(x)\mathbf{e}_y, \qquad \frac{1}{t}\int_0^t \hat{A}_y(x) = J^0.$$

Then (4.21) can be written as

$$\begin{cases} \xi^2 \dfrac{d^2}{dx^2}\hat{u} + \hat{u} - \hat{u}^3 + \dfrac{\hat{u}\hat{A}_y^2}{8\pi\lambda^2} = 0 & \forall\, x \in I\!R, \\ \lambda^2 \dfrac{d^2}{dx^2}\hat{A}_y = \hat{u}^2\hat{A}_y & \forall\, x \in I\!R. \end{cases}$$

5. Single-vortex solution with no transport supercurrent.

We seek a solution of the form

$$u = u(r), \qquad \tilde{\mathbf{A}} = A_\theta(r)\mathbf{e}_\theta,$$

and

$$(u, (rA_\theta)'/r) \to \begin{cases} (u_\infty, 0) & \text{as } \ r \to +\infty, \\ (0, H^e) & \text{as } \ x \to 0. \end{cases}$$

Then (4.21) can be written as

$$\begin{cases} -\dfrac{\hbar^2}{2m^*}\dfrac{d}{rdr}r\dfrac{d}{dr}u + \alpha u + \beta u^3 + \dfrac{uA_\theta^2}{8\pi\hat{\lambda}^2} = 0 & \forall\, x \in I\!R, \\ \dfrac{d}{rdr}r\dfrac{d}{dr}A_\theta - \dfrac{A_\theta}{r^2} = \dfrac{u^2}{\hat{\lambda}^2}A_\theta & \forall\, x \in I\!R. \end{cases}$$

4.3 Interaction with paramagnetic inhomogeneity: no transport current

In this section we consider pinning interaction of a magnetic flux line to the interface of paramagnetic inhomogeneity without transport current. In the section 4.5, external transport current will be introduced to fulfill the picture of mechanism of interaction force.

The system of the pinning center considered shall be at dilute limit, which means that the system of pinning center (e.g., the inhomogeneity) is widely spaced so that the distortion of the vortex current due to any pinning center is at a low level comparing to its maximum value.

A heterogeneous superconducting thin film in the xy-plane is pieced by a columnar linear paramagentic inhomogeneities whose radius is R as shown in Fig. 4.1. The film consists of rectangle arrays with each unit includes one paramagnetic inhomogeneity. The thickness of film is t and lateral sizes of the film are L_x, L_y ($L_x, L_y \gg t$). For simplicity, neglecting the fringe effects we assume that order parameter ψ, magnetic field $\mathbf{B} = B_z\mathbf{e}_z$ and magnetization $\mathbf{M} = M_z\mathbf{e}_z$ inside the inhomogeneity are independent of $\mathbf{e}_z$ within the film.

If the size of unit cell is large comparing to the size of inhomogeneity and the distance between magnetic vortex and inhomogeneity, the periodic boundary condition shall degenerate into dilute limit. When there is no transport current appears in the thin film, we rewrite the total free energy in a unit cell as follows:

$$\begin{aligned} G[\psi, \mathbf{A}, \mathbf{M}; \mathbf{H}^e] =& t\int_{\tilde{\Omega}_s}\left[f_{n0} + \alpha|\psi|^2 + \frac{\beta}{2}|\psi|^4 + \frac{1}{2m^*}|(\frac{\hbar}{i}\tilde{\nabla} - \frac{e^*}{c}\mathbf{A})\psi|^2\right] \\ &+ \frac{t}{8\pi}\int_{\tilde{\Omega}}|\nabla\times\mathbf{A} - \mathbf{H}^e - 4\pi\mathbf{M}\chi_{\tilde{\Omega}_m}|^2 \\ &+ t\int_{\tilde{\Omega}_m}[\frac{a_{\text{ex}}}{2}|\tilde{\nabla}\mathbf{M}|^2 + \phi(\mathbf{M}) - \mathbf{H}^e\cdot\mathbf{M}], \end{aligned} \tag{4.26}$$

where $\tilde{\nabla}$ is planar vector differential operator, $\tilde{\Omega}_s$ denotes the planar superconductor region, $\tilde{\Omega}_m$ denotes the planar paramagnetic inhomogeneities, $\tilde{\Omega}$ is the union of $\tilde{\Omega}_s$ and $\tilde{\Omega}_m$, which represents the planar thin film composite.

Remark that there is no transport current and external electric field in the vacuum. Therefore, we can exclude $\nabla\times\mathbf{B}^{\text{sf}}$ in equation (4.26) due to Maxwell equations

$$\nabla\times\mathbf{B} = \nabla\times(\mathbf{H}^e + \mathbf{B}^{\text{sf}}) = \nabla\times\mathbf{B}^{\text{sf}} = \frac{4\pi}{c}\mathbf{J} + \frac{1}{c}\frac{\partial\mathbf{E}}{\partial t} = 0 \qquad \text{in } [\tilde{\Omega}\times(0,t)]^c. \tag{4.27}$$

Also the cross product term $\mathbf{A}^{\text{sf}}\times\mathbf{B}^{\text{sf}}$ is perpendicular to normal direction $\mathbf{n}$ on top and

bottom film surface, we have

$$\frac{1}{8\pi}\int_{\partial[\tilde{\Omega}\times(0,t)]^c}\mathbf{n}\cdot(\mathbf{A}^{\rm sf}\times\mathbf{B}^{\rm sf})=0. \tag{4.28}$$

We employ a planar model derived from total free energy of the unit cell in equation (4.26) by variational method, which implies the boundary value problem:

$$\begin{cases}\alpha\psi+\beta|\psi|^2\psi+\frac{1}{2m^*}(\frac{\hbar}{i}\tilde{\nabla}-\frac{e^*}{c}\mathbf{A})^2\psi=0 & \text{in } \tilde{\Omega}_s,\\ \tilde{\nabla}\times(\tilde{\nabla}\times\mathbf{A}-4\pi\mathbf{M}\chi_{\tilde{\Omega}_{\rm inh}})=\frac{4\pi}{c}\mathbf{J}_s\chi_{\tilde{\Omega}_s} & \text{in } I\!R^2,\\ \frac{\mu}{\mu-1}4\pi\mathbf{M}=\tilde{\nabla}\times\mathbf{A} & \text{in } \tilde{\Omega}_m,\end{cases} \tag{4.29}$$

subject to the boundary conditions

$$\begin{cases}\left[(\frac{\hbar}{i}\tilde{\nabla}-\frac{e^*}{c}\mathbf{A})\psi\right]\cdot\mathbf{N}=0 & \text{on } \partial\tilde{\Omega}_s,\\ [\![\tilde{\nabla}\times\mathbf{A}-\mathbf{M}]\!]\big|_{\Gamma_{sinh}}\times\mathbf{N}=0 & \text{on } \Gamma_{sinh},\\ |\tilde{\nabla}\times\mathbf{A}-\mathbf{H}^e|\to 0 & \text{as } |\mathbf{x}|\to\infty,\\ |\tilde{\nabla}\times\tilde{\nabla}\times\mathbf{A}|\to 0 & \text{as } |\mathbf{x}|\to\infty\chi_{\Omega_s}.\end{cases} \tag{4.30}$$

where supercurrent $\mathbf{J}_s$ is

$$\mathbf{J}_s=[\frac{\hbar e^*}{2m^*i}(\psi^*\tilde{\nabla}\psi-\psi\tilde{\nabla}\psi^*)-\frac{e^{*2}}{m^*c}\psi\psi^*\mathbf{A}] \qquad \text{in } \tilde{\Omega}_s. \tag{4.31}$$

Notice that the equation $(4.30)_4$ is given because no transport current passing through the thin film.

The equations (4.29) associated with boundary conditions (4.30) are well-posed boundary value problem. The free energy of the composite system can be obtained by multiplying the thickness of the thin film t over the planar energy. With an abuse of notation, by equation (4.16) we also rewrite the total free energy of the system in a form of planar model

$$G[u,\theta,\mathbf{M};\mathbf{A}^e]=\tilde{G}^s[u,\theta;\mathbf{A}^e]+\tilde{G}^m[\mathbf{M};\mathbf{A}^e]+\tilde{G}^{int}[u,\theta,\mathbf{M};\mathbf{A}^e]+G^{\rm sf}[u,\theta,\mathbf{M};\mathbf{A}^e]. \tag{4.32}$$

where

$$\tilde{G}^{s}[u,\theta;\mathbf{A}^{e}] = t\int_{\tilde{\Omega}_s}\Big[\frac{\hbar^2}{2m^*}|\nabla u|^2+\frac{\beta}{2}(u^2+\frac{\alpha}{\beta})^2+\frac{u^2}{8\pi\lambda^2}|-\mathbf{A}^{e}-\mathbf{A}^{\mathrm{sf}}+\frac{c\hbar}{e^*}\nabla\theta|^2\Big],$$
$$\tilde{G}^{m}[\mathbf{M};\mathbf{A}^{e}] = t\int_{\tilde{\Omega}_m}[\frac{a_{\mathrm{ex}}}{2}|\nabla\mathbf{M}|^2+\phi(\mathbf{M})+8\pi|\mathbf{M}|^2-\mathbf{H}^{e}\cdot\mathbf{M}],$$
$$\tilde{G}^{int}[u,\theta,\mathbf{M};\mathbf{A}^{e}] = -t\int_{\tilde{\Omega}_m}\mathbf{M}\cdot(\nabla\times\mathbf{A}^{\mathrm{sf}}),$$
$$G^{\mathrm{sf}}[u,\theta,\mathbf{M};\mathbf{A}^{e}] = \frac{1}{8\pi}\int_{I\!R^3}|\nabla\times\mathbf{A}^{\mathrm{sf}}|^2.$$

The self field energy term G^{sf} can be rewritten by *Divergence Theorem* as

$$\begin{aligned}G^{\mathrm{sf}} =&\frac{1}{8\pi}\int_{I\!R^3}|\nabla\times\mathbf{A}^{\mathrm{sf}}|^2\\ =&\frac{t}{8\pi}\int_{\tilde{\Omega}}|\nabla\times\mathbf{A}^{\mathrm{sf}}|^2+\frac{1}{8\pi}\int_{\partial[\tilde{\Omega}\times(0,t)]^c}\mathbf{n}\cdot(\mathbf{A}^{\mathrm{sf}}\times\mathbf{B}^{\mathrm{sf}})+\frac{1}{8\pi}\int_{[\tilde{\Omega}\times(0,t)]^c}(\nabla\times\mathbf{B}^{\mathrm{sf}})\cdot\mathbf{A}^{\mathrm{sf}}.\end{aligned} \tag{4.33}$$

In this case there is no transport current and electric field in the vacuum. This allows us to exclude the last term in equation (4.33) due to Maxwell equations

$$\nabla\times\mathbf{B}=\nabla\times(\mathbf{H}^{e}+\mathbf{B}^{\mathrm{sf}})=\nabla\times\mathbf{B}^{\mathrm{sf}}=\frac{4\pi}{c}\mathbf{J}+\frac{1}{c}\frac{\partial\mathbf{E}}{\partial t}=0 \qquad \text{in } [\tilde{\Omega}\times(0,t)]^c. \tag{4.34}$$

For the second term in the equation (4.33), the cross product term $\mathbf{A}^{\mathrm{sf}}\times\mathbf{B}^{\mathrm{sf}}$ is perpendicular to normal direction $\mathbf{n}$ on top and bottom film surface. Hence, the self field energy term is written as

$$G^{\mathrm{sf}}[u,\theta,\mathbf{M};\mathbf{A}^{e}]=\tilde{G}^{\mathrm{sf}}[u,\theta,\mathbf{M};\mathbf{A}^{e}]=\frac{t}{8\pi}\int_{\tilde{\Omega}}|\nabla\times\mathbf{A}^{\mathrm{sf}}|^2. \tag{4.35}$$

4.3.1 A single vortex at the vicinity of an inhomogeneity at dilute limit

In this section, our interest is to investigate the interaction force of individual flux line to the interface of a single paramagnetic inhomogeneity at dilute system and thermal equabilium state at low magnetic fields, which is close to the lower critical field H_{c1} for type II superconductor. One linear paramagnetic columnar inhomogeneity embedded by the superconductor matrix is modeled. The schematic diagram is shown in Fig. 4.3.1.

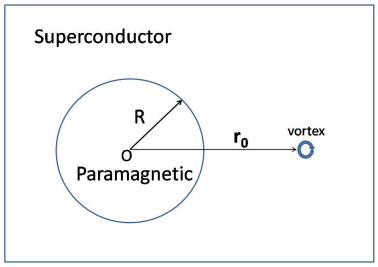

Figure 4.2: Schematic diagram

Depending on the governing equations (4.29) associated with the boundary conditions (4.30), our strategy to compute the vortex pinning force due to the existance of paramagnetic inhomogeneity is as follows:

1. Using a standard free-boundary trial solution of individual magnetic vortex to derive well-posed near-field governing equations of vector potential. Show that the magnetization of the inhomogeneity is uniform by *Coulomb* gauge under our assumption.

2. Obtain an approximated solution of magnetic field $\mathbf{B}$ in terms of unknown uniform magnetization $\mathbf{M}$.

3. Rewrite the total free energy of the system in terms of the position vector of the vortex.

4. In principle of minimum free energy in the equilibrium state, find the unknown magnetization $\mathbf{M}$ and then determine the effective total free energy of the system.

5. Differentiate the total free energy with respect to the position vector of vortex to derive the pinning force.

In particular, for thin film, the absolute value of order parameter ψ, or say the density of superconducting electrons, has the same value everywhere inside the superconducting phase region. This is because the variation of $|\psi|$ would occur in a thin thickness so that the term in the free energy proportional to $(\nabla|\psi|)^2$ would provide an excessively large contribution if any substantial variations occurred. In dilute limit, a single vortex will appear in the superconductor region when the external field H^e reaches the critical field $H_{c1} = \frac{\Phi_0}{4\pi\lambda^2}$,

where Φ_0 is single fluxoid and $\lambda = \sqrt{\frac{m^* c^2 \beta}{4\pi e^{*2}(-\alpha)}}$ is the penetration depth. For simplicity, we consider trial solution to a single vortex in the superconducting phase at $\mathbf{r}_0$ with the order parameter given by

$$\psi = |\psi_0| f(\mathbf{r} - \mathbf{r}_0) e^{i\theta_c} \qquad \text{in } \tilde{\Omega}_s, \tag{4.36}$$

where $|\psi_0|$ is a constant value, function $f(\mathbf{r}) \approx \tanh \frac{|\mathbf{r}|}{\xi}$ will decay to one exponentially by the coherence length ξ away from the vortex center (Tinkham, 1975). This solution is axial symmetric. And based on the fact that the phase of ψ varies by 2π in making a complete circuit, corresponding to the existence of a single flux quantum associated with the vortex, equation (4.29) $_2$ can be simplified as

$$\tilde{\nabla} \times (\tilde{\nabla} \times \mathbf{A} - 4\pi \mathbf{M} \chi_{\tilde{\Omega}_m}) = [\frac{4\pi\hbar e^*}{m^* c} f^2(\mathbf{r} - \mathbf{r}_0) |\psi_0|^2 \tilde{\nabla}\theta_c - \frac{1}{\lambda^2}\mathbf{A}] \chi_{\tilde{\Omega}_s} \qquad \text{in } I\!R^2 \setminus \tilde{\Omega}_{\text{co}}, \tag{4.37}$$

where $\tilde{\Omega}_{\text{co}}$ is planar normal core region.

The vector potential $\mathbf{A}$ shall be determined by the governing equations (4.29)

$$\begin{cases} \tilde{\nabla} \times (\tilde{\nabla} \times \mathbf{A} - 4\pi \mathbf{M} \chi_{\tilde{\Omega}_m}) = [\frac{4\pi\hbar e^*}{m^* c} f^2(\mathbf{r} - \mathbf{r}_0) |\psi_0|^2 \tilde{\nabla}\theta_c - \frac{1}{\lambda^2}\mathbf{A}] \chi_{\tilde{\Omega}_s} & \text{in } \tilde{\Omega} \setminus \tilde{\Omega}_{\text{co}}, \\ \frac{\mu}{\mu - 1} 4\pi \mathbf{M} = \tilde{\nabla} \times \mathbf{A} & \text{in } \tilde{\Omega}_m \end{cases} \tag{4.38}$$

subject to boundary conditions

$$\begin{cases} [\![\tilde{\nabla} \times \mathbf{A} - \mathbf{M}]\!]\big|_{\Gamma_{sinh}} \times \mathbf{N} = 0 & \text{on } \Gamma_{\text{sinh}}, \\ |\tilde{\nabla} \times \tilde{\nabla} \times \mathbf{A}| \to 0 & \text{as } |\mathbf{x}| \to \infty \chi_{\Omega_s}. \end{cases} \tag{4.39}$$

Now we write the above boundary value problem in terms of magnetic field $\mathbf{B}$. This is because inside the composite thin film, magntic field $\mathbf{B}$ only has one component and it is convenient for us to obtain an approximate solution under our planar assumption.

The first equation in (4.38) can be manipulated by take curl operation on both sides as

$$\begin{aligned}\tilde{\nabla}\times\tilde{\nabla}\times(\tilde{\nabla}\times\mathbf{A}-4\pi\mathbf{M}\chi_{\tilde{\Omega}_m}) = [\nabla\times\frac{4\pi\hbar e^*}{m^*c}f^2(\mathbf{r}-\mathbf{r}_0)|\psi_0|^2\tilde{\nabla}\theta_c \\ -\frac{1}{\lambda^2}\nabla\times\mathbf{A}]\chi_{\tilde{\Omega}_s} \quad \text{in } I\!R^2\setminus\tilde{\Omega}_{\text{co}},\end{aligned} \tag{4.40}$$

We use a two-dimensional delta function δ at the location of the core to replace the first term in the right hand side in the above equation as an approximate form. This kinds of approximation let the equation degenerate into London equation and core structure would be ignored and the equation shall be expressed as

$$\tilde{\nabla}^2\mathbf{B}+4\pi\tilde{\nabla}\times\tilde{\nabla}\times\mathbf{M}\chi_{\tilde{\Omega}_m} = [-\frac{\Phi_0\delta_2(\mathbf{r}-\mathbf{r}_0)\mathbf{e}_z}{\lambda^2}+\frac{1}{\lambda^2}\mathbf{B}]\chi_{\tilde{\Omega}_s} \qquad \text{in } I\!R^2\setminus\partial\tilde{\Omega}_{\text{co}}. \tag{4.41}$$

Another point is that magnetic field in the inhomogeneity is uniform based on *Coulomb* gauge under our planar model. Vector potential $\mathbf{A}$ will only has nonzero components A_x and A_y for the reason that magnetic field $\mathbf{B}$ is independent of z within the film and has only nonzero component along $\mathbf{e}_z$ direction. Therefore, we can prescribe vector potential $\mathbf{A}$ has only $\mathbf{e}_x$ and $\mathbf{e}_y$ component, $\mathbf{A}=(A_x(x,y),A_y(x,y),0)$.

Without loss of generality, we choose *Coulomb* gauge for the vector potential $\mathbf{A}$:

$$\tilde{\nabla}\cdot\mathbf{A}=0. \tag{4.42}$$

We introduce a scalar function $\phi(x,y)$ that satisfies the *Coulomb* gauge to replace the vector potential $\mathbf{A}$ by

$$A_x=\phi_{,y}, \qquad A_y=-\phi_{,x}. \tag{4.43}$$

Notice that magnetic field $\mathbf{B}=\tilde{\nabla}\times\mathbf{A}=B_z\mathbf{e}_z=\tilde{\Delta}\phi\mathbf{e}_z$, since there is no current in the inhomogeneity, according to Maxwell equation, we can show that

$$\nabla\times\mathbf{B}=\tilde{\nabla}\times(\tilde{\Delta}\phi\mathbf{e}_z)=(\tilde{\Delta}\phi)_{,x}\mathbf{e}_x+(\tilde{\Delta}\phi)_{,y}\mathbf{e}_y=0 \qquad \text{in } \tilde{\Omega}_m. \tag{4.44}$$

which implies that $\tilde{\Delta}\phi$ in the inhomogeneity is a constant, or say magnetic field $\mathbf{B}$ in

the inhomogeneity is uniform. To seek the solution of magnetic field $\mathbf{B}$, we prescribe a uniform magnetization $\mathbf{M} = M\mathbf{e}_z$ within the paramagnetic inhomogeneity $\tilde{\Omega}_m$. Now that the uniform magnetic field $\mathbf{B}$ in the paramagentic inhomogeneity can be expressed in terms of magnetization $\mathbf{M}$ as

$$\mathbf{B} = \frac{\mu}{\mu - 1} 4\pi \mathbf{M} \qquad \text{in } \tilde{\Omega}_m. \tag{4.45}$$

Applying the boundary condition $(4.38)_3$ on the interface Γ_{sinh}, we find the magnetic field on the interface on the side of superconductor region shall satisfy

$$\mathbf{B}|_{\Gamma_{\text{sinh}+}} = \frac{1}{\mu - 1} 4\pi \mathbf{M} \qquad \text{on } \Gamma_{\text{sinh}+}, \tag{4.46}$$

where $\Gamma_{\text{sinh}+}$ is the interface between the superconductor and paramagentic inhomogeneity on superconductor side.

We anticipate magnetic field governed by (4.38) shall decay exponentially away from the inhomogeneity $\tilde{\Omega}_m$ and vortex at $\mathbf{r}_0$. Neglecting the fringe effect, in London limit $\kappa \to \infty$, the magnetic field $\mathbf{B}$ in the superconductor region $\tilde{\Omega}_m$ can be safely approximated by the solution to the following boundary value problem:

$$\begin{cases} -\frac{1}{\lambda^2}\mathbf{B} + \tilde{\nabla}^2 \mathbf{B} = -\frac{\Phi_0 \delta_2(\mathbf{r} - \mathbf{r}_0)\mathbf{e}_z}{\lambda^2} & \text{in } I\!R^2 \setminus \tilde{\Omega}_{\text{inh}}, \\ \mathbf{B} = \frac{1}{\mu - 1} 4\pi \mathbf{M} & \text{on } \Gamma_{\text{sinh}+}, \end{cases} \tag{4.47}$$

subject to the boundary condition

$$\mathbf{B} \to 0 \quad \text{ at } \infty \chi_{\tilde{\Omega}_s}. \tag{4.48}$$

Notice that for dilute system, far away from the vortex in the superconductor region, the magnetic field $\mathbf{B}$ is screened. This is represented in equation (4.48). In addition, equation $(4.47)_1$ is usually called the modified London equation.

The single vortex is represented by a source term using δ function. Because of the

existence of the paramagnetic inhomogeneity, supercurrent is distorted. It is not easy to get the accurate analytic solution for the boundary value problem (4.47) in a closed form. However, we can obtain an approximate solution in the cylindrical coordinate system (r,θ,z) as follows (see *Appendix* 4.7.2 for details)

$$\mathbf{B}=\begin{cases}\frac{4\pi M^p}{\mu-1}\frac{K_0(|\frac{\mathbf{r}}{\lambda}|)}{K_0(\frac{R}{\lambda})}\mathbf{e}_z+\frac{\Phi_0}{2\pi\lambda^2}K_0(|\frac{\mathbf{r}-\mathbf{r}_0}{\lambda}|)\mathbf{e}_z+\Big[\frac{1}{K_0(\frac{R}{\lambda})}\frac{1}{\pi}\int_0^\pi Q(\theta)\mathrm{d}\theta\Big]K_0(|\frac{\mathbf{r}}{\lambda}|)\mathbf{e}_z+ & \\ \Big[\frac{1}{K_1(\frac{R}{\lambda})}\frac{2}{\pi}\int_0^\pi Q(\theta)\cos\theta\mathrm{d}\theta\Big]K_1(|\frac{\mathbf{r}}{\lambda}|)\cos\theta\mathbf{e}_z & \text{in } \tilde{\Omega}_s, \\ \frac{\mu}{\mu-1}4\pi M^p\mathbf{e}_z & \text{in } \tilde{\Omega}_m.\end{cases} \tag{4.49}$$

where

$$Q(\theta)=-\frac{\Phi_0}{2\pi\lambda^2}K_0(|\frac{\sqrt{R^2+|\mathbf{r}_0|^2-2R|\mathbf{r}_0|\cos\theta}}{\lambda}|),\qquad \mathbf{r}_0=\mathbf{r}_0(R+d,0,0). \tag{4.50}$$

$K_0(K_1)$ is the zeroth(first)-order of modified Bessel function of the second kind. Remark that the solution of magnetic field $\mathbf{B}$ is not accurate near the core region, we need a cut-off to make an approximation. The core energy is almost independent of the position of vortex under our assumption, it does not play an important role in the magnetic energy associated with paramagnetic boundary.

4.3.2 Vortex energy associated with magnetic field and pinning force to paramagnetic boundary in the dilute limit

To determine the total free enengy in the dilute limit, the magnetization $\mathbf{M}$ shall be solved by the minimum principle of free energy. Then the profile of the magnetic field can be obtained. Moreover, we can calculate the pinning force of the single vortex due to distortion of supercurrent changed by the effect of inhomogeneity.

Applying *Divergence Theorem*, the total free energy can be decomposed as follows:

$$G=T1+T2+T3+T4+T5+T6, \tag{4.51}$$

where Ti $(i = 1, ..., 6)$ are integrals given by

$$
\begin{aligned}
T1 &= t \int_{\tilde{\Omega}_s} \Big[f_{n0} + \frac{\beta}{2}(u^2 + \frac{\alpha}{\beta})^2 - (\frac{\alpha}{\beta})^2 \Big], \\
T2 &= \frac{t}{8\pi} \int_{\tilde{\Omega}_s} |\mathbf{B}| \Phi_0 \delta_2(\mathbf{r} - \mathbf{r}_0) dS, \\
T3 &= t \oint_{\partial \tilde{\Omega}_{\text{sinh}}} \frac{\lambda^2}{8\pi} \mathbf{B} \times (\nabla \times \mathbf{B}) \cdot d\mathbf{s}, \\
T4 &= t \int_{\tilde{\Omega}_m} (\frac{2\pi}{\mu - 1} + 8\pi)(\frac{\mu - 1}{4\pi\mu} \mathbf{B})^2 - \mathbf{M} \cdot \mathbf{H}^e, \\
T5 &= -t \int_{\tilde{\Omega}_m} \mathbf{M} \cdot (\mathbf{B} - \mathbf{H}^e), \\
T6 &= \frac{t}{8\pi} \int_{\tilde{\Omega}_m} |\mathbf{B} - \mathbf{H}^e|^2.
\end{aligned}
$$

The first three terms $T1 + T2 + T3$ is superconducting free energy including the kinetic energy in the superconducting domain. We shall notice that $T1$ is an unchanged with fixed location of magnetic vortex $\mathbf{r}_0$ under the thermal equilibrium condition. $T2$ is the estimation of the core energy and it is independent of the location of the vortex $\mathbf{r}_0$. $T3$ is the free energy with integral on the interface of paramagnetic inhomogeneity derived by *Divergence theorem*. $T4$ represents the free energy induced by magnetization in the inhomogeneity. $T5$ indicates the interaction energy between magnetization and magnetic self field. And $T6$ is the self field energy in the paramagnetic inhomogeneity.

Through the above argument, we can ignore Ti(i=1,2) in equation (4.51) in the calculation of the pinning force because these two terms are independent of the position of vortex. Keeping the terms Ti(i=3,4,5,6), we treat them as the effective total free energy of the system

$$
G^{\text{eff}}(\mathbf{r}_0) = T3 + T4 + T5 + T6. \tag{4.52}
$$

To determine the total free enengy in terms of the magnetic field in dilute limit, the magnetization $\mathbf{M}$ can be solved by the minimum principle of free energy. In the principle of minimum energy for the equilibrium state of the system, we can minimize G^{eff} against

the magnetization $\mathbf{M}$ so that $\mathbf{M}$ could be solved by

$$\frac{\partial G^{\text{eff}}(M)}{\partial M} = 0. \tag{4.53}$$

Once the magnetization $\mathbf{M}$ is obtained, the profile of the magnetic field $\mathbf{B}$ and the effective total free energy G^{eff} are determined and only depend on the external field $\mathbf{H}^e$, the permeability of the paramagnetic inhomogeneity μ and the radius of the inhomogeneity R. The pinning force F associated with the position vector $\mathbf{r}_0(R+d,0,0)$ is given by

$$F(\mathbf{r}_0) = -\frac{\partial G^{\text{eff}}}{\partial d}\mathbf{e}_r, \tag{4.54}$$

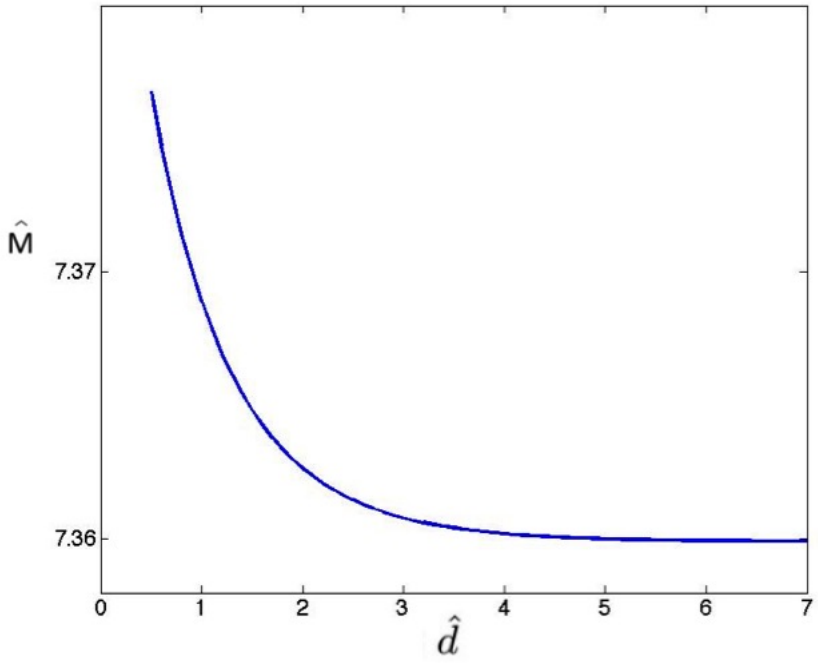

Figure 4.3: Dimensionless magnetization $\hat{M}$ in the paramagnetic domain versus the position of vortex $\hat{d}$. The radius of the inhomogeneity $\hat{R} = 0.2$, the magnetic permeability of the paramagnetic inclusion $\mu = 100$ and the external magnetic field strength $\hat{H}^e = 1$.

To simplify the calculation, we nondimensionalize the parameters in the following table 4.1 so that we can avoid to consider the penetration length of superducting materials

Table 4.1: Dimensionless variables I

Dimensionless Variable	$\hat{R}$	$\hat{\mathbf{r}_0}$	$\hat{d}$	$\hat{M}$	$\hat{H}^e$	$\hat{G}^{\text{eff}}$
Variable	R/λ	$\mathbf{r}_0/\lambda$	d/λ	$M/(\frac{\Phi_0}{2\pi\lambda^2})$	$H^e/(\frac{\Phi_0}{2\pi\lambda^2})$	$G^{\text{eff}}/\frac{\Phi_0^2}{16\pi^2\lambda^2}$

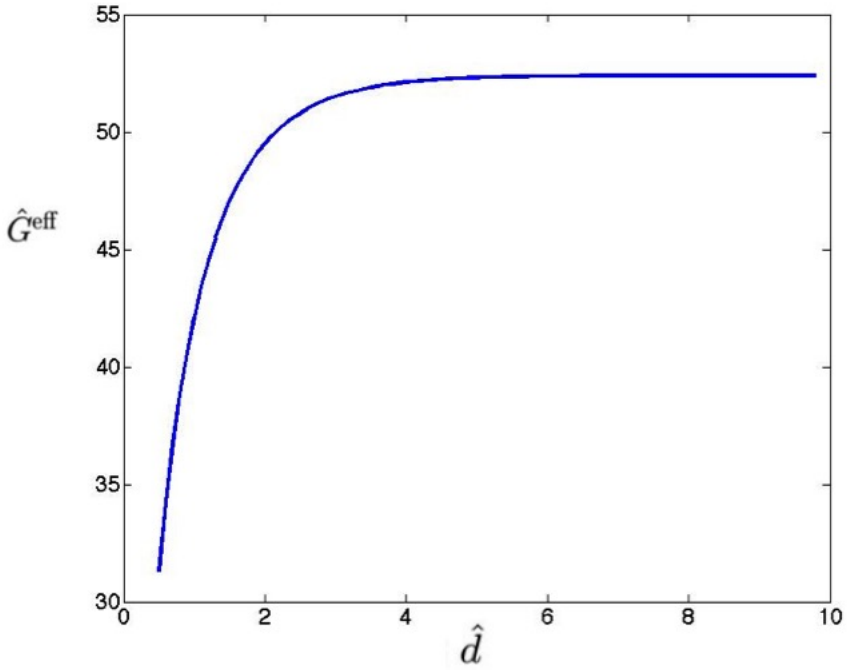

Figure 4.4: Dimensionless effective total free energy $\hat{G}^{\text{eff}}$ versus the position of vortex $\hat{d}$. The radius of the inhomogeneity $\hat{R} = 0.2$. The magnetic permeability of the paramagnetic inclusion $\mu = 100$. And the external magnetic field strength $\hat{H}^e = 1$.

4.3.3 Results

Figure. 4.3 shows the magnetization $\mathbf{M}$ depends on the distance of the vortex to the interface. We can see that the uniform magnetization $\mathbf{M}$ is enhanced as the vortex approaches the interface. The enhanced magnetization $\mathbf{M}$ results in two effects on the total free energy of system. Firstly, the Zeeman energy of the paramagnetic inhomogeneity will reduce. Secondly, the line energy of the vortex decreases due to the change of the profile of magnetic field $\mathbf{B}$ in equation (4.49).

The effective total free energy of the system versus the distance between the magnetic vortex to the interface of inhomogeneity is shown in the Fig. 4.5. Energy decreases when vortex is close to the interface. This trendency will cause an attractive force between

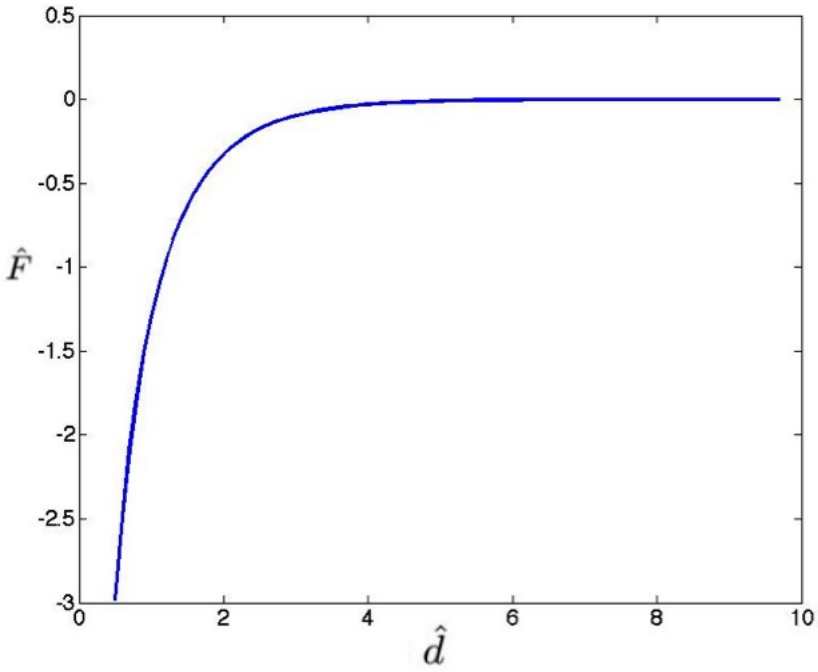

Figure 4.5: Dimensionless pinning force $\hat{F}$ versus the position of vortex $\log_{10}\hat{d}$. The radius of the inhomogeneity $\hat{R} = 0.2$. The magnetic permeability of the paramagnetic inclusion $\mu = 100$. And the external magnetic field strength $\hat{H}^e = 1$.

magnetic vortex and interface of inhomogeneity.

In Fig. 4.6, Fig. 4.7 and Fig. 4.8, we can see the pinning force of vortex depends on the size of inhomogeneity $\hat{R}$, external magnetic field $\hat{H}^e$ and magnetic permeability of paramagnetic inhomogeneity μ. In Fig. 4.6, pinning force shows attraction to the interface and is enhanced with large radius $\hat{R}$ of the inhomogeneity. The magnitude of the pinning force will decay to a zero when the distance $\hat{d}$ is away from the interface. Another conclusion that can be drawn is the dependence of the pinning force on the external magnetic field $\hat{H}^e$ and magnetic permeability μ. The higher external magnetic field and magnetic permeability, the stronger is the pinning force. More details will be discussed in section 4.5.

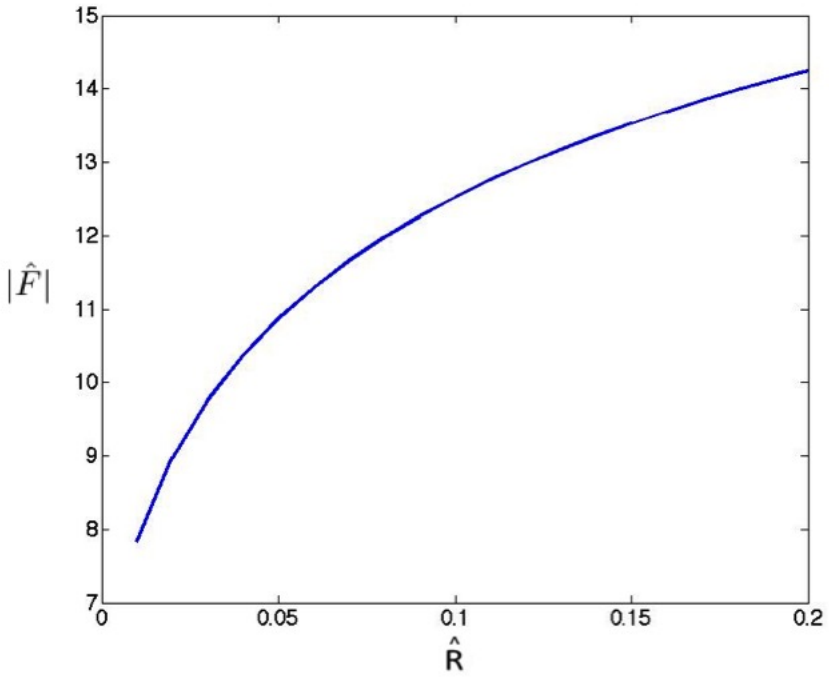

Figure 4.6: Dimensionless pinning force versus the position of vortex depends on the radius of the inclusion $\hat{R}$. The magnetic permeability of the paramagnetic inclusion $\mu = 1$, the external magnetic field strength $\hat{H}^e = 1$.

4.4 Driving force on a single vortex with transport current: derivation of Lorentz force in thin film

When external transport currents pass through the superconducting thin film, velocity of electrons varies along the thickness direction and an in-plane magnetic field will be generated. Therefore, a planar model (4.32) does not work anymore. In this section, we study a simple scenario: interaction force on a single vortex in an infinit pure superconducting thin film when a uniform external transport current exists at infinity.

4.4.1 Current density near vortex core area

Consider an external uniform transport current with density $j_0\mathbf{e}_y$ far away from the vortex core area. Transport current cannot penetrate into vortex core and only has tangential component on the vortex interface. Transport current density $\mathbf{J}_t : \Omega_s \to \mathbb{C}$ shall satisfy the

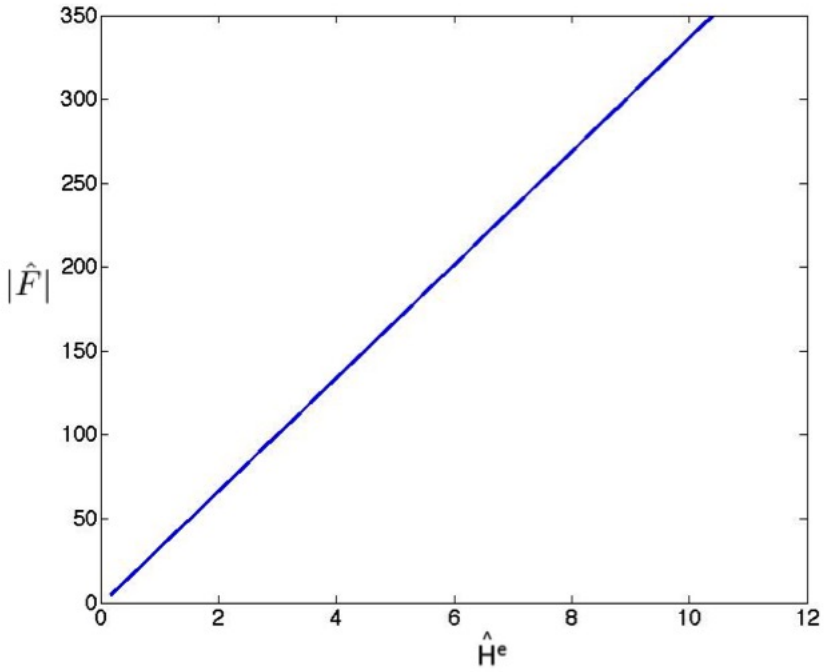

Figure 4.7: Dimensionless interaction force versus the position of vortex depends on the external magnetic field strength $\hat{H}^e$. The magnetic permeability of the paramagnetic inclusion $\mu = 100$, the radius of the columnar inhomogeneity $\hat{R} = 0.2$.

following boundary value problem based on the GL equation:

$$\lambda^2 \Delta \mathbf{J}_t - \mathbf{J}_t = 0 \qquad \text{in } \tilde{\Omega}_s \times (0, t), \tag{4.55}$$

subjects to the boundary conditions

$$\begin{cases} \mathbf{J}_t \cdot \mathbf{n} = 0 & \text{on } \partial\Omega_{\text{co}}, \\ \fint_{\text{end}} \mathbf{J}_t = j_0 \mathbf{e}_y & \text{at } \infty. \end{cases} \tag{4.56}$$

In the above three-dimensional problem, we infer that the solution to the boundary value problem satisfies

$$\mathbf{J}_t = j_p(z)(-\frac{\xi^2}{r^2}\sin 2\theta, 1 + \frac{\xi^2}{r^2}\cos 2\theta, 0), \tag{4.57}$$

$$where \qquad j_p(z) = C\frac{e^{z/\lambda} + e^{-z/\lambda}}{2}, \tag{4.58}$$

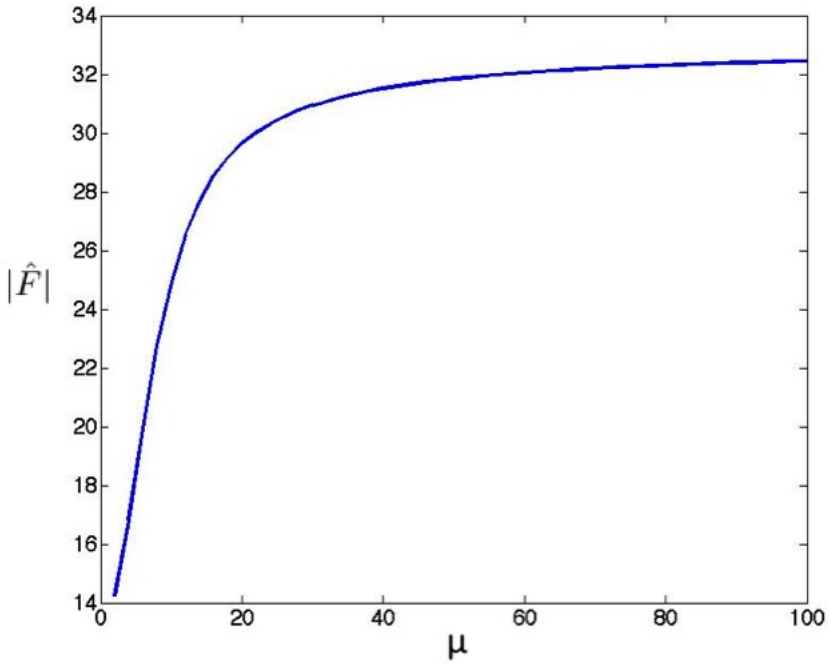

Figure 4.8: Dimensionless interaction force versus the position of vortex depends on the magnetic permeability of the paramagnetic inclusion μ. The external magnetic field strength $\hat{H}^e = 1$, the radius of the columnar inhomogeneity $\hat{R} = 1$.

where coherence length ξ is characteristic length of vortex core, C is a constant determined by j_0 and film thickness t (see *Appendix* 4.7.3 for details). We can easily observe that transport current density is hypobolic tangent distributed in thickness direction away from the vortex.

4.4.2 Free energy and Lorentz force

Denote by vector potential $\mathbf{A}_t$ induced by the transport supercurrent $\mathbf{J}_t : \Omega_s \to \mathbb{C}$ and vector potential $\mathbf{A}_v$ induced by a single vortex at location $\mathbf{r}_0$. The total magnetic vector potential $\mathbf{A}_{\text{tot}}$ consists of the above two terms:

$$\mathbf{A}_{\text{tot}} = \mathbf{A}_t + \mathbf{A}_v. \tag{4.59}$$

From the prior discussion, we see that $\mathbf{A}_t$ and $\mathbf{A}_v$ satisfy that [1]

$$\nabla \times \nabla \times \mathbf{A}_t = \frac{4\pi}{c}\mathbf{J}_t\chi_{\Omega_s} \qquad \text{in } I\!R^3, \tag{4.60}$$

and

$$\begin{cases} \nabla \times \nabla \times \mathbf{A}_v = [\frac{4\pi\hbar e^*}{m^*c} f^2(\mathbf{r}-\mathbf{r}_0)|\psi_0|^2\nabla\theta_c - \frac{1}{\lambda^2}\mathbf{A}_v]\chi_{\Omega_s} & \text{in } I\!R^3\backslash\Omega_{co}, \\ \nabla \times \mathbf{A}_v \to 0 & \text{as } |\mathbf{x}| \to +\infty, \end{cases} \tag{4.61}$$

respectively. In addition, according to the total free energy (4.1) deduced from section 4.2, the total free energy can be written as

$$G = G_{\text{nc}} + G_{\text{co}}, \tag{4.62}$$

where G_{nc} is the free energy outside vortex core and G_{co} is the free energy associated with vortex core, which we are not interested in and treat it as a constant value.

The free energy G_{nc} is given by

$$G_{\text{nc}} = \int_{\Omega_s\backslash\Omega_{\text{co}}} \left[f_{n0} + \alpha|\psi|^2 + \frac{\beta}{2}|\psi|^4 + \frac{1}{8\pi}(\frac{4\pi}{c})^2\lambda^2\mathbf{J}^2\right] + \frac{1}{8\pi}\int_{I\!R^3\backslash\Omega_{\text{co}}} |\nabla \times \mathbf{A}^{\text{sf}}|^2, \tag{4.63}$$

Remark that we assume the variation of density of superconducting electrons $|\psi|^2$ is constant.

The last term in equation (4.63) represents the free energy associated with self field and

[1] $(\mathbf{A}_t)_{,y} \to 0$ as $|y| \to +\infty$ and $|\nabla\mathbf{A}_t| \to 0$ as $|x| + |z| \to +\infty$.

it can be manipulated as

$$\begin{aligned}\int_{\mathbb{R}^3\setminus\Omega_{co}} |\nabla\times\mathbf{A}^{\mathrm{sf}}|^2 &= \int_{\mathbb{R}^3\setminus\Omega_{co}} |\nabla\times\mathbf{A}_t+\nabla\times\mathbf{A}_v-\nabla\times\mathbf{A}^e|^2\\ &= \int_{\mathbb{R}^3\setminus\Omega_{co}} |\nabla\times\mathbf{A}_t|^2+|\nabla\times\mathbf{A}_v|^2+|\nabla\times\mathbf{A}^e|^2\\ &+2\int_{\partial\Omega_s}\mathbf{n}\cdot[\![(\mathbf{A}_v\times(\nabla\times\mathbf{A}_t))]\!]\\ &+2\int_{\Omega_s\setminus\Omega_{co}}(\nabla\times(\nabla\times\mathbf{A}_t))\cdot\mathbf{A}_v\\ &= \int_{\mathbb{R}^3\setminus\Omega_{co}} |\nabla\times\mathbf{A}_t|^2+|\nabla\times\mathbf{A}_v|^2+|\nabla\times\mathbf{A}^e|^2\\ &+2\int_{\partial\Omega_s}\mathbf{n}\cdot[\![(\mathbf{A}_v\times(\nabla\times\mathbf{A}_t))]\!]+2\int_{\Omega_s\setminus\Omega_{co}}\frac{4\pi}{c}\mathbf{J}_t\cdot\mathbf{A}_v.\end{aligned} \tag{4.64}$$

Therefore, the free energy G_{nc} is

$$G_{nc}=G_s+G_m+G_b+\frac{1}{c}\int_{\Omega_s\setminus\Omega_{co}}\mathbf{J}_t\cdot\mathbf{A}_v, \tag{4.65}$$

where

$$G_s=\int_{\Omega_s}\left[f_{n0}+\alpha|\psi|^2+\frac{\beta}{2}|\psi|^4\right]+\frac{1}{8\pi}(\frac{4\pi}{c})^2\int_{\Omega_s}\lambda^2\mathbf{J}^2, \tag{4.66}$$

$$G_m=\frac{1}{8\pi}\int_{\mathbb{R}^3\setminus\Omega_{co}}|\nabla\times\mathbf{A}_t|^2+|\nabla\times\mathbf{A}_v|^2+|\nabla\times\mathbf{A}^e|^2, \tag{4.67}$$

$$G_b=\frac{1}{4\pi}\int_{\partial\Omega_s}\mathbf{n}\cdot[\![(\mathbf{A}_v\times(\nabla\times\mathbf{A}_t))]\!]. \tag{4.68}$$

G_s is the superconducting energy associated with kinetic part, G_m is the magnetic field energy associated with transport current, vortex current and external field and G_b is the free energy associated with the interface. They are all independent of position of vortex $\mathbf{r}_0$.

Taking the gradient of free energy with respect to $\mathbf{r}_0$, the interaction force F is

$$F=-\nabla_{\mathbf{r}_0}G=-\frac{1}{c}\int_{\Omega_s\setminus\Omega_{co}}\nabla_{\mathbf{r}_0}(\mathbf{J}_t\cdot\mathbf{A}_v)\mathrm{d}\mathbf{r}. \tag{4.69}$$

Notice that transport current $\mathbf{J}_t$ and vector potential $\mathbf{A}_v$ are the functions of $|\mathbf{r}-\mathbf{r}_0|$, resulting in $\nabla_{\mathbf{r}_0}=-\nabla_{\mathbf{r}}$.

Applying *Divergence Theorem*, equation (4.69) can be rewritten as

$$\begin{aligned} F &= \frac{1}{c}\int_{\Omega_s\backslash\Omega_{co}} \nabla_{\mathbf{r}}(\mathbf{J}_t\cdot\mathbf{A}_v)\mathrm{d}\mathbf{r}, \\ &= \frac{1}{c}\int_{\partial(\Omega_s\backslash\Omega_{co})} \mathbf{n}(\mathbf{J}_t\cdot\mathbf{A}_v)\mathrm{d}\mathbf{r}. \end{aligned} \tag{4.70}$$

Since vector potential $\mathbf{A}_v$ decays to zero exponentially, it results in the line integral over the exterior boundary is zero. Therefore, we only need calculate the interior boundary intergral.

By the solution of governing equation (4.61) using the similar technique in section 4.3, vector potential $\mathbf{A}_v$ has an approximate expression

$$\mathbf{A}_v = (\mathbf{A}_{vx}, \mathbf{A}_{vy}), \tag{4.71}$$

where

$$\mathbf{A}_{vx} = \frac{\Phi_0}{8\pi^2\lambda^2}\int\int -\frac{1}{|\mathbf{r}-\mathbf{r}_0|}\frac{\partial}{\partial y_0}|\frac{\mathbf{r}_0}{\lambda}|\mathrm{d}\mathbf{r}_0, \quad \mathbf{A}_{vy} = \frac{\Phi_0}{8\pi^2\lambda^2}\int\int \frac{1}{|\mathbf{r}-\mathbf{r}_0|}\frac{\partial}{\partial x_0}|\frac{\mathbf{r}_0}{\lambda}|\mathrm{d}\mathbf{r}_0. \tag{4.72}$$

The interaction force is

$$F = (F_x, F_y) \tag{4.73}$$

where $F_x = \frac{1}{c}\int_0^t\int_{\partial(\tilde{\Omega}_s\backslash\tilde{\Omega}_{co})} J_y(-A_{vx}n_y + A_{vy}n_x)\mathrm{d}S\mathrm{d}z$ and $F_y = \frac{1}{c}\int_0^t\int_{\partial(\tilde{\Omega}_s\backslash\tilde{\Omega}_{co})} J_x(A_{vx}n_y - A_{vy}n_x)\mathrm{d}S\mathrm{d}z$.

According to the solution of current density given in the equation (4.96), the component of interaction force F_y along $\mathbf{e}_y$ direction can be written as

$$\begin{aligned} F_y &= \frac{1}{c}\int_0^t j_p(z)\int_{\partial(\tilde{\Omega}_s\backslash\tilde{\Omega}_{co})} \frac{\xi^2}{r^2}\big|_{r=\xi}\cos 2\theta(A_{vx}n_y - A_{vy}n_x)\mathrm{d}S\mathrm{d}z \\ &= \frac{1}{c}\int_0^t j_p(z)\int_{\partial(\tilde{\Omega}_s\backslash\tilde{\Omega}_{co})} \frac{\Phi_0\cos 2\theta}{8\pi^2\lambda^2}[\int\int -\frac{1}{|\mathbf{x}-\mathbf{x}_0|}\frac{\partial}{\partial|\mathbf{x}_0|}(K_0|\frac{\mathbf{x}_0}{\lambda}|)\frac{1}{2|\mathbf{x}_0|^{\frac{1}{2}}}\mathrm{d}\mathbf{x}_0]\big|_{|\mathbf{x}|=\xi}\mathrm{d}S\mathrm{d}z \\ &= 0. \end{aligned} \tag{4.74}$$

Similary, the component of interaction force F_x along $\mathbf{e}_x$ direction is

$$\begin{aligned} F_x &= [\frac{1}{c}\int_0^t j_p(z)\int_{\partial(\tilde{\Omega}_s\setminus\tilde{\Omega}_{co})}(-A_x n_y + A_y n_x)\mathrm{d}S\mathrm{d}z] \\ &+ \frac{1}{c}\int_0^t j_p(z)\int_{\partial(\tilde{\Omega}_s\setminus\tilde{\Omega}_{co})}\frac{\xi^2}{r^2}\big|_{r=\xi}\sin 2\theta(-A_{vx}n_y + A_{vy}n_x)\mathbf{e}_x\mathrm{d}S\mathrm{d}z \\ &= [\frac{1}{c}\int_0^t j_p(z)\int_{\partial(\tilde{\Omega}_s\setminus\tilde{\Omega}_{co})}(\mathbf{A}\cdot d\mathbf{l})] \\ &= \frac{1}{c}j_0\Phi_0. \end{aligned} \tag{4.75}$$

Thus the interaction force, or the so-called *Lorentz Force* in thin film is written as

$$F = \frac{1}{c}j_0\mathbf{e}_y \times \Phi_0\mathbf{e}_z. \tag{4.76}$$

Generally speaking, for transport current density $\mathbf{J}$ passing through an individual vortex in a thin film, the interaction force is given by $\frac{1}{c}\mathbf{J}\times\mathbf{\Phi_0}$, which is shown in most literature as *Lorentz Force*. Moreover, the force is actually not uniform along the vortex line column. It concentrates on the surfaces and is weaker in the middle of the vortex line.

4.5 Interaction with paramagnetic inhomogeneity: nonzero transport current

With the appearance of transport current, there is variation of velocity of supercurrent electrons along $\mathbf{e}_z$ direction. For this reason, we can not employ planar model to deal with nonzero transport current scenario. Applying an in-plane external transport current $\mathbf{J}_t$ as described in equation (4.55), total supercurrent $\mathbf{J}_{\mathrm{tot}}$ satisfies

$$\oint_{\mathrm{end}}\mathbf{J}_{\mathrm{tot}} = j_0\mathbf{e}_y \qquad \text{at } \infty\chi_{\Omega_s}. \tag{4.77}$$

To investigate the problem, we consider the same geometric model in section 4.3: an individual vortex with a paramagentic inhomogeneity in a superconducting composite thin film under an external magnetic field $\mathbf{H}^e$ and periodic boundary conditions. We first clarify the total free energy of the system and decompose it based on the supercurrent induced by

different kinds of mechanisms.

4.5.1 A decomposition on supercurrent-based free energy

To determine the interaction force between a single magnetic vortex and interface of paramagnetic inhomogeneity, we formulate the free energy, decompose it based on the supercurrents induced by different kinds of mechanims.

The total supercurrent $\mathbf{J}_{\text{tot}} : \Omega_s \to \mathbb{C}$ consists of four parts: supercurrent $\mathbf{J}_v : \Omega_s \to \mathbb{C}$ induced by a single vortex, external transport current $\mathbf{J}_t : \Omega_s \to \mathbb{C}$ which shall satisfy the boundary value problem described in section 4.4, the perturbated supercurrent $\mathbf{J}_p : \Omega_s \to \mathbb{C}$ due to the geometic configuration without considering magnetic permeability μ and supercurrent $\mathbf{J}_m : \Omega_s \to \mathbb{C}$ generated by paramagnetic effect. Therefore, we have

$$\mathbf{J}_{\text{tot}} = \mathbf{J}_v + \mathbf{J}_t + \mathbf{J}_p + \mathbf{J}_m \qquad \text{on } \Omega_s \backslash \Omega_{\text{co}}. \tag{4.78}$$

The corresponding total magnetic vector potential $\mathbf{A}_{\text{tot}} : I\!R^3 \to I\!R^3$ can be written as

$$\begin{aligned} \mathbf{A}_{\text{tot}} &= \mathbf{A}^{\text{sf}} + \mathbf{A}^e \\ &= \mathbf{A}_v + \mathbf{A}_t + \mathbf{A}_p + \mathbf{A}_m \qquad \text{in } I\!R^3, \end{aligned} \tag{4.79}$$

where vector potential $\mathbf{A}_v$(resp. $\mathbf{A}_t, \mathbf{A}_p, \mathbf{A}_{\text{inh}}$): $I\!R^3 \to I\!R^3$ is associated with the single magnetic vortex (resp. transport current $\mathbf{J}_t$, perturbated current $\mathbf{J}_p$ and supercurrent $\mathbf{J}_m$). And vector potential $\mathbf{A}^e$ (resp. $\mathbf{A}^{\text{sf}}$): $I\!R^3 \to I\!R^3$ is associated with the external magnetic field $\mathbf{H}^e$(resp. self field $\mathbf{H}^{\text{sf}}$).

Consider the local density of superconducting electrons $|\psi|^2$ as constant, the kinetic part of superconducting energy in equation (4.1) can be written as

$$\begin{aligned} \int_{\Omega_s} \frac{1}{2m^*} |(\frac{\hbar}{i}\nabla - \frac{e^*}{c}\mathbf{A}_{\text{tot}})\psi|^2 &= \int_{\Omega_s} \frac{1}{2m^*} [\hbar(\nabla|\psi|)^2 + (\hbar\nabla\theta - \frac{e^*\mathbf{A}_{\text{tot}}}{c})^2 |\psi|^2] \\ &= \int_{\Omega_s} \frac{1}{8\pi} \lambda^2 |\nabla \times \nabla \times \mathbf{A}_{\text{tot}}|^2. \end{aligned} \tag{4.80}$$

The total free energy in equation (4.1) becomes

$$\begin{aligned} G[\psi, \mathbf{A}_{\text{tot}}, \mathbf{M}; \mathbf{H}^e] = & \int_{\Omega_s} \left[f_{n0} + \alpha|\psi|^2 + \frac{\beta}{2}|\psi|^4 + \frac{1}{8\pi}\lambda^2 |\nabla \times \nabla \times \mathbf{A}_{\text{tot}}|^2 \right] \\ & + \frac{1}{8\pi} \int_{I\!R^3} |\nabla \times \mathbf{A}_{\text{tot}} - \mathbf{H}^e - 4\pi \mathbf{M} \chi_{\Omega_m}|^2 \\ & + \int_{\Omega_m} [\frac{a_{\text{ex}}}{2} |\nabla \mathbf{M}|^2 + \phi(\mathbf{M}) - \mathbf{H}^e \cdot \mathbf{M}]. \end{aligned} \tag{4.81}$$

Ignoring the exchange energy term $\frac{a_{\text{ex}}}{2}|\nabla \mathbf{M}|^2$ and assuming a linear paramagnetic inhomogeneity, we define an effective free energy associated with the relative distance of a single magnetic vortex to the interface of paramagnetic inhomogeneity.

The total free energy can be decomposed into

$$G^{\text{eff}}[\mathbf{A}^{\text{sf}}, \mathbf{M}; \mathbf{A}^e] = G_s^{\text{eff}}[\mathbf{A}^{\text{sf}}; \mathbf{A}^e] + G_m^{\text{eff}}[\mathbf{M}; \mathbf{A}^e] + G_{\text{sf}}^{\text{eff}}[\mathbf{A}^{\text{sf}}, \mathbf{M}; \mathbf{A}^e] + G_{\text{int}}^{\text{eff}}[\mathbf{A}^{\text{sf}}, \mathbf{M}; \mathbf{A}^e] \tag{4.82}$$

where

$$\begin{aligned} G_s^{\text{eff}}[\mathbf{A}^{\text{sf}}; \mathbf{A}^e] &= \int_{\Omega_s} \left[\frac{1}{8\pi} \lambda^2 |\nabla \times \nabla \times (\mathbf{A}^e + \mathbf{A}^{\text{sf}})|^2 \right], \\ G_m^{\text{eff}}[\mathbf{M}; \mathbf{A}^e] &= \int_{\Omega_m} [\frac{2\pi}{\mu - 1} \mathbf{M}^2 + 8\pi \mathbf{M}^2 - \mathbf{H}^e \cdot \mathbf{M}], \\ G_{\text{sf}}^{\text{eff}}[\mathbf{A}^{\text{sf}}, \mathbf{M}; \mathbf{A}^e] &= \frac{1}{8\pi} \int_{I\!R^3} |\nabla \times \mathbf{A}^{\text{sf}}|^2, \\ G_{\text{int}}^{\text{eff}}[\mathbf{A}^{\text{sf}}, \mathbf{M}; \mathbf{A}^e] &= - \int_{\Omega_m} \mathbf{M} \cdot (\nabla \times \mathbf{A}^{\text{sf}}). \end{aligned}$$

Here G_s^{eff} indicates the superconducting kinetic energy, G_m^{eff} indicates the energy induced by magnetization, $G_{\text{sf}}^{\text{eff}}$ is the self field energy and $G_{\text{int}}^{\text{eff}}$ is the interaction energy between magnetization and self field. On another hand, It can also be rewritten based on the decompostion of supercurrent (4.78) as

$$G^{\text{eff}}[\mathbf{A}_{\text{tot}}, \mathbf{M}; \mathbf{H}^e] = G_v^{\text{eff}}[\mathbf{A}; \mathbf{H}^e] + G_t^{\text{eff}}[\mathbf{A}; \mathbf{H}^e] + G_p^{\text{eff}}[\mathbf{A}; \mathbf{H}^e] + G_{m*}^{\text{eff}}[\mathbf{A}, \mathbf{M}; \mathbf{H}^e], \tag{4.83}$$

where

$$
\begin{aligned}
G_v^{\text{eff}}[\mathbf{A};\mathbf{H}^e] &= \frac{1}{8\pi}(\frac{4\pi}{c})^2\int_{\Omega_s\setminus\Omega_{co}}\lambda^2(\mathbf{J}_v+\mathbf{J}_{pv})^2+\frac{1}{8\pi}\int_{I\!R^3\setminus\Omega_{\text{co}}}|\nabla\times(\mathbf{A}_v+\mathbf{A}_{pv}-\mathbf{A}^e)|^2,\\
G_t^{\text{eff}}[\mathbf{A};\mathbf{H}^e] &= \frac{1}{8\pi}(\frac{4\pi}{c})^2\int_{\Omega_s\setminus\Omega_{co}}\lambda^2(\mathbf{J}_t+\mathbf{J}_{pt})^2+\frac{1}{8\pi}\int_{I\!R^3\setminus\Omega_{\text{co}}}|\nabla\times(\mathbf{A}_t+\mathbf{A}_{pt}-\mathbf{A}^e)|^2,\\
G_p^{\text{eff}}[\mathbf{A};\mathbf{H}^e] &= \frac{1}{8\pi}(\frac{4\pi}{c})^2\int_{\Omega_s\setminus\Omega_{\text{co}}}2\lambda^2(\mathbf{J}_v+\mathbf{J}_{pv})\cdot(\mathbf{J}_t+\mathbf{J}_{pt})\\
&\quad+\frac{1}{8\pi}\int_{I\!R^3\setminus\Omega_{\text{co}}}2[\nabla\times(\mathbf{A}_v+\mathbf{A}_{pv})]\cdot[\nabla\times(\mathbf{A}_t+\mathbf{A}_{pt})]-2|\nabla\times\mathbf{A}^e|^2,\\
G_{m*}^{\text{eff}}[\mathbf{A},\mathbf{M};\mathbf{H}^e] &= \frac{1}{8\pi}(\frac{4\pi}{c})^2\int_{\Omega_s\setminus\Omega_{co}}\lambda^2[\mathbf{J}_m^2+2\mathbf{J}_m\cdot(\mathbf{J}_v+\mathbf{J}_{pv}+\mathbf{J}_t+\mathbf{J}_{pt})]\\
&\quad+\int_{\Omega_m}(\frac{2\pi}{\mu-1}+8\pi)\mathbf{M}^2-\nabla\times(\mathbf{A}_v+\mathbf{A}_t+\mathbf{A}_p+\mathbf{A}_m)\cdot\mathbf{M}\\
&\quad+\frac{1}{8\pi}\int_{I\!R^3\setminus\Omega_{\text{co}}}|\nabla\times\mathbf{A}_m|^2+2\nabla\times\mathbf{A}_m\cdot[\nabla\times(\mathbf{A}_v+\mathbf{A}_{pv}+\mathbf{A}_t+\mathbf{A}_{pt}-\mathbf{A}^e)].
\end{aligned}
$$

G_v^{eff} is the effective interaction energy with zero external transport current associated with a single magnetic vortex and an inhomogeneity, which magnetic permeability $\mu=1$. Alternatively speaking, the inhomgeneity is nonmagnetic material. G_t^{eff} is the additional effective free energy corresponding to external transport current $\mathbf{J}_t$. And G_p^{eff} represents the interaction energy among the vortex supercurrent $\mathbf{J}_v+\mathbf{J}_{pv}$, transport current $\mathbf{J}_t+\mathbf{J}_{pt}$ and their related magnetic field. When inhomogeneity is paramagnetic material, G_{m*}^{eff} is the additional energy including the coupling term of the interactions associated with inhomogeneity and its magnetization $\mathbf{M}$.

For a specific case, if there is no inhomogeneity, perturbated currents $\mathbf{J}_{pt}$ and $\mathbf{J}_{pv}$ will be zero, only the term $\frac{1}{8\pi}\int_{I\!R^3\setminus\Omega_{\text{co}}}2(\nabla\times\mathbf{A}_v)\cdot(\nabla\times\mathbf{A}_t)$ in G_p^{eff} contributes the driving force $\frac{1}{c}\mathbf{J}\times\mathbf{\Phi_0}$, which is the lorentz force on a single vortex by the transport current as described in section 4.4.

In summary, we could have the following five scenarios:

1. No inhomogeneity in the composite, transport current $\mathbf{J}_t\neq 0$. The effective free energy is

$$G^{\text{eff}}=G_p^{\text{eff}}. \tag{4.84}$$

Remark that the pertubated currents $\mathbf{J}_{pv} = 0$ and $\mathbf{J}_{pt} = 0$, G_v^{eff} is unchanged with the location of vortex so that it will not contribute the effective energy, which is used to calculate the interaction force.

2. One inhomogeneity with magnetic permeability $\mu = 1$ in the composite, transport current $\mathbf{J}_t = 0$. The effective free energy is

$$G^{\text{eff}} = G_v^{\text{eff}} + G_p^{\text{eff}}. \tag{4.85}$$

3. One inhomogeneity with magnetic permeability $\mu = 1$ in the composite, transport current $\mathbf{J}_t \neq 0$. The effective free energy is

$$G^{\text{eff}} = G_v^{\text{eff}} + G_t^{\text{eff}} + G_p^{\text{eff}}. \tag{4.86}$$

4. One inhomogeneity with magnetic permeability $\mu \neq 1$ in the composite, transport current $\mathbf{J}_t = 0$. The effective free energy is

$$G^{\text{eff}} = G_v^{\text{eff}} + G_p^{\text{eff}} + G_{m*}^{\text{eff}}. \tag{4.87}$$

5. One inhomogeneity with magnetic permeability $\mu \neq 1$ in the composite, transport current $\mathbf{J}_t \neq 0$. The effective free energy is

$$G^{\text{eff}} = G_v^{\text{eff}} + G_t^{\text{eff}} + G_p^{\text{eff}} + G_{m*}^{\text{eff}}. \tag{4.88}$$

4.5.2 Euler-Lagrange equations associated with boundary conditions

In the principle of free energy, Euler-Lagrange equations (4.81) necessarily satisfies

$$\begin{cases} \nabla \times (\nabla \times \mathbf{A}_{\text{tot}} - 4\pi \mathbf{M} \chi_{\Omega_m}) = -\lambda^2 \nabla \times \nabla \times \nabla \times \nabla \times \mathbf{A}_{\text{tot}} \chi_{\Omega_s} & \text{in } I\!R^3, \\ -\nabla \times \mathbf{A}_{\text{tot}} + 4\pi \mathbf{M} + D_{\mathbf{M}} \phi(\mathbf{M}) = 0 & \text{in } \Omega_m, \end{cases} \tag{4.89}$$

By Maxwell equations, we can also rewrite the equation $(4.89)_1$ as

$$\lambda^2 \Delta \mathbf{J}_{\text{tot}} - \mathbf{J}_{\text{tot}} = 0 \qquad \text{in } \Omega_s/\Omega_{\text{co}}. \tag{4.90}$$

If a single magnetic vortex exists in the superconducting domain, the above equation shall be modified as

$$\lambda^2 \Delta \mathbf{J}_{\text{tot}} - \mathbf{J}_{\text{tot}} = -\nabla \times \nabla \times \frac{\Phi_0 \delta_2(\mathbf{r} - \mathbf{r}_0)\mathbf{e}_z}{\lambda^2} \qquad \text{in } \Omega_s/\Omega_{\text{co}}. \tag{4.91}$$

Upon the above discussion, we determine the complete boundary value problem as:

$$\begin{cases} \lambda^2 \Delta \mathbf{J}_{\text{tot}} - \mathbf{J}_{\text{tot}} = -\nabla \times \nabla \times \frac{\Phi_0 \delta_2(\mathbf{r}-\mathbf{r}_0)\mathbf{e}_z}{\lambda^2} & \text{in } \Omega_s/\Omega_{\text{co}}, \\ -\nabla \times \mathbf{A} + 4\pi \mathbf{M} + D_{\mathbf{M}} \phi(\mathbf{M}) = 0 & \text{in } \Omega_m, \end{cases} \tag{4.92}$$

associated with the boundary conditions that shall satisfy the reasonable physical behaviors:

$$\begin{cases} |\nabla \times \mathbf{A}_{\text{tot}} - \mathbf{H}^e| \to 0 & \text{as } |\mathbf{x}| \to +\infty, \\ \fint_{\text{end}} \mathbf{J}_{\text{tot}} = j_0 \mathbf{e}_y & \text{at } \infty \chi_{\Omega_s}, \\ \mathbf{J}_{\text{tot}} \cdot \mathbf{n} = 0 & \text{on } \partial\Omega_m, \\ \mathbf{J}_{\text{tot}} \cdot \mathbf{n} = 0 & \text{on } \partial\Omega_{\text{co}}. \end{cases} \tag{4.93}$$

The first boundary condition indicates that magnetic field is close to the applied external field $\mathbf{H}^e$ away from the composite in the vacuum. The second boudary condition is derived from the prescribed external transport current. And the last two boundary conditions shows that supercurrent cannot penerate into the normal phase or paramagentic inhomgeneity.

The above boundary value problem is linear. By the property of linearity, we could solve the partial differential equations through the decomposition of supercurrent $\mathbf{J}_{\text{tot}}$ in equation (4.78) and magnetic vector potential $\mathbf{A}_{\text{tot}}$ in equation (4.79). We now illustrate the detail calculation as follows.

The supercurrent $\mathbf{J}_v$ is generated by a single magnetic vortex. We assume that the

vortex is straight and is independent of direction $\mathbf{e}_z$. The magnetic field $\mathbf{B}_v$ generated by the vortex can be expressed approximately in terms of zeroth-order of modified Bessel function of the second kind as

$$\mathbf{B}_v = \frac{\Phi_0}{2\pi\lambda^2} K_0(|\frac{\mathbf{r}-\mathbf{r}_0}{\lambda}|)\mathbf{e}_z \qquad \text{in } \Omega_s\backslash\Omega_{\text{co}}, \tag{4.94}$$

and the related supercurrent $\mathbf{J}_v$ is determined by magnetic field $\mathbf{B}_v$ according to Maxwell equation as

$$\mathbf{J}_v = \frac{c}{4\pi}\nabla\times\mathbf{B}_v \qquad \text{in } \Omega_s\backslash\Omega_{\text{co}}. \tag{4.95}$$

For the external transport current $\mathbf{J}_t$ calculated in section 4.4, it has the form of

$$\mathbf{J}_t = C\frac{e^{z/\lambda}+e^{-z/\lambda}}{2}(-\frac{\xi^2}{r^2}\sin 2\theta, 1+\frac{\xi^2}{r^2}\cos 2\theta, 0) \qquad \text{in } \Omega_s\backslash\Omega_{\text{co}} \tag{4.96}$$

where C is a constant determined by boundary condition $(4.93)_2$.

Due to the change of geometic configuration by the existence of inhomogeneity, there must be a perturbed current density $\mathbf{J}_p$ so that the total current $\mathbf{J}_{\text{tot}}$ can satisfy the boundary condition $(4.93)_{3,4}$, where no supercurrent is allowed to penetrate into normal phase or paramagnetic inhomgeneity. We have the following governing equation

$$\lambda^2\Delta\mathbf{J}_p - \mathbf{J}_p = 0 \qquad \text{in } \Omega_s\backslash\Omega_{\text{co}}, \tag{4.97}$$

$$\tag{4.98}$$

subject to the boudary conditions

$$\begin{cases} \mathbf{J}_p\cdot\mathbf{n} = 0 & \text{on } \partial\Omega_{\text{co}}, \\ \mathbf{J}_p = 0 & \text{at } \infty_{\Omega_s}. \end{cases} \tag{4.99}$$

Remark that we assume magnetic permeability $\mu = 1$.

Due to the linearity of govening equation, perturbed current $\mathbf{J}_p$ could be considered as the sum of perturbed current $\mathbf{J}_{pt}$ corresponding to transport current $\mathbf{J}_t$ and perturbed

current $\mathbf{J}_{pv}$ corresponding to supercurrent $\mathbf{J}_v$

$$\mathbf{J}_p = \mathbf{J}_{pt} + \mathbf{J}_{pv}. \tag{4.100}$$

Hence we can decompose the boundary value problem as follows:

$$\begin{cases} \lambda^2 \Delta \mathbf{J}_{pi} - \mathbf{J}_{pi} = 0 & \text{in } \Omega_s \backslash \Omega_{\text{co}}, \\ (\mathbf{J}_{pi} + \mathbf{J}_i) \cdot \mathbf{n} = 0 & \text{on } \partial\Omega_m, \\ \mathbf{J}_{pi} \cdot \mathbf{n} = 0 & \text{on } \partial\Omega_{\text{co}}, \\ \mathbf{J}_{pi} = 0 & \text{at } \infty_{\Omega_s}, \end{cases} \quad \text{where } i = t, v. \tag{4.101}$$

The magnetic field $\mathbf{B}_t(\mathbf{B}_p)$ associated with current $\mathbf{J}_t(\mathbf{J}_p)$ in the superconducting region Ω_s could be obtained according to Maxwell equations

$$\nabla \times \mathbf{B}_i = \nabla \times \nabla \times \mathbf{A}_i = \frac{4\pi}{c} \mathbf{J}_i \chi_{\Omega_s \backslash \Omega_{\text{co}}} \quad \text{in } I\!R^3 \qquad i = t, p. \tag{4.102}$$

In the inhomogeneity domain, the magnetic vector potential $\mathbf{A}_v$, $\mathbf{A}_t$ and $\mathbf{A}_p$ satisfy the following boundary value problem

$$\begin{cases} \nabla \times \nabla \times \Sigma \mathbf{A}_i = 0 & \text{in } \Omega_m \\ [\![\Sigma \mathbf{A}_i]\!] = 0 & \text{on } \partial\Omega_m \\ [\![\nabla \times \Sigma \mathbf{A}_i]\!] \cdot \mathbf{t} = 0 & \text{on } \partial\Omega_m \end{cases} \quad i = v, t, p. \tag{4.103}$$

Since the inhomogeneity is paramagnetic material, it will generate magnetization $\mathbf{M}$ in the inhomogeneity. The magnetization $\mathbf{M}$ and current $\mathbf{J}_{\text{tot}}$ are coupled with each other, it is more convenicent to investigate the problem from the viewpoint of vector potential $\mathbf{A}_m$. The governing equations followed by equation (4.89) are

$$\begin{cases} \lambda^2 \nabla \times \nabla \times \mathbf{A}_m + \mathbf{A}_m = 0 & \text{in } \Omega_s \setminus \Omega_{\text{co}} \\ \nabla \times (\nabla \times \mathbf{A}_m - 4\pi \mathbf{M}) = 0 & \text{in } \Omega_m \end{cases} \tag{4.104}$$

By constitutive law (4.6), we have

$$\nabla \times \mathbf{A}_{\text{tot}} = \frac{\mu}{\mu - 1} 4\pi \mathbf{M} \quad \text{in } \Omega_m. \tag{4.105}$$

The curl of $\mathbf{A}_m$ in the inhomogeneity Ω_m can be expressed

$$\nabla \times \mathbf{A}_m = \frac{\mu}{\mu - 1} 4\pi \mathbf{M} - \nabla \times (\mathbf{A}_v + \mathbf{A}_t + \mathbf{A}_p) \quad \text{in } \Omega_m \tag{4.106}$$

Therefore equation $(4.104)_1$, (4.106) will form a boundary value problem for $\mathbf{A}_m$:

$$\begin{cases} \lambda^2 \nabla \times \nabla \times \mathbf{A}_m + \mathbf{A}_m = 0 & \text{in } \Omega_s \setminus \Omega_{\text{co}}, \\ \nabla \times \mathbf{A}_m = \frac{\mu}{\mu - 1} 4\pi \mathbf{M} - \nabla \times (\mathbf{A}_v + \mathbf{A}_t + \mathbf{A}_p) & \text{in } \Omega_m. \end{cases} \tag{4.107}$$

subject to boundary conditions

$$\begin{cases} [\![\mathbf{A}_m]\!] = 0 & \text{on } \partial\Omega_m \& \partial\Omega_{\text{co}}, \\ [\![\nabla \times \mathbf{A}_m]\!] \cdot \mathbf{t} = 0 & \text{on } \partial\Omega_{\text{co}}, \\ [\nabla \times \mathbf{A}_m] \cdot \mathbf{t}\big|_{\partial\Omega_{m+}} = [\frac{1}{\mu} \nabla \times \mathbf{A}_m + (\frac{1}{\mu} - 1) \nabla \times (\mathbf{A}_v + \mathbf{A}_t + \mathbf{A}_p)] \cdot \mathbf{t}\big|_{\partial\Omega_{m-}}, \\ \nabla \times \mathbf{A}_m = 0 & \text{at } \infty \chi_{\Omega_s}. \end{cases} \tag{4.108}$$

Supercurrent $\mathbf{J}_m$ can be easily determined as

$$\mathbf{J}_m = \frac{c}{4\pi} \nabla \times \nabla \times \mathbf{A}_m \qquad \text{in } \Omega_s \backslash \Omega_{\text{co}}. \tag{4.109}$$

4.5.3 An approximate analytical solution with small inhomogeneity

In this section, we continue the calculation based on the governing equations derived in the last section and estimate the pinning force of a single vortex under the prescribed length scale (excludes *Lorenze Force*). To clarify the problem, we again claim some important assumptions:

1. High temperature type II superconductors are considered. Alternatively, London

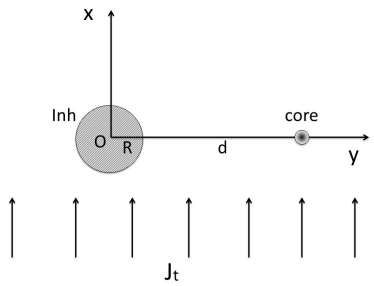

Figure 4.9: Schematic diagram for composite film with transport current $\mathbf{J}_t$ (a)

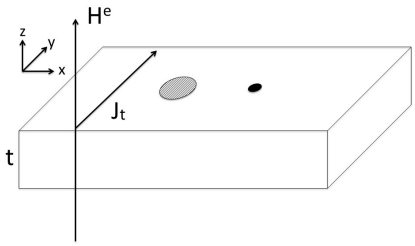

Figure 4.10: Schematic diagram for composite film with transport current $\mathbf{J}_t$ (b)

limit, which is the ratio of the penetration length λ and coherence length ξ, is infinity: $\kappa = \frac{\lambda}{\xi} \to \infty$.

2. The distance between magnetic vortex and the interface of inhomogeneity d is comparable to penetration length λ: $d \sim \lambda$. Under this length scale, the magnetic field and supercurrent around the vortex core area is independent of the existance of inhomogeneity.

3. We suppose that the radius of the inhomgeneity R is much smaller then penetration length λ: $R \ll \lambda$. Therefore, for simplicity's sake, we do not consider the perturbed current $\mathbf{J}_p$ and its related perturbed field $\mathbf{B}_p$.

4. We asssume magnetic field $\mathbf{B}_m$ induced by inhomogeneity and magnetization $\mathbf{M}$ only have a uniform $\mathbf{e}_z$ component.

5. The origion point O is set at the center of the inhomogeneity, external magnetic field $\mathbf{B}^e$ is along $\mathbf{e}_z$ direction and transport current $\mathbf{J}_t$ is along $\mathbf{e}_y$ direction as shown in Fig. 4.9 and Fig. 4.10.

Upon the above assumptions, both of the total supercurrent $\mathbf{J}_{\text{tot}}$ and magnetic field $\mathbf{B}_{\text{tot}}$ in superconducting region Ω_s consist of three parts

$$\mathbf{J}_{\text{tot}} = \mathbf{J}_v + \mathbf{J}_t + \mathbf{J}_m \qquad \text{in } \Omega_s \backslash \Omega_{\text{co}}. \tag{4.110}$$

$$\mathbf{B}_{\text{tot}} = \mathbf{B}_v + \mathbf{B}_t + \mathbf{B}_m \qquad \text{in } \Omega_s \backslash \Omega_{\text{co}}. \tag{4.111}$$

The magnetic field $\mathbf{B}_v$ induced by single magnetic vortex outside the core area satisfies the equation

$$\begin{cases} -\frac{1}{\lambda^2}\mathbf{B}_v + \nabla^2\mathbf{B}_v = -\frac{\Phi_0\delta_2(\mathbf{r}-\mathbf{r}_0)\mathbf{e}_z}{\lambda^2} & \text{in } \Omega_s \setminus \Omega_{\text{co}}, \\ \mathbf{B}_v \to 0 & \text{at } \infty_{\chi_{\Omega_s}}. \end{cases} \tag{4.112}$$

The solution to the above equation is

$$\mathbf{B}_v = \frac{\Phi_0}{2\pi\lambda^2}K_0(|\frac{\mathbf{r}-\mathbf{r}_0}{\lambda}|)\mathbf{e}_z = \frac{\Phi_0}{2\pi\lambda^2}K_0(\frac{\sqrt{r_0^2+r^2-2rr_0\cos\theta}}{\lambda})\mathbf{e}_z \qquad \text{in } \Omega_s\backslash\Omega_{\text{co}}, \tag{4.113}$$

where $r_0 = R + d$. This is the standard solution for a single vortex in the infinite pure superconducting region we used in the previous sections.

And the supercurrent $\mathbf{J}_v$ induced by $\mathbf{B}_v$ is determined by Maxwell equation

$$\mathbf{J}_v = \frac{c}{4\pi}\nabla\times\mathbf{B}_v = -\frac{c}{4\pi}\frac{\Phi_0}{2\pi\lambda^2}\frac{\partial}{\partial r}(K_0(\frac{\sqrt{r_0^2+r^2-2rr_0\cos\theta}}{\lambda}))\mathbf{e}_\theta \qquad \text{in } \Omega_s\backslash\Omega_{\text{co}}. \tag{4.114}$$

In addition, transport current $\mathbf{J}_t$ is prescribed. According to the previous analysis, it has the form

$$\mathbf{J}_t = C_1\frac{e^{z/\lambda}+e^{-z/\lambda}}{2}\mathbf{e}_y \qquad \text{in } \Omega_s\backslash\Omega_{\text{co}}. \tag{4.115}$$

where C_1 is the prescribed constant determined by strength of the transport current. Remark that the boundary condition on the vortex core area does not count here and *Lorenze Force* is excluded in the calculation of pinning force.

Magnetic field $\mathbf{B}_t$ will not have $\mathbf{e}_z$ component. By symmetry and continuity of potential $\mathbf{A}_t$, the magnetic field $\mathbf{B}_t$ is

$$\mathbf{B}_t = B_t(z)\mathbf{e}_x = \frac{4\pi}{c}\lambda C_1\frac{e^{z/\lambda}-e^{-z/\lambda}}{2}\mathbf{e}_x\chi_{\Omega_s\backslash\Omega_{\text{co}}}. \tag{4.116}$$

The partial differential equations (4.104) for $\mathbf{B}_m$ and its boundary conditions can be solved as a function of magnetization $\mathbf{M}$. Based on the assumption that $\mathbf{B}_m$ and $\mathbf{M}$ only have a uniform $\mathbf{e}_z$ compoment, we assume $\mathbf{M} = M\mathbf{e}_z$ in the inhomogeneity Ω_m. And the

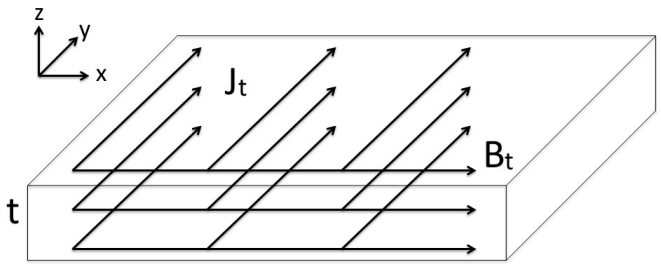

Figure 4.11: Magnetic field $\mathbf{B}_t$ induced by transport current.

magnetic field $\mathbf{B}_m$ is determined by the governing equations

$$\begin{cases} \mathbf{B}_m = (\frac{\mu}{\mu-1}4\pi M - (\mathbf{B}_v + \mathbf{B}_t)\cdot\mathbf{e}_z)\mathbf{e}_z & \text{in } \Omega_m, \\ -\frac{1}{\lambda^2}\mathbf{B}_m + \nabla^2\mathbf{B}_m = 0 & \text{in } \Omega_s, \end{cases} \tag{4.117}$$

subject to the boudary conditions

$$\begin{cases} \mathbf{B}_m\big|_{\partial\Omega_m+} = (\frac{1}{\mu-1}4\pi M - (\mathbf{B}_v + \mathbf{B}_t)\cdot\mathbf{e}_z)\mathbf{e}_z\big|_{\partial\Omega_m-}, \\ \mathbf{B}_m = 0 \qquad\qquad \text{at } \infty. \end{cases} \tag{4.118}$$

Using the method of separation of variables, which is similar as the one in section 4.3, the magnetic field $\mathbf{B}_m$ in the superconducting domain is

$$\mathbf{B}_m = \mathbf{B}_{m1} + \mathbf{B}_{m2} \qquad \text{in } \Omega_s\backslash\Omega_{\text{co}}, \tag{4.119}$$

where

$$\mathbf{B}_{m1} = \frac{K_0(\frac{|\mathbf{r}|}{\lambda})}{K_0(\frac{|\mathbf{R}|}{\lambda})}\frac{4\pi M}{\mu-1}\mathbf{e}_z \qquad \text{in } \Omega_s\backslash\Omega_{\text{co}}, \tag{4.120}$$

$$\begin{aligned}\mathbf{B}_{m2} = &\frac{K_0(\frac{|\mathbf{r}|}{\lambda})}{K_0(\frac{|\mathbf{R}|}{\lambda})}\frac{1}{2\pi}\int_{-\pi}^{\pi} Q_2 \mathrm{d}\theta \\ &+ \frac{K_1(\frac{|\mathbf{r}|}{\lambda})}{K_1(\frac{|\mathbf{R}|}{\lambda})}\frac{\cos\theta}{\pi}\int_{-\pi}^{\pi} Q_2\cos\theta \mathrm{d}\theta + \frac{K_1(\frac{|\mathbf{r}|}{\lambda})}{K_1(\frac{|\mathbf{R}|}{\lambda})}\frac{\sin\theta}{\pi}\int_{-\pi}^{\pi} Q_2\sin\theta \mathrm{d}\theta \mathbf{e}_z \qquad \text{in } \Omega_s\backslash\Omega_{\text{co}}.\end{aligned} \tag{4.121}$$

And the inhomogeneous current $\mathbf{J}_m$ is

$$\mathbf{J}_m = \frac{c}{4\pi}\nabla\times\mathbf{B}_m = \frac{c}{4\pi}(\frac{\partial B_{m2}}{r\partial\theta}\mathbf{e}_r + (-\frac{\partial B_{m1}}{\partial r} - \frac{\partial B_{m2}}{\partial r})\mathbf{e}_\theta). \tag{4.122}$$

Substitute the above solutions of $\mathbf{B}^{\text{tot}}$ and $\mathbf{J}^{\text{tot}}$ back into the effective total free energy in equation (4.82), we have

$$\begin{aligned}G^{\text{eff}} =&\frac{1}{8\pi}\int_{\Omega_s\backslash\Omega_{\text{co}}}\Phi_0\delta(\mathbf{r}-\mathbf{r}_0) + \frac{1}{8\pi}\oint_{\Omega_s\backslash\Omega_{\text{co}}}\lambda^2\mathbf{B}\times(\nabla\times\mathbf{B}) \\ &-\frac{1}{8\pi}\int_{\Omega_s\backslash\Omega_{\text{co}}} 2(\mathbf{B}_v+\mathbf{B}_t+\mathbf{B}_m)\cdot\mathbf{H}^e \\ &+\int_{\Omega_m}[\frac{2\pi}{\mu-1}\mathbf{M}^2 - (\mathbf{B}_v+\mathbf{B}_t+\mathbf{B}_m)\cdot\mathbf{M} + 8\pi|\mathbf{M}|^2] + \frac{1}{8\pi}\int_{\Omega_m}(\frac{4\pi\mu}{\mu-1}\mathbf{M}-\mathbf{H}^e)^2 \\ &+\frac{1}{8\pi}\int_{\partial\Omega_{top}} -2A_{my}(x,y)B_t(t_0/2).\end{aligned} \tag{4.123}$$

In order to find the pinning force, we employ the same strategy in section 4.3. In the principle of minimum energy, we first minimize the total free energy (4.82) against M. The magnetization will be determined by distance d, radius of inhomogeneity R, magnetic permeability μ, transport current j_0 and external magnetic field $\mathbf{H}^e$

$$\frac{\partial G}{\partial M} = 0 \qquad \Rightarrow \qquad M = M(d,\mu,j_0,R,\mathbf{H}^e). \tag{4.124}$$

Finally, taking the derivative of G^{eff} with respect to d, we obtain the pinning force of vortex to the interface of inhomogeneity

$$F^{\text{pin}} = -\frac{\partial G^{\text{eff}}}{\partial d} = F^{\text{pin}}(d,\mu,j_0,R,\mathbf{H}^e). \tag{4.125}$$

Remark that this pinning force does not count the *Lorentz Force* that we have derived in section 4.4. It only indicates the interface effect of inhomogeneity on a single magnetic

vortex.

For simplicity's sake, we can nondimensionalize the parameters in the same way in table 4.1 with additional term C_1 and $\mathbf{J}_t$ as shown in table 4.2

Table 4.2: Dimensionless variables II

Dimensionless Variable	$\hat{C_1}$	$\hat{\mathbf{J}}_t$
Variable	$C_1/(\frac{\Phi_0 c}{8\pi^2\lambda^4}(e^{\hat{d}} - e^{-\hat{d}}))$	$\mathbf{J}_t/(\frac{\Phi_0 c}{8\pi^2\lambda^4}(e^{\hat{d}} - e^{-\hat{d}}))$

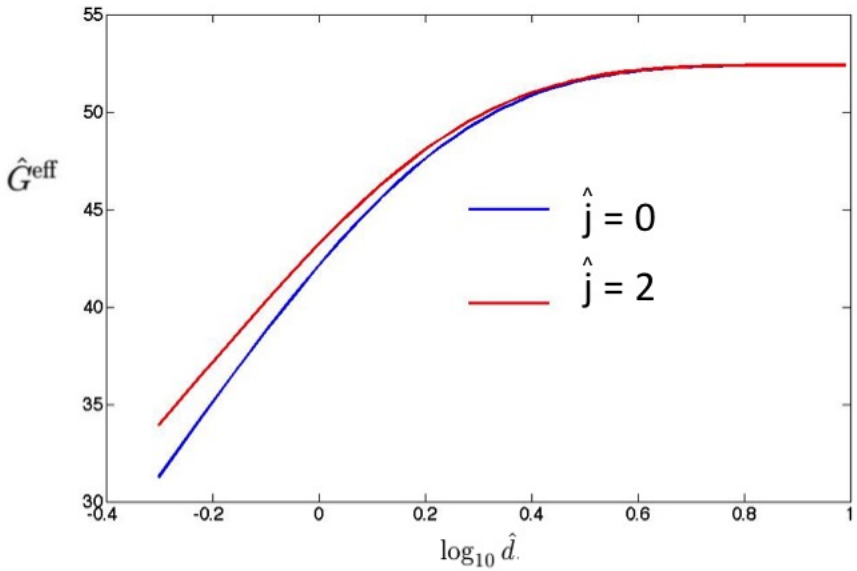

Figure 4.12: Dimensionless effective energy versus the position of vortex with/without transport current density $\hat{j}$. The magnetic permeability of the paramagnetic inhomogeneity $\mu = 100$, the external magnetic field strength $\hat{H}^e = 1$, the radius of the columnar inhomogeneity $\hat{R} = 0.2$ and the thichness $\hat{t} = 1$.

4.5.4 Results and discussion

After considering external transport currents, now we can have a reliable picture on the pinning force of vortex. Figure. 4.12 and Figure. 4.13 show the effective total free energy and pinning force as a funtion of distance $\hat{d}$ with/without external transport current. We can see that the existance of paramagnetic inhomogeneity results in an attractive force of the

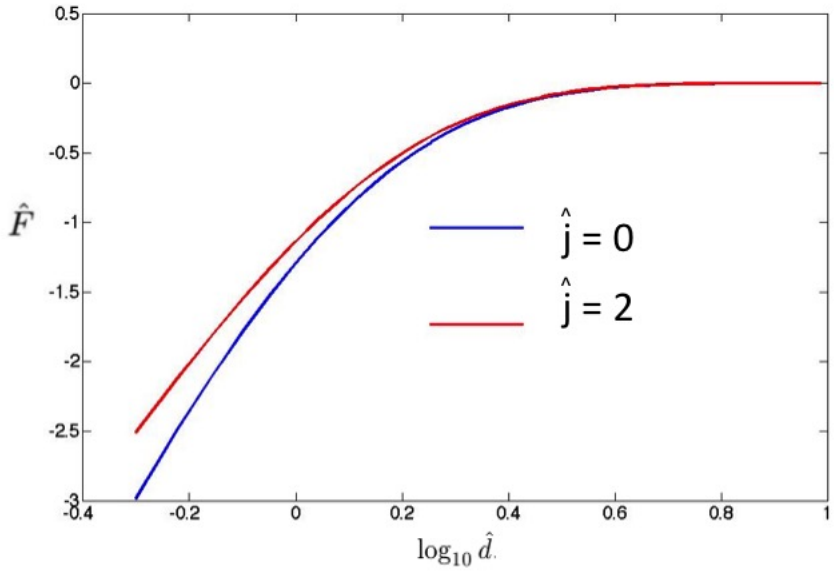

Figure 4.13: Dimensionless pinning force versus the position of vortex with/without transport current density $\hat{j}$. The magnetic permeability of the paramagnetic inhomogeneity $\mu = 100$, the external magnetic field strength $\hat{H}^e = 1$, the radius of the columnar inhomogeneity $\hat{R} = 0.2$ and the thichness $\hat{t} = 1$.

magnentic vortex to the interface of inhomogeneity, which is in agreement with our previous result in section 4.3. On the other hand, we observe that external transport current could weaken the magnitude of attractive pinning force slightly by increasing the free energy. And the magnitude of the pinning force will decay to zero when the distance d reaches several λs.

To illustrate the dependence of all the variables (external magnetic field, magnetic permeability, size of inhomogeneity, thichness of film and transport current) on the pinning force, we define the maximum pinning force happens at distance $\hat{d} = 0.5$. We monitor the variation of the defined maximum pinning force with the above mentioned variables. In Fig. 4.15, Fig. 4.18 and Fig. 4.14, we observe that external field $\hat{H}^e$ and thickness $\hat{t}$ can enchance the pinning force linearly and transport current will weaken the pinning force. In Figure. 4.16, we see that pinning force can be enhanced by the magnetic permeability μ, but it will be satuation with large μ. And in Fig. 4.17, the enhancement of pinning force

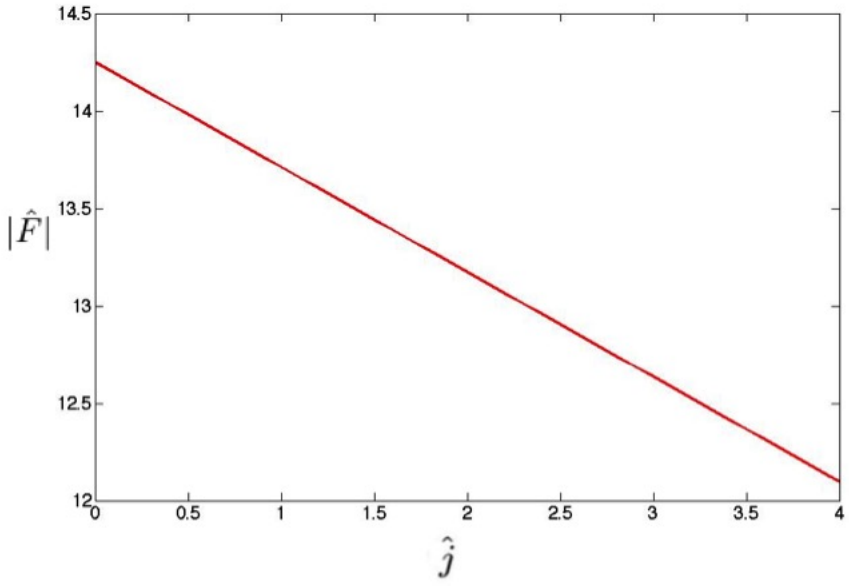

Figure 4.14: Dimensionless pinning force transport current density $\hat{j}$. Magnetic permeability of the paramagnetic inhomogeneity $\mu = 100$, the external magnetic field strength $\hat{H}^e = 1$, the radius of the columnar inhomogeneity $\hat{R} = 0.2$ and the thichness $\hat{t} = 1$.

due to the radius of paramagnetic inhomogenetiy is slightly lower then linearity.

According to the above observation, we see that the dimensionless pinning force $\hat{F}^{\text{pin}}$ has the following relationship with distance of magnetic vortex $\hat{d}$, magnetic permeability μ, extenal magnetic field $\hat{H}^e$, thickness $\hat{t}$, radius of inhomogneity $\hat{R}$ and transport current density $\hat{j}$ as follows:

$$
\begin{aligned}
\hat{F}^{\text{pin}} &\propto -c_1(\mu, \hat{H}^e, \hat{t}, \hat{R}, \hat{j}) e^{-c_2(\mu, \hat{H}^e, \hat{t}, \hat{R}, \hat{j})\hat{d}} \\
\hat{F}^{\text{pin}} &\propto c_3(\hat{d}, \hat{H}^e, \hat{t}, \hat{R}, \hat{j}) - c_4(\hat{d}, \hat{H}^e, \hat{t}, \hat{R}, \hat{j}) e^{-c_5(\hat{d}, \hat{H}^e, \hat{t}, \hat{R}, \hat{j})\hat{\mu}} \\
\hat{F}^{\text{pin}} &\propto -c_6(\hat{d}, \mu, \hat{t}, \hat{R}, \hat{j})\hat{H}^e \\
\hat{F}^{\text{pin}} &\propto -c_7(\hat{d}, \mu, \hat{H}^e, \hat{R}, \hat{j})\hat{t} \\
\hat{F}^{\text{pin}} &\propto c_8(\hat{d}, \mu, \hat{H}^e, \hat{t}, \hat{j})\hat{R}^{c_9(\hat{d}, \mu, \hat{H}, \hat{t}, \hat{j})} \\
\hat{F}^{\text{pin}} &\propto -c_{10}(\hat{d}, \mu, \hat{H}, \hat{t}, \hat{R})\hat{j}
\end{aligned}
\tag{4.126}
$$

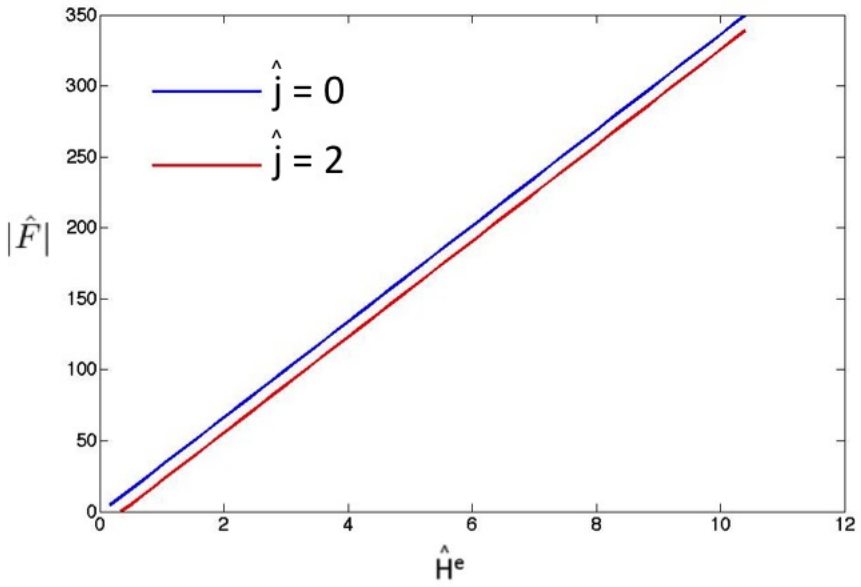

Figure 4.15: Dimensionless pinning force versus the position of vortex depends on external magnetic field $\hat{H}^e$ with/without transport current density $\hat{j}$. Magnetic permeability of the paramagnetic inhomogeneity $\mu = 100$, the radius of the columnar inhomogeneity $\hat{R} = 0.2$ and the thichness $\hat{t} = 1$

where the parameters $c_i (i = 1, ..., 10)$ are determined by material properties, geometric configuration and state variables.

Based on our calculation for *Lorantz Force* in section 4.4, the driving force on a single vortex also increases with higher transport current. Since we investigate the mechanism of pinning force which is caused by paramagnetic inhomogeneity, we can estimate the amount of increasing critical current enhanced by the pinning force due to the inhomogeneity. It happens when vortex is pinned at some location so that the increasing *Lorantz Force* is balanced with attractive pinning force of the inhomogeneity. In dilute limit, we provide a naive defination on the increasing critical current: the increasing value of *Lorantz Force* equals to the magnitude of maximum attractive pinning force, see Fig. 4.19. In this state, the enhanced critical current is obtained.

We observe the dependence of increasing critical current on variation of size of inhomogeneity $\hat{R}$ and variation of magnetic permeability μ. In Fig. 4.20, there is a optimum point

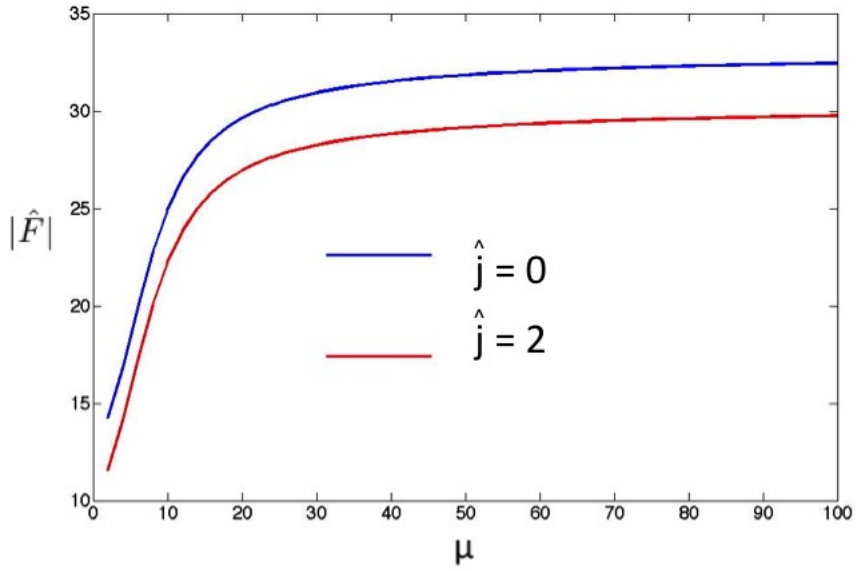

Figure 4.16: Dimensionless pinning force versus magnetic permeability of paramagnetic inhomogeneity μ with/without transport current density $\hat{j}$. External magnetic field $\hat{H}^e = 1$, the radius of the columnar inhomogeneity $\hat{R} = 0.2$ and the thichness $\hat{t} = 1$.

for $\hat{R}$ to generate the maximum increasing critical current. In another hand, in Fig. 4.22, increaing critical current is enchanced with larger magnetic permeability μ and approaches to satuation finally.

Theoretically speaking, pinning force is caused by two mechanisms: the core interaction and the magnetic interaction. In this dilute limit case, only magnetic interaction exists. The total free energy of the system is determined by two characteristic geometric length: the coherence lenth ξ and the penetration depth λ. Wave function changes dramatically over ξ while magnetic field and supercurrent decays over λ. In high temperature superconductors, λ is much larger than ξ. Thus, the interface between superconducting matrix and paramagnetic inclusion is determined by the length scale λ. Moreover, with larger radius R and permeability μ, more magnetic fluxes will transfer from the superconductor into the inhomogeneity. This could make the total free energy of the system increase and result in the enhancement of pinning force.

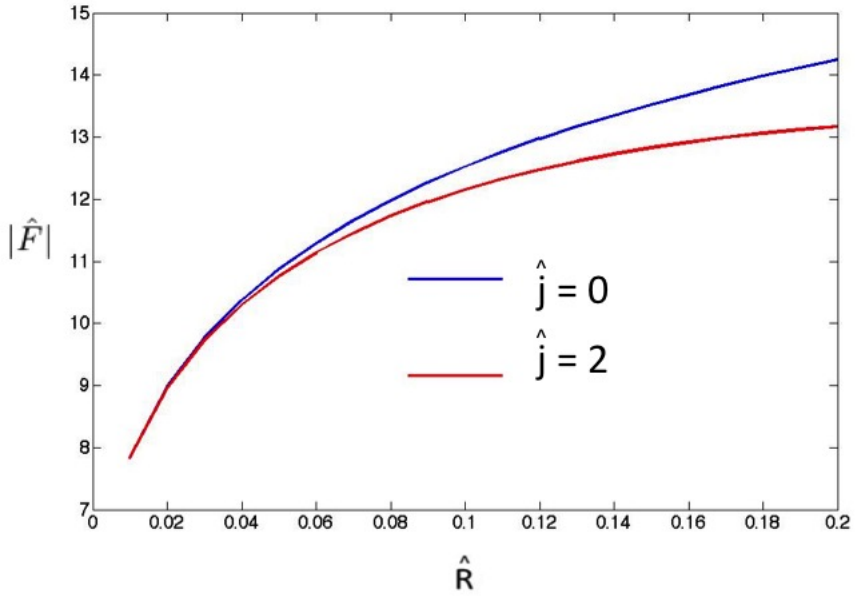

Figure 4.17: Dimensionless pinning force versus the radius of the columnar inhomogeneity $\hat{R}$ with/without transport current density $\hat{j}$. Magnetic permeability of the paramagnetic inhomogeneity $\mu = 100$, the external magnetic field $\hat{H}^e = 1$ and the thichness $\hat{t} = 1$.

Significant contribution to the overall flux pinning strength due to an interface or additives has been reported by recent experiments[124]. Higher current density J_c with self-field and in-field by a factor of 1.5-7 is achieved by adding Ba_2RENbO_6 paramagnetic material into high-temperature superconducting YBCO film compared to un-doped one. With higher volume fraction of BYNO from 0.3 to 5.1%, critical current density is enhanced. In these volume fraction senarios, they can be considered at the dilute limit. Thus, the result is in agreement with our calculation on the pinning force effected by the size of inhomogeneity qualitatively as shown in Fig. 4.22. Moreover for BYNO-doped sample, a stronger peak of J_c is observed when the external field is perpendicular to the film plane.

4.6 Summary

In conclusion, we have proposed a general form of total free energy system for a superconducting composite with paramagnetic inhomogeneities, and derived the Euler-Lagrange

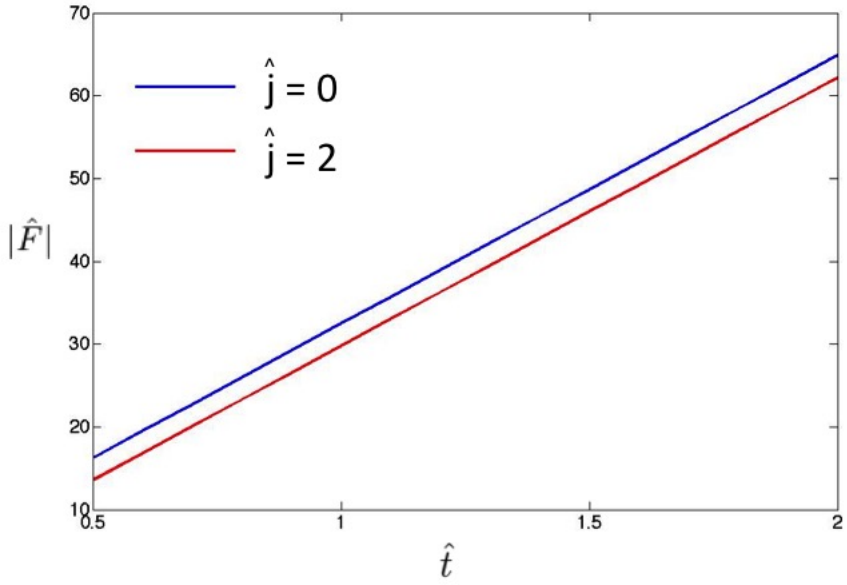

Figure 4.18: Dimensionless pinning force versus thichness of thin film $\hat{t}$ with/without transport current density $\hat{j}$. Magnetic permeability of the paramagnetic inhomogeneity $\mu = 100$, the external magnetic field $\hat{H}^e = 1$ and the radius of the columnar inhomogeneity $\hat{R} = 0.2$.

equations associated with boundary conditions in the principle of free energy. Specifically, we degenarate the energy into two-dimensional planar model for zero external transport current scenario. We then consider the dilute limit case for a single magnetic vortex without core interaction and with magnetic interaction. We solve the magnetic field, obtain an approximate solution and calculate the pinning force for different configurations of inhomogeneity and external magnetic field. It is shown that as the size of inhomogeneity, the magnetic permeability and external magnetic field increases, the pinning force is enchanced. Then a three-dimensional model with external transport current is considered in dilute limit from the viewpoint of supercurrent. The problem is decomposed into several parts by the linearity of the approximated governing equations. The attractive pinning force of a single vortex to the interface of the inhomogeneity is calculated. Based on a naive definition on increasing critical current, we find the critical current will be optimized by the size of inhomogeneity in some range and approach to saturation with higher magnetic permeability.

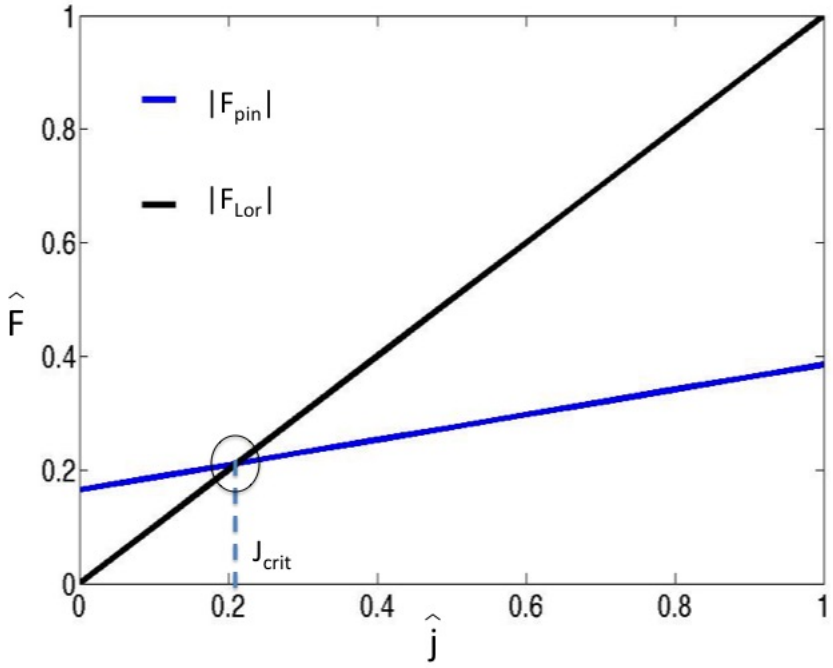

Figure 4.19: A naive definition on the amount of enhanced critical current as the absolute value of pinning force equals to the absolute value of lorentz force

And some experimental results agree with our analysis qualitatively.

4.7 Appendix

4.7.1 Calculus of variational method to Euler-Lagrange equations of total free energy

To find the change of total free energy to the leading order, we assume that

$$\psi_\delta = \psi + \delta\psi_1, \qquad \mathbf{M}_\delta = \mathbf{M} + \delta\mathbf{M}_1, \qquad \mathbf{A}_\delta = \mathbf{A} + \delta\mathbf{A}_1, \tag{4.127}$$

For variation of order parameter ψ, the minimum energy shall satisfy

$$\frac{d}{d\delta} G[\psi_\delta, \mathbf{A}, \mathbf{M} : \mathbf{H}^e]\Big|_{\delta=0} = 0 \qquad \forall\ \psi_1. \tag{4.128}$$

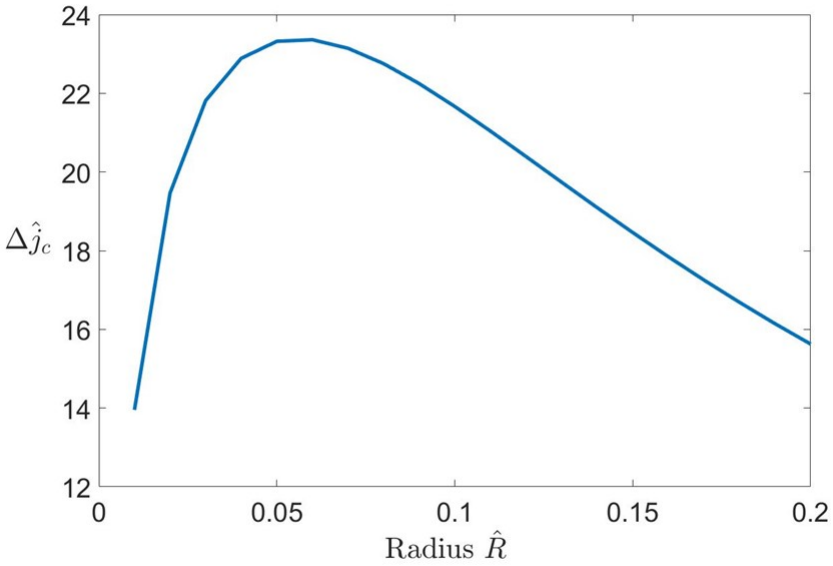

Figure 4.20: Increase of critical current j_{crit} versus radius of inhomogeneity $\hat{R}$

After manipulating the equation, we have

$$\begin{aligned}\frac{d}{d\delta}G[\psi_\delta,\mathbf{A},\mathbf{M};\mathbf{H}^e]\Big|_{\delta=0} &= \int_{\Omega_s}[\alpha\psi+\beta|\psi|^2\psi+\frac{1}{2m^*}(\frac{\hbar}{i}\nabla-\frac{e^*}{c}\mathbf{A})^2\psi]\psi_1^* \\ &+\int_{\Omega_s}[\alpha\psi^*+\beta|\psi|^2\psi^*+\frac{1}{2m^*}(\frac{\hbar}{i}\nabla+\frac{e^*}{c}\mathbf{A})^2\psi^*]\psi_1 \\ &-\int_{\partial\Omega_s}\frac{1}{2m^*}[(\frac{\hbar}{i})^2\nabla\psi\cdot\mathbf{N}-\frac{\hbar e^*}{ic}\psi\mathbf{A}\cdot\mathbf{N}]\psi_1^* \\ &-\int_{\partial\Omega_s}\frac{1}{2m^*}[(\frac{\hbar}{i})^2\nabla\psi^*\cdot\mathbf{N}+\frac{\hbar e^*}{ic}\psi^*\mathbf{A}\cdot\mathbf{N}]\psi_1=0 \qquad \forall\ \psi_1,\psi_1^*.\end{aligned} \tag{4.129}$$

where $\mathbf{N}$ is the unit outward normal on the boundary $\partial\Omega_s$.

Therefore, the Euler-Lagrange equation associated with ψ is

$$\alpha\psi+\beta|\psi|^2\psi+\frac{1}{2m^*}(\frac{\hbar}{i}\nabla-\frac{e^*}{c}\mathbf{A})^2\psi=0 \qquad \text{in } \Omega_s. \tag{4.130}$$

And the boundary condition on the interface is

$$[(\frac{\hbar}{i}\nabla-\frac{e^*}{c}\mathbf{A})\psi]\cdot\mathbf{N}=0 \qquad \text{on } \partial\Omega_s. \tag{4.131}$$

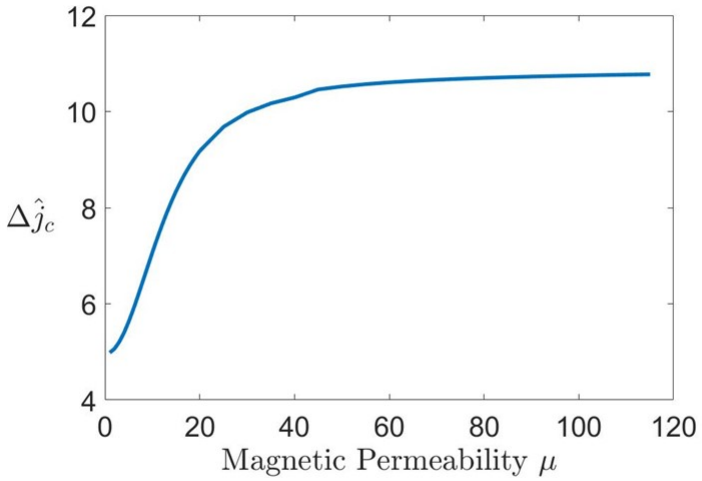

Figure 4.21: Increase of critical current j_{crit} versus magnetic permeability μ

For variation of magnetic vector potential $\mathbf{A}$, the minimum energy shall satisfy

$$\frac{d}{d\delta} G[\psi, \mathbf{A}_\delta, \mathbf{M}; \mathbf{H}^e]\Big|_{\delta=0} = 0 \qquad \forall\ \psi_1. \tag{4.132}$$

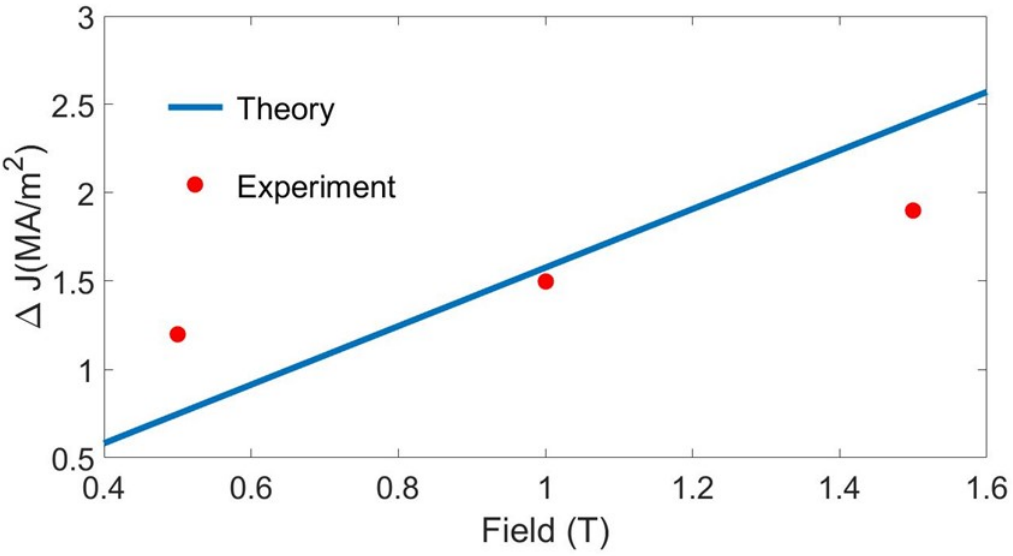

Figure 4.22: Incerase of critical current j_{crit} versus external magnetic field H^e. Experiment data are reproduced from Wee *et al.* [124]

From (4.132), we have

$$\begin{aligned}\frac{d}{d\delta}G[\psi,\mathbf{A}_\delta,\mathbf{M};\mathbf{H}^e] = &\int_{\Omega_s}\frac{1}{2m^*}[-\frac{\hbar e^*}{ic}(\psi^*\nabla\psi-\psi\nabla\psi^*)+2(\frac{e^*}{c})^2\psi\psi^*\mathbf{A}]\cdot\mathbf{A}_1\\ &+\frac{1}{4\pi}\int_{\Omega_s}[\nabla\times(\nabla\times\mathbf{A}-\mathbf{H}^e)]\cdot\mathbf{A}_1+\frac{1}{4\pi}\int_{\partial\Omega_s}[\mathbf{A}_1\times(\nabla\times\mathbf{A}-\mathbf{H}^e)]\cdot\mathbf{N}\\ &+\frac{1}{4\pi}\int_{\Omega_m}[\nabla\times(\nabla\times\mathbf{A}-\mathbf{H}^e-4\pi\mathbf{M})]\cdot\mathbf{A}_1\\ &-\frac{1}{4\pi}\int_{\partial\Omega_m}[\mathbf{A}_1\times(\nabla\times\mathbf{A}-\mathbf{H}^e-4\pi\mathbf{M})]\cdot\mathbf{N}\\ &=0\qquad\forall\,\mathbf{A}_1.\end{aligned}$$

The Euler-Lagrange equation associated with $\mathbf{A}$ is

$$\nabla \times (\nabla \times \mathbf{A} - 4\pi \mathbf{M}\chi_{\Omega_m}) = \frac{4\pi}{c}\mathbf{J}_s\chi_{\Omega_s} \quad \text{in } I\!R^3, \tag{4.133}$$

where

$$\mathbf{J}_s = \frac{\hbar e^*}{2m^* i}(\psi^*\nabla\psi - \psi\nabla\psi^*) - \frac{e^{*2}}{m^* c}\psi\psi^*\mathbf{A} \qquad \text{in } \Omega_s.$$

is the supercurrent.

The boundary on the interface Γ_{sinh} and Γ_{vinh} is also given by (4.132),

$$\begin{cases} [\![\nabla \times \mathbf{A} - \mathbf{M}]\!]\big|_{\Gamma_{sinh}} \times \mathbf{N} = 0 & \text{on } \Gamma_{sinh}, \\ [\![\nabla \times \mathbf{A} - \mathbf{M}]\!]\big|_{\Gamma_{vinh}} \times \mathbf{N} = 0 & \text{on } \Gamma_{vinh}. \end{cases} \tag{4.134}$$

For variation of magnetization $\mathbf{M}$, the minimum energy shall satisfy

$$\frac{d}{d\delta}G[\psi, \mathbf{A}, \mathbf{M}_\delta : \mathbf{H}^e]\Big|_{\delta=0} = 0 \qquad \forall\ \psi_1. \tag{4.135}$$

It is easy to obtain the Euler-Lagrange equation associated with $\mathbf{M}$

$$-\nabla \times \mathbf{A} + 4\pi\mathbf{M} + D_{\mathbf{M}}\phi(\mathbf{M}) - a_{\text{ex}}\Delta\mathbf{M} = 0 \quad \text{in } \Omega_m, \tag{4.136}$$

and the associated boundary condition

$$(\nabla\mathbf{M})\mathbf{N} = 0 \qquad \text{on } \partial\Omega_m. \tag{4.137}$$

4.7.2 Approximation solution of magnetic field in single vortex state

Due to the linearity of equation (4.47), in order to obtain an approximate solution, we suppose $\mathbf{B} = \mathbf{B}_1 + \mathbf{B}_2 + \mathbf{B}_3$. The meaning of $\mathbf{B}_i (i = 1, 2, 3)$ is as follows:

The magnetic field $\mathbf{B}_1$ represents the magnetic field in the superconductor domain when

there is no single vortex appears. The boundary value problem is

$$-\frac{1}{\lambda^2}\mathbf{B}_1 + \nabla^2\mathbf{B}_1 = 0 \qquad \text{in } \Omega_s, \tag{4.138}$$

subject to

$$\begin{cases} \mathbf{B}_1 = \frac{1}{\mu}H^e\mathbf{e}_z & \text{on } \Gamma_+, \\ \mathbf{B}_1 = 0 & \text{at } \infty_{\chi_{\Omega_s}}. \end{cases} \tag{4.139}$$

This modified helmholtz equation $(4.138)_1$ with the boundary conditions (4.139) are solvable:

$$\mathbf{B}_1 = \frac{H^e}{\mu}\frac{K_0(|\frac{\mathbf{r}}{\lambda}|)}{K_0(\frac{R}{\lambda})}\mathbf{e}_z. \tag{4.140}$$

The magnetic field $\mathbf{B}_2$ repersents the magnetic field when there is no inhomogeneity in the domain. The equations are as follows

$$\begin{cases} -\frac{1}{\lambda^2}\mathbf{B}_2 + \nabla^2\mathbf{B}_2 = -\frac{\Phi_0\delta_2(\mathbf{r}-\mathbf{r}_0)}{\lambda^2}\mathbf{e}_z & \text{in } \Omega_s, \\ \mathbf{B}_2 = 0 & \text{at } \infty_{\chi_{\Omega_s}}. \end{cases} \tag{4.141}$$

This is a free boundary problem and the solution is

$$\mathbf{B}_2 = \frac{\Phi_0}{2\pi\lambda^2}K_0(|\frac{\mathbf{r}-\mathbf{r}_0}{\lambda}|)\mathbf{e}_z. \tag{4.142}$$

Finally, we introduce the magnetic field $\mathbf{B}_3$ to compensate the effect of magnetic field $\mathbf{B}_2$ on the interface of inhomogeneity. The boundary value problem for $\mathbf{B}_3$ is

$$-\frac{1}{\lambda^2}\mathbf{B}_3 + \nabla^2\mathbf{B}_3 = 0 \qquad \text{in } \Omega_s, \tag{4.143}$$

Subject to

$$\begin{cases} \mathbf{B}_3 = -\mathbf{B}_2\big|_{\Gamma_+} & \text{on } \Gamma_+, \\ \mathbf{B}_3 = 0 & \text{at } \infty_{\chi\Omega_s}. \end{cases} \tag{4.144}$$

By separation of variables and symmetry of the model, we have

$$\mathbf{B}_3 = \Sigma_{n=0}^{\infty} a_n K_n(|\frac{\mathbf{r}}{\lambda}|)\cos(n\theta)\mathbf{e}_z. \tag{4.145}$$

By boundary condition $(4.143)_2$, we have

$$\Sigma_{n=0}^{\infty} a_n K_n(\frac{R}{\lambda})\cos(n\theta)\mathbf{e}_z = Q(\theta)\mathbf{e}_z = -\frac{\Phi_0}{2\pi\lambda^2} K_0(|\frac{\sqrt{R^2+|\mathbf{r}_0|^2-2R|\mathbf{r}_0|\cos\theta}}{\lambda}|)\mathbf{e}_z. \tag{4.146}$$

We expand the right hand side by *Fourier Series* and compare it to the left hand side, therefore we can obtain the coefficient of the first two leading order terms

$$a_0 = \frac{1}{K_0(\frac{R}{\lambda})}\frac{1}{\pi}\int_0^{\pi} Q(\theta)\mathrm{d}\theta, \qquad a_1 = \frac{1}{K_1(\frac{R}{\lambda})}\frac{2}{\pi}\int_0^{\pi} Q(\theta)cos\theta\mathrm{d}\theta. \tag{4.147}$$

In the end, the approximation of magnetic field $\mathbf{B}$ is

$$\begin{aligned} \mathbf{B} =& \frac{H^e}{\mu}\frac{K_0(|\frac{\mathbf{r}}{\lambda}|)}{K_0(\frac{R}{\lambda})}\mathbf{e}_z + \frac{\Phi_0}{2\pi\lambda^2}K_0(|\frac{\mathbf{r}-\mathbf{r}_0}{\lambda}|)\mathbf{e}_z + \big[\frac{1}{K_0(\frac{R}{\lambda})}\frac{1}{\pi}\int_0^{\pi} Q(\theta)\mathrm{d}\theta\big]K_0(|\frac{\mathbf{r}}{\lambda}|)+ \\ & \big[\frac{1}{K_1(\frac{R}{\lambda})}\frac{2}{\pi}\int_0^{\pi} Q(\theta)cos\theta\mathrm{d}\theta\big]K_1(|\frac{\mathbf{r}}{\lambda}|)\cos\theta. \end{aligned} \tag{4.148}$$

4.7.3 Derivation for current distribution in the thin film passing with a columnar inhomogeneity

Consider a infinite plane xy with thickness t in $\mathbf{e}_z$ direction, one columnar inhomogeneity with radius R is located in the center of the plane. Decompose the transport current density $\mathbf{J}_t$ into planar current density $\mathbf{J}_0(z)$ without a columnar inhomogeneity and perturbated current density $\mathbf{J}_1(x,y,z)$ considering the existence of inhomogeneity

$$\mathbf{J}_t = \mathbf{J}_0(z) + \mathbf{J}_1(x,y,z). \tag{4.149}$$

The boundary condition of $\mathbf{J}_t$ can be written as

$$\lambda^2 \Delta \mathbf{J}_t - \mathbf{J}_t = 0 \qquad \text{in } \tilde{\Omega} \times (0, d) \tag{4.150}$$

subject to

$$\begin{cases} \mathbf{J}_t \cdot \mathbf{n} = 0 & \text{on } \partial\tilde{\Omega}_m \\ \oint_{\text{end}} \mathbf{J}_t = j_0 \mathbf{e}_y. \end{cases} \tag{4.151}$$

Because of the linearity of (4.149), the above equation is decomposed into two parts. For the planar current density $\mathbf{J}_0(z)$, we have

$$\begin{cases} \lambda^2 \Delta \mathbf{J}_0(z) - \mathbf{J}_0(z) = 0 & \text{in } \tilde{\Omega} \times (0, d) \\ \oint \mathbf{J}_0(z) \cdot \mathbf{n} = j_0 & \text{on } \partial\tilde{\Omega} \end{cases} \tag{4.152}$$

For the perturbation current density $\mathbf{J}_1(x, y, z)$, we have

$$\begin{cases} \lambda^2 \Delta \mathbf{J}_1(x, y, z) - \vec{J}_1(x, y, z) = 0 & \text{in } \tilde{\Omega} \times (0, d) \\ (\mathbf{J}_0(z) + \mathbf{J}_1(x, y, z)) \cdot \mathbf{n} = 0 & \text{on } \partial\tilde{\Omega}_m \\ \mathbf{J}_1(x, y, z) = 0 & \text{at } \infty \end{cases} \tag{4.153}$$

We shall notice that $\mathbf{J}_0(z)$ only have $\mathbf{e}_y$ component $\mathbf{J}_0(z) = (0, J_{0y}(z), 0)$ and $\mathbf{J}_1(x, y, z)$ only have $\mathbf{e}_x$ and $\mathbf{e}_y$ component $\mathbf{J}_1 = (J_{1x}(x, y, z), J_{1y}(x, y, z), 0)$.

By symmetry, component $J_{0y}(z)$ can be easily solved as

$$J_{0y}(z) = C \frac{e^{z/\lambda} + e^{-z/\lambda}}{2}, \tag{4.154}$$

where C is determined by the average current density j_0.

Since $\mathbf{J}_1$ is treated as a perturbated term, for convenience, we make the following transformation

$$\mathbf{J}_1(x, y, z) = J_{0y}(z)(\hat{J}_x(x, y), \hat{J}_y(x, y), 0) = J_{0y}(z)\hat{\mathbf{J}}_1(x, y). \tag{4.155}$$

Substitute (4.155) into (4.153), we obtain a two dimensional planar Laplace equation which only has $\mathbf{e}_x$, $\mathbf{e}_y$ components and only depends on x and y.

$$\begin{cases} \tilde{\Delta}\hat{\mathbf{J}}_1(x,y) = 0 & \text{on } \tilde{\Omega} \\ (\mathbf{e}_y + \hat{\mathbf{J}}_1(x,y)) \cdot \mathbf{n} = 0 & \text{on } \partial\tilde{\Omega}_m \\ \hat{\mathbf{J}}_1(x,y) = 0 & \text{at } \infty \end{cases} \tag{4.156}$$

We now consider the problem in cylindrical coordinate (r, θ, z). The fundamental solution for a general Laplace equation using separation of variable is given

$$S(r,\theta) = A\ln r + B + \Sigma_{n=1}^{\infty} r^n (A_n \sin n\theta + B_n \cos n\theta) + \Sigma_{n=-\infty}^{-1} r^n (C_n \sin n\theta + D_n \cos n\theta) \tag{4.157}$$

Both of $\mathbf{e}_x$ and $\mathbf{e}_y$ components of $\hat{\mathbf{J}}_1$ can be expressed in the above form. Meanwhile, $\hat{J}_x$ and $\hat{J}_y$ have the following symmetric properties

$$\begin{aligned} \hat{J}_x(r,\theta) &= \hat{J}_x(r,-\theta) \qquad \hat{J}_x(r,\theta) = -\hat{J}_x(r,\pi-\theta) \\ \hat{J}_y(r,\theta) &= \hat{J}_y(r,-\theta) \qquad \hat{J}_y(r,\theta) = \hat{J}_y(r,\pi-\theta) \end{aligned} \tag{4.158}$$

Thus, $\hat{J}_x$ and $\hat{J}_y$ shall satisfy the following general solutions

$$\begin{aligned} \hat{J}_x &= \Sigma_{n=1}^{\infty} \frac{C_n}{r^n} \sin n\theta, \\ \hat{J}_y &= \Sigma_{n=1}^{\infty} \frac{D_n}{r^n} \cos n\theta. \end{aligned} \tag{4.159}$$

Then the boundary condition $(4.153)_2$ can be rewritten as

$$[\Sigma_{n=1}^{\infty} \frac{C_n}{R^n} \sin n\theta] \cos\theta + [\Sigma_{n=1}^{\infty} \frac{D_n}{R^n} \cos n\theta + 1] \sin\theta = 0 \tag{4.160}$$

Using the identities of trigonometric functions

$$\cos\alpha\sin\beta = \frac{\sin(\alpha+\beta)-\sin(\alpha-\beta)}{2},$$
$$\sin\alpha\cos\beta = \frac{\sin(\alpha+\beta)+\sin(\alpha-\beta)}{2}. \tag{4.161}$$

The boundary condition can be manipulated as

$$\Sigma_{n=1}^{\infty}\frac{C_n}{R_n}\frac{\sin(n+1)\theta+\sin(n-1)\theta}{2}+\Sigma_{n=1}^{\infty}\frac{D_n}{R_n}\frac{\sin(n+1)\theta-\sin(n-1)\theta}{2}=-2\sin\theta, \tag{4.162}$$

We can obtain the coefficient C_i and D_i as follows

$$C_i=\begin{cases}-R^2 & i=2,\\ 0 & \text{otherwise}\end{cases}\qquad D_i=\begin{cases}R^2 & i=2,\\ 0 & \text{otherwise}\end{cases} \tag{4.163}$$

And the solution of $\hat{J}_x$ and $\hat{J}_y$ are

$$\hat{J}_x = -\frac{R^2}{r^2}\sin 2\theta,$$
$$\hat{J}_y = \frac{R^2}{r^2}\cos 2\theta. \tag{4.164}$$

Thus, the total current density can be written as

$$\mathbf{J}_t = C\frac{e^{z/\lambda}+e^{-z/\lambda}}{2}(-\frac{R^2}{r^2}\sin 2\theta, 1+\frac{R^2}{r^2}\cos 2\theta, 0). \tag{4.165}$$

Chapter 5

Applications

5.1 High T_c Superconducting Magnet Excited by Composite Thermoelectric Element

High temperature superconductors have advantages in their working temperature, low enegy loss and high magnetic field over low temperture superconductors. Combined with thermoelectric composites, we design a High Temperature Superconducting (HTS) magnet which is excited by thermoelectric element. Instead of requiring an external power source for converntional HTS, the proposed HTS magnet requires no external power source through being excited by a thermo-electromotive force of a thermoelectic composite. This could make the magnet system compact and lightweight so that it is more suitable for applications in the place where the space and weight are limited.

The proposed HTS magnet system consists of a thermoelectric composite element, HTS coils and a pair of HTS leads to connenct the coils and element as shown in Fig. 5.1. The thermoelectic compsite element is used in place of an external power source, provides an electromotive force by transfering heat energy into electrical energy. The working temperature of the thermoelectric composite element has limitation due to the usage of superconductor. Both of temperature of cold junction and hot junction must below the critical temperature of the supercoducting material. The system is under cryogenic temperature and heater is attached one side of the junctions of the element to generate and control the temperature difference on the thermoelectric difference.

Consider the thermoelectric composite with a sandwich structure of two TE materials as a plate with thickness L. The TE properties are given by σ_r, κ_r and s_r (r=1,2). Recall that by the continuum theory for thermoelectric materials in chapter 3, the effective electrical

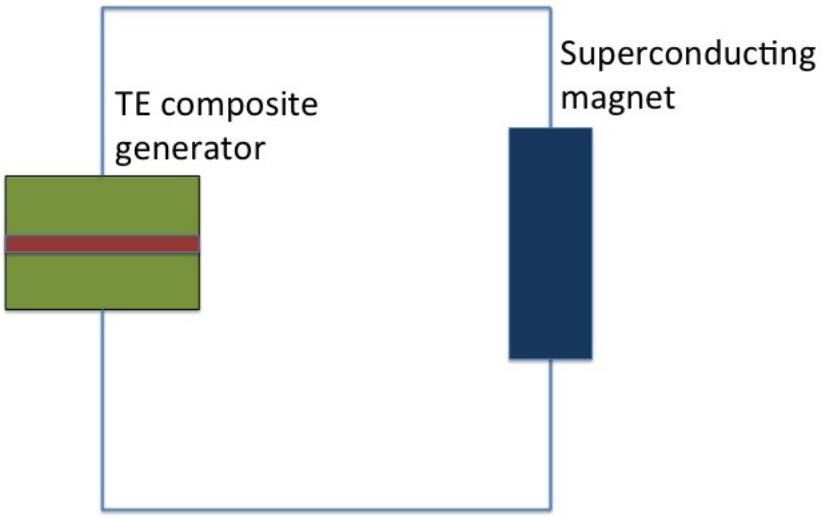

Figure 5.1: Superconductor magnet

conductivity, effective thermal conductivity and effective Seebeck coefficient of the overall composite can be written as

$$\begin{bmatrix} \sigma^e & T_0\sigma^e s^e \\ T_0\sigma^e s^e & T_0[\kappa^e + T_0\sigma^e (s^e)^2] \end{bmatrix} = \\ \left\{ \theta_1 \begin{bmatrix} \sigma_1 & T_0\sigma_1 s_1 \\ T_0\sigma_1 s_{\mathrm{mt}} & T_0[\kappa_1 + T_0\sigma_1 (s_1)^2] \end{bmatrix}^{-1} + \theta_2 \begin{bmatrix} \sigma_2 & T_0\sigma_2 s_2 \\ T_0\sigma_2 s_2 & T_0[\kappa_2 + T_0\sigma_2 (s_2)^2] \end{bmatrix}^{-1} \right\}^{-1}, \tag{5.1}$$

where $\theta_1(\theta_2)$ is the volume fraction of materials1(2).

The boundary temperature and electrochemical potential are maintained as

$$\begin{cases} T = T_2, \quad \mu = \mu_0, & \text{on top surface,} \\ T = T_1, \quad \mu = -\mu_0, & \text{on bottom surface,} \end{cases} \tag{5.2}$$

Assuming temperature difference (i.e., $\delta T = T_2 - T_1 \ll T_0$) across the composite is small

, and upon linearization we can explicitly give the electric and energy fluxes genarated by the TE element as

$$j_e = -T_0\mu_0[\frac{1}{T_2L} + \frac{1}{T_1L}]\sigma + T_0^2[\frac{1}{T_2L} - \frac{1}{T_1L}]\sigma s, \tag{5.3}$$

$$j_u = -T_0^2\mu_0[\frac{1}{T_2L} + \frac{1}{T_1L}]s\sigma + T_0^2[\frac{1}{T_2L} - \frac{1}{T_1L}](\kappa + T_0\sigma s^2). \tag{5.4}$$

Without the electric potential μ_0, they can be written as

$$j_e = T_0^2[\frac{1}{T_2L} - \frac{1}{T_1L}]\sigma s, \tag{5.5}$$

$$j_u = T_0^2[\frac{1}{T_2L} - \frac{1}{T_1L}](\kappa + T_0\sigma s^2). \tag{5.6}$$

The heat density flux j_q is

$$j_q = j_u - \mu j_e = j_u. \tag{5.7}$$

For traditional HTS magnet system, HTS coils are used to connect the external power source in order to minimize the heat leakage to a cryogenic temperature from the ambient temperature. The amount of heat leakage of HTS coil per unit current (Q/I) is an important index to evaluate the performance of superconducting magnet. In this proposed magnet system, the heat leakage is determined by

$$Q/I = j_q/j_e = \frac{k}{\sigma s} + T_0 s. \tag{5.8}$$

To be more precise, if there is a adjusted electric resistence r_{adj} for the whole magnet system, electric potential μ is no longer zero, instead it is determined by

$$r_{adj}j_eS = 2\mu. \tag{5.9}$$

Combine with the solution of electric density flux $(5.3)_1$, we can express electric density

flux j_e and electric potential μ in terms of the adjusted electric resistence as

$$\mu_0 = \frac{T_0^2 \sigma s \frac{T_1 - T_2}{T_1 T_2 L}}{\frac{2}{r_{adj} S} + \frac{T_1 + T_2}{T_1 T_2} \frac{T_0 \sigma}{L}} \tag{5.10}$$

$$j_e = \frac{T_0^2 \sigma s \frac{T_1 - T_2}{T_1 T_2 L}}{2 + r_{adj} S \frac{T_1 + T_2}{T_1 T_2} \frac{T_0 \sigma}{L}} \tag{5.11}$$

Neglecting the adjusted electric resistence due to the HTS coil and the HTS leads, for the composite material consisting of Cu and pB_iT_e, we give the figure for the power factor p_f, heat leakage Q/I and the electric density flux j_e versus the volumn fraction of Cu at temperature $T = 77K$ in Fig. 5.2:

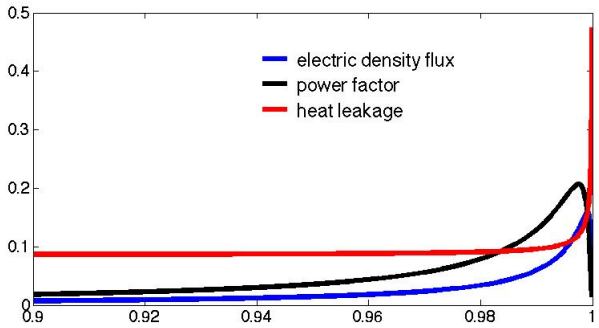

Figure 5.2: Power factor p_f, heat leakage Q/I and the electric density flux j_e versus the volumn fraction of Cu

In the conventional magnet system, the minimized heat leakage is about $0.09W/A$. Now comparing to our proposed magnet system, the maximum electric flux density reaches at a pretty low volume fraction of TE materials in the composite while the heat leakage at that point is less then 0.15 W/A, which is acceptable. To increase the transport current, it can be obtained by fabricating a larger cross-section area of thermoelectric composite to get rid of rising the temperature applied on the hot junction.

5.2 Cooler for Superconducting Transmission Bulk

A high temperature superconductor (HTS) transmission bulk for carrying electric currents could be widely used because of its zero energy loss dissipation. However, the amount of transport current has its limitation on the geometric design, external magnetic field,

materials properties and working termperature. Especially for achieving a stable working temperature, a cooling system which is thermally coupled by a high electrical conductivity material to the plurality of HTS transmission bulk shall be applied. In this proposed cooling application design, the self-motivated thermoelectric (TE) composite coolers are arranged in series along the electric current transporting direction. Then TE cooler would cool superconducting bulk and generate compensation currents.

TE composite used as cooler to stabilize the superconducting current transportation is shown in Fig. 5.3. Each TE cooler is attached on the top surface of the superconducting bulk. The thermal and electrical contacts between superconductor bulk and TE composite are perfect. We assume the ambient temperature is T_c, the effective thermoelectric properties of TE material are s, σ and κ and the temperature T_{sc} inside the superconductor is uniform.

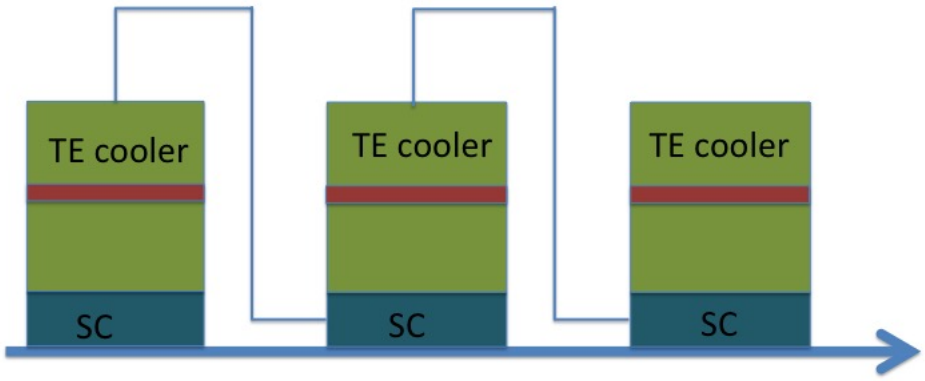

Figure 5.3: Cooler

Once temperature flactuation happens, i.e., temperature T_{sc} is higher than ambient temperature T_c, TE cooler can lower the temperature T_{sc} by transferring heat energy into electric energy through generated heat flux.

The TE composite cooler is designed as a plate. Also, we ignore the temperature on

the fringe. According to the continuum theory in Chapter 3, the electric flux density and energy flux density are in the form of

$$j_e = -T_0\mu_0[\frac{1}{T_2L} + \frac{1}{T_1L}]\sigma + T_0^2[\frac{1}{T_2L} - \frac{1}{T_1L}]\sigma s, \tag{5.12}$$

$$j_u = -T_0^2\mu_0[\frac{1}{T_2L} + \frac{1}{T_1L}]s\sigma + T_0^2[\frac{1}{T_2L} - \frac{1}{T_1L}](\kappa + T_0\sigma s^2). \tag{5.13}$$

In the continuum theory, we have the assumption that the temperature difference is small

$$T_1 \approx T_2 \approx T_0. \tag{5.14}$$

If we add a large electric resistence r_{adj} in the circuit, as calculated in the last section, we have

$$\begin{aligned} \mu_0 &= \frac{T_0^2\sigma s\frac{T_1-T_2}{T_1T_2L}}{\frac{2}{r_{adj}S} + \frac{T_1+T_2}{T_1T_2}\frac{T_0\sigma}{L}} = \frac{(T_1-T_2)\sigma s r_{adj}S}{2L + 2r_{adj}S\sigma}, \\ j_e &= \frac{T_0^2\sigma s\frac{T_1-T_2}{T_1T_2L}}{2 + r_{adj}S\frac{T_1+T_2}{T_1T_2}\frac{T_0\sigma}{L}} = \frac{(T_1-T_2)\sigma s}{2L + 2\sigma r_{adj}S}. \end{aligned} \tag{5.15}$$

Where S is the cross-section of the TE cooler. Notice that this electric density j_e flux can be regarded as compensation for the loss of current when critical current decreases with a higher temperature.

The energy density flux is

$$\begin{aligned} j_u &= -T_0^2\mu_0[\frac{1}{T_2L} + \frac{1}{T_1L}]s\sigma + T_0^2[\frac{1}{T_2L} - \frac{1}{T_1L}](\kappa + T_0\sigma s^2) \\ &= -\frac{2T_0s\sigma}{L}\frac{(T_1-T_2)\sigma s r_{adj}S}{2L + 2r_{adj}S\sigma} + \frac{T_1-T_2}{L}(\kappa + T_0\sigma s^2) \\ &= (\frac{\kappa + T_0\sigma s^2}{L} - \frac{2T_0s\sigma}{L}\frac{\sigma s r_{adj}S}{2L + 2r_{adj}S\sigma})(T_1-T_2). \end{aligned} \tag{5.16}$$

Therefore the heat density flux is determined by

$$\begin{aligned} j_q &= j_u - \mu_0 j_e \\ &= (\frac{\kappa + T_0\sigma s^2}{L} - \frac{2T_0 s\sigma}{L}\frac{\sigma s r_{adj} S}{2L + 2r_{adj} S\sigma})(T_1 - T_2) \\ &- [\frac{\sigma s}{2L + 2r_{adj} S\sigma}]^2 r_{adj} S(T_1 - T_2)^2 \\ &= A(T_1 - T_2) - B(T_1 - T_2)^2, \end{aligned} \tag{5.17}$$

where $A = \frac{\kappa + T_0\sigma s^2}{L} - \frac{2T_0 s\sigma}{L}\frac{\sigma s r_{adj} S}{2L + 2r_{adj} S\sigma}$ and $B = [\frac{\sigma s}{2L + 2r_{adj} S\sigma}]^2 r_{adj} S$. Remark that if $r_{adj} \to \infty$, the electric density flux $j_e \to 0$ and the electric potential is

$$\mu_0 \to \frac{(T_1 - T_2)s}{2}. \tag{5.18}$$

The energy density j_u is given

$$\begin{aligned} j_u &= -T_0^2\mu_0[\frac{1}{T_2 L} + \frac{1}{T_1 L}]s\sigma + T_0^2[\frac{1}{T_2 L} - \frac{1}{T_1 L}](\kappa + T_0\sigma s^2) \\ &= -\frac{s^2\sigma}{L}T_0(T_1 - T_2) + \frac{\kappa + T_0\sigma s^2}{L}(T_1 - T_2) \\ &= \frac{\kappa}{L}(T_1 - T_2), \end{aligned} \tag{5.19}$$

which degenerates to Fourier's law.

We can also calculate the characteristic time of the system to recover the temperature. Given the heat capacity C_v for each superconductor, it is determined by

$$\begin{cases} j_q S = A(T_c - T_{sc}) - B(T_c - T_{sc})^2 = C_v \frac{\mathrm{d}T_{sc}}{\mathrm{d}t}, \\ T_{sc}(0) = T_h. \end{cases} \tag{5.20}$$

The solution for the above boundary value problem is

$$\frac{T_{sc} - T_c}{T_h - T_c} \cdot \frac{A - B(T_h - T_c)}{A - B(T_{sc} - T_c)} = e^{-\frac{A}{c}t}. \tag{5.21}$$

Chapter 6

Conclusions

In this thesis, we have investigated three kinds of physical coupling problems using variantional energy formulation method. Firstly, to deal with the problem that determing the equilibrium shape of a bubble in an electric field, we proposed a general variational method in account of electro-mechanical couplings. Our analysis shows that this variational formulation is equivalent to the classic field equation approach based on the Young-Laplace equation and the concept of Maxwell stress. And a fixed mesh level-set gradient method for simulating the equalibrium shape of the bubble is then developed based on the energy formulation. The numerical scheme is validated by comparing with analytical solutions [8] and experimental results [6].

Secondly, we reviewed Liping Liu's continuum theory for the thermoelectric bodies. Boundary value problems are formulated and explicit formula of effective TE properties of thermoeletric composites with simple laminates structure can be obtained by the continuum theory. We have shown that power factor can be significantly improved by heterogeneous TE structures. We implement a FEM simulation to solve generic TE boundary value problems for general geometries, heterogeneities and boundary conditions. In particular, to account for the effect of small electrical contacts, we numerically compute the local fields and electrical power output of simple laminates in real-world working condition. The results demonstrated that the optimal power output of the TE sandwich is still 75 times larger then pure TE structure at the same size and boundary conditions even small electrical contacts do have a significant effect on power output.

Thirdly, we studied the phase transitions of superconducting materials and proposed the free energy system which is combined with phenomenological Ginzburg-Landau theory and Landau theory of micromagnetics. In particular, we analyze the magnetic vortex pinning by

paramagnetic boundary in high temperature type II superconducting materials. With the help of framework we developed, we conclude that (i) Euler-Lagrange equations associated with boundary conditions is derived in the principle of free energy. (ii) In two-dimensional planar model for zero external transport current scenario, we calculate the pinning force on a single magnetic vortex for different configurations of inhomogeneity and external magnetic field in the dilute limit case. (iii) Consider three-dimensional model with external transport current, a decomposition on supercurrent-based total free energy system is investigated. We give explanation on the mechanisms for each energy terms in the system. Also the attractive pinning force of a single vortex to the interface of the inhomogenity is calculated associated with the size of inhomogeneity, magnetic permeability, thickness of film, strength of external transport current and external magnetic field. (iv) Based on a naive definition on the critical current, we find the critical current shall be optimized by a larger size of inhomogeneity in some range and critical current approaches to saturation with higher magnetic permeability of inhomgeneity which agrees with some experimental results quanlitatively.

Finally, we proposed two potential applications: (i) A high temperature superconducting magnet excited by thermoelectric element. (ii) A cooler for superconducting transmission bulk. The proposed magnetic can reach the maximum electric flux density at a pretty low volume fraction of pure TE materials in the composite while the heat leakage at that point is less then 0.15 W/A. And the proposed TE composite cooler can not only stabilize the superconducting transportation bulk but also provide a compensation of transport currents. The characteristic time for the system to recover the temperature is given in equation 5.21.

References

[1] G. Allaire and F. Jouve. Minimum stress optimal design with the level set method. *Engineering Analysis With Boundary Elements*, 32(11):909–918, 2008.

[2] Grégoire Allaire, François Jouve, and Anca-Maria Toader. Structural optimization using sensitivity analysis and a level-set method. *Journal of Computational Physics*, 194(1):363 – 393, 2004.

[3] Peter Berg, Sven-Joachim Kimmerle, and Arian Novruzi. Modeling, shape analysis and computation of the equilibrium pore shape near a pem–pem intersection. *Journal of Mathematical Analysis and Applications*, 410(1):241 – 256, 2014.

[4] R. Bustamante, A. Dorfmann, and R.W. Ogden. On electric body forces and maxwell stresses in nonlinearly electroelastic solids. *International Journal of Engineering Science*, 47:1131 – 1141, 2009.

[5] P. Carrica, P. Dimarco, and W. Grassi. Nucleate pool boiling in the presence of an electric field: Effect of subcooling and heat-up rate. *Experimental Thermal and Fluid Science*, 15(3):213–220, 1997.

[6] F. Chen, Y. Peng, and and M.Chen Y. Z.Song. Ehd behavior of nitrogen bubbles in dc electric fields. *Experimental Thermal and Fluid Science*, 32(1):174–181, 2007.

[7] K. J. Cheng and J. B. Chaddock. Deformation and stability of drops and bubbles in an electric field. *Physics Letters*, 106A(1):51–53, 1984.

[8] K.J. Cheng and J.B. Chaddock. Maximum size of bubbles during nucleate boiling in an electric field. *International Journal of Heat and Fluid Flow*, 7(4):278 – 282, 1986.

[9] H. J. Cho, I. S. Kang, Y. C. Kweon, and M. H. Kim. Study of the behavior of a bubble attached to a wall in a uniform electric field. *International Journal of Multiphase Flow*, 22(5):909–922, 1996.

[10] H. J. Cho, I. S. Kang, Y. C. Kweon, and M. H. Kim. Numerical study of the behavior of a bubble attached to a tip in a non-uniform electric field. *International Journal of Multiphase Flow*, 24(3):479–498, 1998 1998.

[11] W. Dong, R. Y. Li, H. L.Yu, and Y. Y. Yan. An investigation of behaviours of a single bubble in a uniform electric field. *Experimental Thermal and Fluid Science*, 30(6):579–586, 2006.

[12] J. D. Eshelby. Energy relations and the energy-momentum tensor in continuum mechanics. pages 77–115. M.F. Kanninen, W.F. Adler, A.R. Rosenfield, and R.I. Jaffee (Eds.). *Inelastic behavior of solids*, McGraw-Hill: New York, 1970.

[13] C. G. Garton and Z. Krasucki. Bubbles in insulating liquid: stability in an electric field. *Proceedings of the Royal Society*, 280(1382):383–397, 1964.

[14] Yury Grabovsky, Vladislav A. Kucher, and Lev Truskinovsky. Weak variations of Lipschitz graphs and stability of phase boundaries. *Continuum Mechanics and Thermodynamics*, 23(2):87–123, 2011.

[15] F. J. Higuera. Injection of bubbles in a quiescent inviscid liquid under a uniform electric field. *Journal of Fluid Mechanics*, 568:203–222, 2006.

[16] Y. Hristov, D. Zhao, D. Kenning, K. Sefiane, and T. Karayiannis. A study of nucleate boiling and critical heat flux with ehd enhancement. *Heat and Mass Transfer*, 45(7):999–1017, 2009.

[17] Chen J, M. Abdelgawad, L. Yu, N. Shakiba, W-Y Chien, Z. Lu, W. R. Geddie, M. Jewett, and Y. Sun. Electrodeformation for single cell mechanical characterization. *J. Micromech. Microeng.*, 21:054012, 2011.

[18] J.Simon. Differentiation with respect to the domain in boundary value problems. *Numerical Functional Analysis and Optimization*, 2(7):649–687, 1980.

[19] T. G. Karayiannis. Ehd boiling heat transfer enhancement of r123 and r11 on a tube bundle. *Applied Thermal Engineering*, 18(9-10):809–817, 1988.

[20] Sven-Joachim Kimmerle, Peter Berg, and Arian Novruzi. An electrohydrodynamic equilibrium shape problem for polymer electrolyte membranes in fuel cells. In *IFIP Conference on System Modeling and Optimization*, pages 387–396. Springer, 2011.

[21] Wolfgang Kuhnel. *Differential Geometry: Curves - Surfaces - Manifolds*. American Mathematical Society, 2005.

[22] Y. C. Kweon and M. H. Kim. Experimental study on nucleate boiling enhancement and bubble dynamic behavior in saturated pool boiling using a nonuniform dc electric field. *International Journal of Multiphase Flow*, 26(8):1351–1368, 2000.

[23] Kehinde O. Ladipo, Peter Berg, Sven-Joachim Kimmerle, and Arian Novruzi. Effects of radially dependent parameters on proton transport in polymer electrolyte membrane nanopores. *The Journal of Chemical Physics*, 134(7):074103, 2011.

[24] Liping Liu. On energy formulations of electrostatics for continuum media. *Journal of the Mechanics and Physics of Solids*, 61(4):968 – 990, 2013.

[25] Liping Liu. An energy formulation of continuum magneto-electro-elasticity with applications. *Journal of the Mechanics and Physics of Solids*, 63:451–480, FEB 2014.

[26] P. Di Marco, W. Grassi, G. Memoli, T. Takamasa, A. Tomiyama, and S. Hosokawa. Influence of electric field on single gas-bubble growth and detachment in microgravity. *International Journal of Multiphase Flow*, 29(4):559–578, 2003.

[27] P. Di Marco, R. Kurimoto, G. Saccone, K. Hayashi, and A. Tomiyama. Bubble shape under the action of electric forces. *Experimental Thermal and Fluid Science*, 49:160–168, 2013.

[28] J. C. Maxwell. *A treatise on electricity and magnetism*. Oxford, United Kindgdom: Clarendon Press, 1873.

[29] M.E.Gurtin and A.I.Murdoch. A continuum theory of elastic material surfaces. *Arch. Rat. Mech. Anal.*, 57(4):291–323, 1975.

[30] J. R. Melcher. *Continuum Electromechanics*. The MIT Press, 1981.

[31] J R Melcher and G I Taylor. Electrohydrodynamics: A review of the role of interfacial shear stresses. *Annual Review of Fluid Mechanics*, 1(1):111–146, 1969.

[32] R. S. Neve and Y. Y. Yan. Enhancement of heat exchanger performance using combined electrohydrodynamic and passive methods. *International Journal of Heat and Fluid Flow*, 17(4):403–409, 1996.

[33] J. Ogata and A. Yabe. Basic study on the enhancement of nucleate boiling heat transfer by applying electric fields. *International Journal of Heat and Mass Transfer*, 36(3):775–782, 1993.

[34] S. D. Oh and H. Y. Kwak. A study of bubble behavior and boiling heat transfer enhancement under electric field. *Heat Transfer Engineering*, 21(4):33–45, 2000.

[35] S Osher and J. A. Sethian. Fronts propagating with curvature-dependent speed-algorithms based on hamilton-jacobi formulations. *J. Comp. Phys.*, 79(1):12–49, 1988.

[36] Stanley J. Osher and Fadil Santosa. Level set methods for optimization problems involving geometry and constraints: I. frequencies of a two-density inhomogeneous drum. *Journal of Computational Physics*, 171(1):272 – 288, 2001.

[37] Carlos Rinaldi and Howard Brenner. Body versus surface forces in continuum mechanics: Is the maxwell stress tensor a physically objective cauchy stress? *Phys. Rev. E*, 65:036615, Feb 2002.

[38] S. Wongwises. S. Laohalertdecha, P. Naphon. A review of electrohydrodynamic enhancement of heat transfer. *Renewable and Sustainable Energy Review*, 11(5):858–876, 2007.

[39] D. A. Saville. Electrohydrodynamics: The taylor-melcher leaky dielectric model. *Annual Review of Fluid Mechanics*, 29:27–64, 1997.

[40] J. A. Sethian. *Level Set Method: Evolving Interfaces in Geometry, Fluid Mechanics, Computer Vision, and Materials Science*. Cambridge University Press, 1996.

[41] J.A. Sethian and Andreas Wiegmann. Structural boundary design via level set and immersed interface methods. *Journal of Computational Physics*, 163(2):489 – 528, 2000.

[42] J. A. Stratton. *Electromagnetic Theory*. Adams Press, 1941.

[43] A.K. Tagantsev. Piezoelectricity and flexoelectricity in crystalline dielectrics. *Physical Review B*, 34:5883–5889, 1986.

[44] G. I. Taylor. Disintegration of water drops in an electric field. *Proceedings of the Royal Society*, 280(1381):221–226, 1964.

[45] R. A. Toupin. The elastic dielectric. *J. Rational Mech. Anal.*, 5:849–914, 1956.

[46] R. A. Toupin. Stress tensors in elastic dielectrics. *Arch. Rational Mech. Anal.*, 5:440–452, 1960.

[47] M. C. Zaghdoudi and M. Lallemand. Nucleate pool boiling under dc electric field. *Experimental Heat Transfer*, 14(3):157–180, 2001.

[48] M. C. Zaghdoudi and M. Lallemand. Electric field effects on pool boiling. *Journal of Enhanced Heat Transfer*, 9(5-6):187–208, 2002.

[49] H.B. Zhang, Y.Y. Yan, and Y.Q. Zu. Numerical modelling of {EHD} effects on heat transfer and bubble shapes of nucleate boiling. *Applied Mathematical Modelling*, 34(3):626 – 638, 2010.

[50] Y.Q. Zu and Y.Y. Yan. A numerical investigation of electrohydrodynamic (ehd) effects on bubble deformation under pseudo-nucleate boiling conditions. *International Journal of Heat and Fluid Flow*, 30(4):761 – 767, 2009.

[51] T. Tritt, and M. Subramanian. Thermoelectric materials, phenomena, and applications: A bird's eye view *MRS Bulletin*, 31(3):188-194, 2006.

[52] D. T. Crane, D. Kossakovski, and L. E. Bell. Modeling the Building Blocks of a 10% Efficient Segmented Thermoelectric Power Generator *Journal of Electronic Materials.*, 38(7): 1382–1386, 2009.

[53] A. Yadav, K. P. Pipe, and M. Shtein. Fiber-based flexible thermoelectric power generator *Journal of Power Sources*, 175(2): 909–913 ,2008.

[54] L. E. Bell. Cooling, heating, generating power, and recovering waste heat with thermoelectric systems *Science*, 321(5895): 1457-1461, 2008.

[55] F. DiSalvo. Thermoelectric cooling and power generation *Science*, 285(5428): 703–706,1999.

[56] G. Nolas, D. Morelli, and T. Tritt. Skutterudites: A phonon-glass-electron crystal approach to advanced thermoelectric energy conversion applications *Annual Review of Materials Science*, 29(71): 89–116, 1999.

[57] L. Hicks, T. Harman, and M. Dresselhaus. Use of quantum-well superlattices to obtain a high figure of merit from nonconventional thermoelectric materials *Applied Physics Letters*, 63(23): 3230–3232, 1993.

[58] L. Hicks, and M. Dresselhaus. Effect of quantum-well structures on the thermoelectric figure of merit *Physical Review B*, 47(19): 12727, 1993.

[59] G. Joshi, H. Lee, Y. Lan, X. Wang, G. Zhu, D. Wang, R. W. Gould, D. C. Cuff, M. Y. Tang, M. S. Dresselhaus, G. Chen, and Z. Ren. Enhanced Thermoelectric Figure-of-Merit in Nanostructured p-type Silicon Germanium Bulk Alloys *Nano Letters*, 8(12): 4670–4674, 2008.

[60] H. Lee, D. Vashaee, D. Z. Wang, M. Dresselhaus, Z. F. Ren, and G. Chen. Effects of nanoscale porosity on thermoelectric properties of SiGe *Journal of Applied Physics*, 107(9), 2010.

[61] Y. Lan, A. J. Minnich, G. Chen, and Z. Ren. Enhancement of Thermoelectric Figure-of-Merit by a Bulk Nanostructuring Approach *Advanced Functional Materials*, 20(3): 357–376, 2010.

[62] R. Venkatasubramanian, E. Siivola, T. Colpitts, and B. O'Quinn. Thin-film thermoelectric devices with high room-temperature figures of merit *Nature*, 413(42):597–602, 2001.

[63] O. Yamashita, and H. Odahara. Effect of the thickness of Bi-Te compound and Cu electrode on the resultant Seebeck coefficient in touching Cu/Bi-Te/Cu composites *Journal of Materials Science*, 42(13): 5057-5067, 2007.

[64] K.F Hsu, S. Loo, F. Guo, W. Chen, J.S. Dyck, C. Uher, T. Hogan, E.K. Polychroniadis, and M.G. Kanatzidis. Cubic AgPbmSbTe2+m: Bulk thermoelectric materials with high figure of merit *Science*, 303(5659): 818-821, 2004.

[65] D. Bergman, and O. Levy. Thermoelectric properties of a composite medium *Journal of Applied Physics*, 70(11): 6821-6833, 1991.

[66] D. Narducci. Do we really need high thermoelectric figures of merit? A critical appraisal to the power conversion efficiency of thermoelectric materials *Applied Physics Letters*, 99(10), 2011.

[67] L. P. Liu. Feasibility of large-scale power plants based on thermoelectric effects *New Journal of Physics*, 16, 2014.

[68] H. Imai, Y. Shimakawa, and Y. Kubo. Large thermoelectric power factor in TiS2 crystal with nearly stoichiometric composition *Physics Review B*, 64(24), 2001.

[69] D. Bergman, and L. Fel. Enhancement of thermoelectric power factor in composite thermoelectrics *Journal of Applied Physics*, 85(12), 8205–8216, 1999.

[70] D. Vashaee, and A. Shakouri. Improved thermoelectric power factor in metal-based superlattices *Physical Review Letters*, 92(10), 2004.

[71] L. Liu. A continuum theory of thermoelectric bodies and effective properties of thermoelectric composites *International Journal of Engineering Science*, 55:35-53, 2012.

[72] L. Liu On energy formulations of electrostatics for continuum media *Journal of the Mechanics and Physics of Solids*, 61(4), 968 - 990, 2013.

[73] L. P. Tan, T. Sun, S. Fan, R. V. Ramanujan, and H. H. Hng. Facile precipitation of two phase alloys in SnTe0.75Se0.25 with improved power factor *Journal of Alloys and Compounds*, 587:420–427, 2014.

[74] M. Zebarjadi, K. Esfarjani, A. Shakouri, J. Bahk, Z. Bian, G. Zeng, J. Bowers, H. Lu, J. Zide, and A. Gossard. Effect of nanoparticle scattering on thermoelectric power factor *Applied Physics Letters*, 94(20), 202105 (2009).

[75] J. Zide, D. Klenov, S. Stemmer, A. Gossard, G. Zeng, J. Bowers, D. Vashaee, and A. Shakouri. Thermoelectric power factor in semiconductors with buried epitaxial semimetallic nanoparticles *Applied Physics Letters.*, 87(11), 112102 2005.

[76] K. Malik, D. Das, S. Bandyopadhyay, P. Mandal, A. K. Deb, V. Srihari, and A. Banerjee. Temperature-dependent structural property and power factor of n type thermoelectric Bi0.90Sb0.10 and Bi0.86Sb0.14 alloys *Applied Physics Letters.*, 103(24), 242108 (2013).

[77] G. J. Lehr, D. T. Morelli, H. Jin, and J. P. Heremans. Enhanced thermoelectric power factor in Yb1-xScxAl2 alloys using chemical pressure tuning of the Yb valence *Journal of Applied Physics*, 114(22), 223712 (2013).

[78] T. H. Zou, X. Y. Qin, D. Li, G. L. Sun, Y. C. Dou, Q. Q. Wang, B. J. Ren, J. Zhang, H. X. Xin, and Y. Y. Li. Simultaneous enhancement in thermoelectric power factor and phonon blocking in hierarchical nanostructured beta-Zn4Sb3-Cu3SbSe4 *Applied Physics Letters.*, 104(1), 013904 (2014).

[79] Herbert B. Callen, The Application of Onsager's Reciprocal Relations to Thermoelectric, Thermomagnetic, and Galvanomagnetic Effects *Phys. Rev.*, 73: 1349, 1948.

[80] Camar-Eddine, M and Milton, GW Non-local interactions in the homogenization closure of thermoelectric functionals *Asymptotic analysis*, 41(3-4): 259-276, 2002.

[81] Yang, Y., Xie, S. H., Ma, F. Y., & Li, J. Y. On the effective thermoelectric properties of layered heterogeneous medium *Journal of Applied Physics*, 111, 013510 (2012).

[82] Yang Y., Ma F., Lei C., Liu Y. and Li J., Nonlinear asymptotic homogenization and the effective behavior of layered thermoelectric composites *Journal of the Mechanics and Physics of Solids*, 61: 1768 –1783, 2013.

[83] Yang Y., Gao C. and Li J. The effective thermoelectric properties of core-shell composites *Acta Mechanica*, 225: 1211 –1222, 2014.

[84] Gurevich, A. Pinning size effects in critical currents of superconducting films *Superconductor Science and Technology*, 20(9), 2007

[85] Bezotosny, P. and Gavrilkin, S. and Lykov, A. and Attanasio, C. and Cirillo, C. and Prischepa, S. Asymmetry of the Pinning Force in Thin Nb Films in Parallel Magnetic Field *Journal of Superconductivity and Novel Magnetism*, 24(5): 1553, 2011

[86] Kaname Matsumoto, Paolo Mele, Ataru Ichinose, Masashi Mukaida, Yutaka Yoshida, Shigeru Horii and Ryusuke Kita Flux Pinning Characteristics of Artificial Pinning Centers With Different Dimension *IEEE Transactions on Applied Superconductivity*, 19(3): 3248 –3253, 2009

[87] Wu, T.C., Yang, T.J., Kang, P.C., Horng, L. and Wu, J.C. Anisotropic pinning effect on a Nb thin film with triangular arrays of pinning sites *Journal of Applied Physics*, 95(11 II): 6696-6698, 2004

[88] Silhanek, A.V., Zhu, B.Y., Raedts, S., Moshchalkov, V.V., Van Look, L. and Jonckheere, R. Enhanced vortex pinning by a composite antidot lattice in a superconducting Pb film *Physical Review B - Condensed Matter and Materials Physics*, 72(1), 2005

[89] Yampolskii, S. V. and Genenko, Yu. A. Entry of magnetic flux into a magnetically shielded type-II superconductor filament *Physics Review B*, 71(134519), 2005

[90] Genenko, Y. A. and Rauh, H. Superconductor strip in a closed magnetic environment: exact analytic representation of the critical state *Physica C*, 39(39073330), 2007

[91] Genenko, Yu. A., Rauh, H. and Yampolskii, S. V. The Bean-Livingston barrier at a superconductor/magnet interface *Journal of Physics: Condensed Matter*, 17(10): L93, 2005

[92] Genenko, Yu. A., Yampolskii, S. V. and Pan, A. V. Virgin magnetization of a magnetically shielded superconductor wire: theory and experiment *Applied Physics Letters*, 84(19): 3921 –3923, 2004

[93] Yampolskii, S.V., Genenko, Y.A. and Rauh, H. Distribution of the sheet current in a magnetically shielded superconducting filament *Physica C: Superconductivity and its applications*, 415: 151 –157, 2004

[94] Genenko, Y.A., Rauh, H. and Snezhko, A. A novel magnet/superconductor heterostructure for high-field applications *Superconductor Science and Technology*, 14(9): 669 –703, 2001

[95] Genenko, Yu. A., Snezhko, A. V. Superconductor strip near a magnetic wall of finite thickness *Journal of Applied Physics*, 92(1): 357, 2002

[96] Genenko, Y.A. Magnetic shielding for improvement of superconductor performance *Physica Status Solidi (A) Applied Research* 189(2): 469 –473, 2002

[97] Carneiro, G. Tunable pinning of a superconducting vortex by a magnetic vortex *Physical Review B - Condensed Matter and Materials Physics*, 75(9), 2007

[98] Carneiro, G. Tunable critical current for a vortex pinned by a magnetic dipole *Europhysics Letters*, 71(5): 817 –823, 2005

[99] Carneiro, G. Tunable interactions between vortices and a magnetic dipole *Physical Review B - Condensed Matter and Materials Physics*, 72(14), 2005

[100] Carneiro, G. Simple model for tunable vortex pinning by a magnetic dipole *Physica C: Superconductivity and its applications*, 437-438: 42 –45, 2006

[101] Helseth, L.E. Anomalous interaction between vortices and nanomagnets *Physics Letters, Section A: General, Atomic and Solid State Physics* 319(3-4): 413 –415, 2003

[102] Erdin, S., Lyuksyutov, I.F., Pokrovsky, V.L. and Vinokur, V.M. Topological textures in a ferromagnet-superconductor bilayer *Physical Review Letters*, 88(1): 170011-170014, 2002

[103] Koorevaar, P., Zwart, C., Aarts, J. and Coehoorn, R Interplay between superconductivity and magnetism in various superconducting/ferromagnetic multilayers *Physica B: Physics of Condensed Matter*, 194-196(PART 2): 2385-2386, 1994

[104] Ledvij, M., Dobrosavljević-Grujić, L., Radović, Z. and Clem, J.R. Vortex and nonvortex nucleation of superconductivity in ferromagnetic-superconducting-ferromagnetic triple layers *Physical Review B*, 44(2): 859 –862, 1991

[105] Cao, R., Horng, Lance, Wang, J. C., Wu, J. C., Yang, T. J. and Wu, T. C. Special pinning phenomena in superconductors with regular composite pinning arrays *Journal of Applied Physics*, 107(9), 2010

[106] Martín, J.I., Vélez, M., Nogués, J. and Schuller, I.K. Flux pinning in a superconductor by an array of submicrometer magnetic dots *Physical Review Letters* 79(10): 1929 – 1932, 1997

[107] Gillijns, W., Silhanek, A.V., Moshchalkov, V.V., Milošević, M.V. and Peeters, F.M. Influence of magnet size on magnetically engineered field-induced superconductivity *Physical Review B - Condensed Matter and Materials Physics*, 76(18), 2007

[108] Silhanek, A.V., Gillijns, W., Volodin, A., Moshchalkov, V.V., Milošević, M.V. and Peeters, F.M. Optimization of superconducting critical parameters by tuning the size and magnetization of arrays of magnetic dots *Physical Review B - Condensed Matter and Materials Physics*, 76(10), 2007

[109] Milošević, MV and Peeters, FM Vortex-antivortex nucleation in superconducting films with arrays of in-plane dipoles *Physica C-Superconductivity and its Applications*, 437-38: 208 –212, 2006

[110] Milošević, M.V. and Peeters, F.M. Field-enhanced critical parameters in magnetically nanostructured superconductors *Europhysics Letters*, 70(5): 670 –676, 2005

[111] Milošević, M. V. and Peeters, F. M. Vortex-antivortex nucleation in magnetically nanotextured superconductors: Magnetic-field-driven and thermal scenarios *Physics Review Letters*, 94(227001), 2005

[112] Milošević, M.V. and Peeters, F.M. Vortex–antivortex molecules induced by a magnetic disk on top of a superconducting film—influence of the magnet geometry *Physica C: Superconductivity and its applications*, 404: 281 –284, 2004

[113] Milošević, M.V. and Peeters, F.M. Commensurate vortex configurations in thin superconducting films nanostructured by square lattice of magnetic dots *Physica C: Superconductivity and its applications*, 404: 246 –250, 2004

[114] Milosevic, M. V. and Peeters, F. M. Vortex-Antivortex Lattices in Superconducting Films with Magnetic Pinning Arrays *Journal of Low Temperature Physics*, 139(1-2): 257 –272, 2005

[115] Milošević, M.V. and Peeters, F.M. Vortex matter in the presence of magnetic pinning centra *Journal of Low Temperature Physics*, 130(3-4): 311 –320, 2003

[116] Narayan D. Khatri, Goran Majkic, Renjie Wang, Aarthi Sundaram, Senthil Sambandam and Venkat Selvamanickam Prefabricated Metal Nanorods on Biaxially-Textured Templates on Flexible Substrates for REBCO Superconductors *IEEE Transactions on Applied Superconductivity*, 23(3): 6600705, 2013

[117] Priour, Jr., D.J. and Fertig, H.A. Broken orientational and reflection symmetries in thin film superconductors with mesoscopic magnetic dipoles *Physica C: Superconductivity and its applications*, 404: 293 - 297, 2004

[118] Priour Jr, D. J. and Fertig, H. A. Vortex States of a Superconducting Film from a Magnetic Dot Array *Physics Review Letters*, 93(5): 057003, 2004

[119] Khatri, Narayan, Liu, Y., Yao, Y., Khatri, N. D., Liu, J., Galtsyan, E., Selvamanickam, V., Chen, Y. and Lei, C. Electromagnetic Properties of (Gd, Y)Ba2Cu3Ox Superconducting Tapes With High Levels of Zr Addition *IEEE Transactions on Applied Superconductivity*, 23(3), 2013

[120] Eisenmenger, J., Oettinger, M., Pfahler, C., Plettl, A., Ziemann, P. and Walther, P. Temperature-dependent matching in a flux-line lattice interacting with a triangular array of pinning centers without long-range order *Physical Review B - Condensed Matter and Materials Physics*, 75(14), 2007

[121] Yamada, H., Yamasaki, H., Ohki, K., Nakagawa, Y. and Mawatari, Y. Strong flux pinning in YBa2Cu3O7-δ thin films due to nanometer-sized precipitates *Superconductor Science and Technology*, 21(12), 2008

[122] Selvamanickam, V., Zhang, Y., Guevara, A., Shi, T., Yao, Y., Majkic, G., Galtsyan, E., Chen, Y., Lei, C. and Miller, D. J. Effect of rare-earth composition on microstructure and pinning properties of Zr-doped (Gd, Y)Ba2Cu3Ox superconducting tapes *Superconductor Science and Technology* 25(4), 2012

[123] Wee, Sung Hun, Goyal, Amit, Zuev, Yuri L., Cantoni, Claudia, Selvamanickam, V. and Specht, Eliot D Formation of Self-Assembled, Double-Perovskite, Ba2YNbO6 Nanocolumns and Their Contribution to Flux-Pinning and Jc in Nb-Doped YBa2Cu3O7-δ Films *Applied Physics Express*, 3(2): 1, 2010

[124] Wee, S.H., Goyal, A., Specht, E.D., Cantoni, C., Zuev, Y.L., Cook, S. and Selvamanickam, V. Enhanced flux pinning and critical current density via incorporation of self-assembled rare-earth barium tantalate nanocolumns within YBa2 Cu3 O7-δ films *Physical Review B - Condensed Matter and Materials Physics*, 81(14), 2010

[125] Sudesh, Varma, G. D., Das, S., Bernhard, C. and Shripathi, T. Study of superconducting properties of ferrocene-added MgB2 *Physica Status Solidi A - Applications and Materials Science*, 211(7): 1503 –1511, 2014

[126] Dou, S.X., Soltanian, S., Horvat, J., Wang, X.L., Zhou, S.H., Ionescu, M., Liu, H.K., Munroe, P. and Tomsic, M. Enhancement of the critical current density and flux pinning of MgB 2 superconductor by nanoparticle SiC doping *Applied Physics Letters*, 81(18): 3419-3421, 2002

[127] Woch, W.M., Tokarz, W., Zalecki, R., Kołodziejczyk, A., Deinhofer, C. and Gritzner, G. Critical currents and magnetization of a (Tl0.5Pb 0.5)(Sr0.85Ba0.15)2Ca 2Cu3Oz film on silver substrate *Superconductor Science and Technology*, 23(2), 2010

[128] Polat, A., Thompson, J.R., Christen, D.K., Cook, S.W., Sinclair, J.W., Zuev, Y.L., Kumar, D., Chen, Y. and Selvamanickam, V. Thickness dependence of magnetic relaxation and E-J characteristics in superconducting (Gd-Y)-Ba-Cu-O films with strong vortex pinning *Physical Review B - Condensed Matter and Materials Physics*, 84(2), 2011

[129] Choi, E.-M., Gupta, S.K., Lee, H.-S., Kim, H.-J., Lee, S.-I. and Sen, S. Critical current density of MgB2 thin films and the effect of interface pinning *Superconductor Science and Technology*, 17(9): 5524 –5527, 2004

[130] Haage, T., Zegenhagen, J., Li, J.Q., Habermeier, H.-U., Cardona, M., Jooss, Ch., Warthmann, R., Forkl, A. and Kronmüller, H. Transport properties and flux pinning by self-organization in YBa2Cu3O7-δ films on vicinal SrTiO3 (001) *Physical Review B - Condensed Matter and Materials Physics*, 56(13): 8404 –8418, 1997

[131] Wee, Sung Hun, Goyal, Amit, Zuev, Yuri L., Cantoni, Claudia, Selvamanickam, V. and Specht, Eliot D. Formation of Self-Assembled, Double-Perovskite, Ba2YNbO6 Nanocolumns and Their Contribution to Flux-Pinning and J(c) in Nb-Doped YBa2Cu3O7-delta Films *Applied Physics Express*, 3(2), 2010

[132] Zdravkov, V. I., Kehrle, J., Obermeier, G., Gsell, S., Schreck, M., Mueller, C., von Nidda, H. -A. Krug, Lindner, J., Moosburger-Will, J., Nold, E., Morari, R., Ryazanov, V. V., Sidorenko, A. S., Horn, S., Tidecks, R. and Tagirov, L. R. Reentrant superconductivity in superconductor/ferromagnetic-alloy bilayers *Physical Review B*, 82(5), 2010

[133] Selvamanickam, Venkat, Chen, Yimin, Xiong, Xuming, Xie, Yiyuan Y., Martchevski, Maxim, Rar, Andrei, Qiao, Yunfei, Schmidt, Robert M. , Knoll, Allan, Lenseth, Kenneth P. and Weber, Chuck S. High Performance 2G Wires: From R&D to Pilot-Scale Manufacturing *IEEE Transactions on Applied Superconductivity*, 19(3): 3225 –3230, 2009

[134] Kakimoto, K., Igarashi, M., Hanada, Y., Hayashida, T., Tashita, C., Morita, K., Hanyu, S., Sutoh, Y., Kutami, H., Iijima, Y. and Saitoh, T. High-speed deposition of high-quality RE123 films by a PLD system with hot-wall heating *Superconductor Science and Technology*, 23(1), 2010

[135] Rupich, Martin W., Li, Xiaoping, Thieme, Cees, Sathyamurthy, Srivatsan, Fleshler, Steven, Tucker, David, Thompson, Elliot, Schreiber, Jeff, Lynch, Joseph, Buczek, David, DeMoranville, Ken, Inch, James, Cedrone, Paul and Slack, James Advances in second generation high temperature superconducting wire manufacturing and R&D at American Superconductor Corporation *Superconductor Science and Technology*, 23(1), 2010

[136] Aladyshkin, A. Yu, Silhanek, A. V., Gillijns, W. and Moshchalkov, V. V. Nucleation of superconductivity and vortex matter in superconductor-ferromagnet hybrids *Superconductor Science and Technology*, 22(5), 2009

[137] Stamopoulos, D. and Manios, E. and Pissas, M. Synergy of exchange bias with superconductivity in ferromagnetic-superconducting layered hybrids: the influence of in-plane and out-of-plane magnetic order on superconductivity *Superconductor Science and Technology*, 20(12): 1205–1222, 2007

[138] Koren, G., Kirzhner, T. and Aronov, P. Critical current measurements in superconductor-ferromagnet-superconductor junctions of YBa2Cu3Oy-SrRuO3-YBa2Cu3Oy: No evidence for dominant proximity-induced triplet superconductivity in the ferromagnetic barrier *Physical Review B*, 85(2), 2012

[139] Yampolskii, SV and Yampolskaya, GI and Rauh, H Magnetic dipole-vortex interaction in a bilayered superconductor/soft-magnet heterostructure *Europhysics Letters*, 74(2): 334 –340, 2006

[140] Milosevic, MV and Peeters, FM Superconducting Wigner vortex molecule near a magnetic disk *Physical Review B*, 68(2), 2003

[141] Doria, MM Magnetic regions inside a superconductor and its effects on the vortex matter *Physica C-Superconductivity and Its Applications*, 404(1-4): 145 –152, 2004

[142] Carneiro, G Interaction between vortices in superconducting films and magnetic dipole arrays *Physica C-Superconductivity and Its Applications*, 404(1-4): 78 –86, 2004

[143] Zhao, Y, Feng, Y, Machi, T, Cheng, CH, Huang, DX, Fudamoto, Y, Koshizuka, N and Murakami, M Enhancement of critical current density in MgB2 bulk superconductor by Ti doping *Europhysics Letters*, 57(3): 437 –443, 2002

[144] Palau, A., MacManus-Driscoll, J. L., Blamire, M. G. Magnetic vortex pinning in superconductor/ferromagnet nanocomposites *Superconductor Science and Technology*, 20(9, SI): S136-S140, 2007

[145] Adamopoulos, N and Patapis, SK Role of interface quality in vortex pinning by large nonsuperconducting particles *Physical Review B*, 61(17): 11305-11308, 2000

[146] Kayali, MA Theory of pinning in a superconducting thin film pierced by a ferromagnetic columnar defect *Physical Review B*, 71(2): 1098-0121, 2005

[147] Blamire, M. G., Dinner, R. B., Wimbush, S. C. and MacManus-Driscoll, J. L. Critical current enhancement by Lorentz force reduction in superconductor-ferromagnet nanocomposites *Superconductor Science and Technology*, 22(2), 2009